



SCUOLA DI DOTTORATO  
UNIVERSITÀ DEGLI STUDI DI MILANO-BICOCCA

Department of Materials Science

PhD in Materials Science and Nanotechnology

Cycle: XXIX

Curriculum: Industrial

# **POLYSILSESQUIOXANE AS ADVANCED “MOLECULAR” FILLER FOR RUBBER REINFORCEMENT**

Redaelli Matteo

Matricola: 717162

Tutor: Prof.ssa Franca Morazzoni

Cotutor: Dr. Massimiliano D'Arienzo

Supervisor: Dr. Luca Giannini

Coordinator: Prof. Gianpaolo Brivio

**ANNO ACCADEMICO 2015/2016**



## Abstract

The reinforcement of elastomers (e.g. PolyButadiene PB, Styrene Butadiene Rubber SBR) by addition of inorganic fillers (carbon black, SiO<sub>2</sub>) is a practice widely employed in tire industry. In particular, the control SiO<sub>2</sub> NPs morphology, surface functionalities, and their networking within the polymer matrix (i.e. filler-filler and filler-rubber interactions) plays a key role in achieving desired mechanical properties. These outcomes suggest that the utilization of fillers with tailorable structure and functionalities, able to simultaneously enhance the networking and the interaction with rubber, may be a promising strategy for upgrading the composites properties. Emerging fillers which seems to be suitable candidates are Polysilsesquioxanes (PSQs), a novel class of hybrid materials which exhibit or impart, if included in composites, a number of beneficial properties (e.g. thermal stability, mechanical properties, etc...). Stimulated by this background, the aim of this work is to explore the possibility to employ PSQs with different molecular structure (cage or ladder-like) as innovative fillers in rubber nanocomposites potentially exploitable in tires formulation. In detail, a novel hybrid filler, SiO<sub>2</sub>@POSS, where SiO<sub>2</sub> and cage-like PSQs (POSS) belong to the same functional structure, has been developed by grafting on silanized SiO<sub>2</sub> different loadings of OctaMethacrylPOSS, using a surface reaction mediated by dicumylperoxide. The hybrid filler was then employed for preparing SBR/SiO<sub>2</sub>@POSS nanocomposites, which display outstanding mechanical properties. This has been associated to the peculiar structure of SiO<sub>2</sub>@POSS, constituted by NPs

aggregates partially interconnected and decorated by POSS nanounits which, thanks to the high number of reactive functionalities, promote the formation of a tight filler network which immobilizes filler and rubber, afford a relevant reinforcement and improve the hysteretical properties. A similar approach, has been applied for study the properties of PB nanocomposites including PSQs with tailorable cage or ladder-like structure. Swelling experiments and, more in depth,  $^1\text{H}$  NMR revealed a significant relation between SH-NBBs architecture and their interactions with the polymer, resulting in restricted rubber chains mobility. In summary, the whole results suggest that PSQs can be promising fillers, which grant the transfer of the advanced properties of these nanounits to the final nanocomposites.



## **Contents**

### **Preface**

### **Structure of the thesis 11**

## **Chapter 1**

### **Introduction 18**

#### **1.1 Hybrid materials and rubber nanocomposites for tires applications 19**

#### **1.2 Filler in rubber nanocomposites for tires application 24**

1.2.1 Filler features and their effect on composite properties 25

1.2.2 Filler networking and percolation threshold 27

#### **1.3 Reinforcing properties of rubber nanocomposites 29**

#### **1.4 Silica-based nanofillers in rubber nanocomposites for tires 34**

#### **1.5 Polysilsesquioxanes 38**

1.5.1 Polyhedral Oligomeric Silsesquioxanes with cage structure 39

1.5.2 Ladder-like polysilsesquioxanes 41

#### **1.6 PSQs -Polymer Nanocomposites 43**

#### **1.7 Aim of the thesis 53**

## **Chapter 2**

### **Fundamentals of rubber compounding 55**

#### **2.1 Formulation of rubber compounds 57**

#### **2.2 Rubbers 59**

<b>2.3 Fillers</b>	<b>60</b>
<b>2.4 Antidegradants</b>	<b>61</b>
<b>2.5 Vulcanizing ingredients</b>	<b>62</b>
2.5.1 Vulcanization with sulfur	62
2.5.2 Vulcanization with Peroxide	64

## **Chapter 3**

<b>Experimental</b>	<b>68</b>
<b>3.1 Synthesis of SiO<sub>2</sub>@POSS hybrid filler</b>	<b>69</b>
<b>3.2 Preparation of SBR nanocomposites</b>	<b>71</b>
3.2.1 Preparation of SBR/SiO <sub>2</sub> @POSS and SBR/SiO <sub>2</sub> @MonoPOSS	71
3.2.2 Preparation of SBR/SiO <sub>2</sub> +POSS and SBR/SiO <sub>2</sub> +MonoPOSS	76
<b>3.3 Synthesis of Thiol Functionalized Nano Building Blocks (SH-NBBs)</b>	<b>77</b>
<b>3.4 Preparation of PB/%NBBs Nanocomposites</b>	<b>79</b>

## **Chapter 4**

<b>Results: Morphological and physico-chemical characterization of fillers and related nanocomposites</b>	<b>82</b>
<b>4.1 Spectroscopic and morphological characterization of the hybrid SiO<sub>2</sub>@POSS nanofiller</b>	<b>83</b>
4.1.1 FT-IR spectroscopy	83
4.1.2 Nitrogen adsorption-desorption experiments	88
4.1.3 Thermogravimetric analysis (TGA)	89

4.1.4 Solid state NMR investigation of SiO <sub>2</sub> @POSS hybrid filler	91
4.1.5 TEM investigation of SiO <sub>2</sub> @POSS hybrid filler	94
<b>4.2 Characterization of SBR/SiO<sub>2</sub>@POSS and SBR/SiO<sub>2</sub>+POSS nanocomposites</b>	<b>97</b>
4.2.1 TEM investigation of the nanocomposites	97
4.2.2 Morphology of SBR nanocomposites by SEM	100
4.2.3 Atomic Force Microscopy (AFM) investigation of the nanocomposites	107
4.2.4 Swelling experiments	110
4.2.5 <sup>1</sup> H MAS NMR investigation on SBR nanocomposites	112
<b>4.3 Characterization of SH-NBBs</b>	<b>118</b>
4.3.1 FT-IR spectroscopy	118
4.3.2 NMR investigation of pure SH-NBBs	119
<b>4.4 Characterization of PB/NBBs Nanocomposites</b>	<b>122</b>
4.4.1 FT-IR spectroscopy	122
4.4.2 Thermogravimetric analysis (TGA)	124
4.4.3 Swelling experiments	126
4.4.4 NMR investigation of PB/%NBBs nanocomposites	127

## **Chapter 5**

### **Results: Dynamo-mechanical properties**

#### **of SBR nanocomposites 134**

##### **5.1 Evaluation of the rheological properties of rubber nanocomposites by ODR (Oscillating Disk Rheometry) 135**

##### **5.2 Temperature dependent dynamo-mechanical studies 142**

<b>5.3 Tensile Tests</b>	<b>147</b>
<b>5.4 SiO<sub>2</sub>@MonoPOSS: a probe for understanding the role of POSS nanocages in SiO<sub>2</sub>@POSS hybrid filler</b>	<b>151</b>
<b>Chapter 6</b>	
<b>Conclusion</b>	<b>155</b>
<b>References</b>	<b>161</b>
<b>Appendix A</b>	
<b>Characterization method</b>	<b>171</b>
A1.1 Attenuated Total Reflectance Infrared Spectroscopy (ATR-FTIR)	172
A1.2 Thermal analysis (TGA)	173
A1.3 Nitrogen physisorption measurements	175
A1.4 Solid State NMR	177
A1.5 Scanning Electron Microscope (SEM)	180
A1.6 High-Resolution Transmission Electron Microscopy (HRTEM)	182
A1.7 Swelling experiments	184
A1.8 Atomic Force Microscopy (AFM)	185
A1.9 Oscillating Dish Rheometry (ODR) and stress-strain measurements	188
A1.10 Dynamo Mechanical Thermal Analysis (DMTA)	190
A1.11 Tensile Tests	191
<b>List of abbreviations</b>	<b>195</b>



## **Preface**

### **Structure of the thesis**

Rubber compounds are largely employed in the manufacturing of plastics goods, especially for the production of the tires. Since the mechanical properties of rubber are poor, their improvement is guaranteed through two main processes: the addition of particulate reinforcing fillers and the vulcanization reaction. Reinforcing fillers are mixed with the rubber to improve the rigidity of the obtained compound. Vulcanization is a process which aims at improving the rubber elasticity via a polymeric network made of sulfur crosslinks.

As regards the addition of reinforcing fillers, the tire industry extensively employs carbon black and silica particles. Silica, in particular, allows to enhance the tear strength of the material, to increase abrasion resistance and to reduce rolling resistance of tires. The reinforcement effect of silica in rubber compounds depends on different contributions. It involves either the hydrodynamic effect, due to volume fraction and shape factor of the filler, and the most important filler-rubber and filler-filler interactions. These determine the formation of an interconnected filler network in the rubber matrix, that is essential to provide effective reinforcement. In particular, the filler-rubber interaction has been recognized to control the filler dispersion and networking through the polymer matrix, depending on the filler particle size and shape, on the surface characteristics of the filler and on the chemical nature of the polymer. In this context, our group reported that also the particle shape affected both filler-filler and filler-rubber interactions as well as the filler networking. Along this line, we have reported a systematic discussion of the behavior of rubber composites in relation to the different shapes of silica NPs. The

results revealed that particle anisotropy and alignment can provide, beside an increase of the filler-filler interactions, high percentage of immobilized rubber at the filler/ rubber interface, so-called bound rubber, leading to a higher degree of reinforcement.

These outcomes suggest that the utilization of new fillers with tailored structure and functionalities able to simultaneously enhance the filler networking and the filler-rubber interaction, increasing the amount of immobilized rubber, may to be a promising approach to effectively improve the mechanical properties of the composite and limit the silica amount in compounding.

In this context, we selected as possible units polyhedral oligomeric silsesquioxanes (PSQs), which have been already used as nanofillers in different polymer matrix. It has been demonstrated that PSQs incorporation in polymers, even in small amount, dramatically improves their mechanical properties (strength, modulus, rigidity). These benefits have been related to the well-defined structure and size of the cage or ladder like nanounits as well as to the possibility of tailoring their functionalization and interaction with the polymers. However, the effects of the introduction of PSQs into polymer matrix on the final composite properties is a complex phenomenon and it is not always clear, since one should carefully consider the blending procedure adopted and the chemical nature of their organic functionalities and of the polymer. Moreover, despite all the above described outcomes, further endeavours are needed to establish a clear relation between the structure/morphology of the PSQs and the subsequent mutual interactions (e.g. filler-polymer interface and

segregation) on the properties of the hybrid nanocomposites and, in turn, to select the best materials for a targeted application.

To the best of our knowledge, no work has reported a systematic discussion of the behaviour of rubber composites in relation to the different PSQs structures and functionalities. In particular, no studies have focused on the design and synthesis of rubber nanocomposite applied for tires including POSS nanocages as novel molecular filler, which in conjunction to silica, impart a significant reinforcement.

### **Structure of the thesis**

This thesis is divided in the following chapters:

In **Chapter 1** the background of hybrid materials and nanocomposites is reviewed, in order to point out the material class of filler/rubber systems. The main part of the chapter is dedicated to the morphology-properties relation typical for this kind of materials, and the properties of interest for the tire manufacturers. Particular attention will be dedicated to rubber nanocomposites reinforced with silica-based nanofillers and to the main features requested for tuning the mechanical properties of the final materials.

In **Chapter 2**, the types and the characteristics of rubbers, the fillers, the vulcanization ingredients and the others chemicals used for the preparation of the rubber nanocomposites for tires applications are summarized.

**Chapter 3** reports the experimental details of the synthesis utilized for obtaining the innovative nanofillers employed in this work (i.e SiO<sub>2</sub>@POSS and SH-NBBs) and of the preparation of the styrene-butadiene rubber (SBR) and polybutadiene (PB) nanocomposites.

**In Chapter 4**, the results of the morphological and physico-chemical characterizations of SiO<sub>2</sub>@POSS hybrid and SH-NBBs and of the related SBR and PB nanocomposites are discussed. In detail, the first part is mainly dedicated to the properties of SiO<sub>2</sub>@POSS and of the resulting SBR nanocomposites. In particular, a deeper investigation of the interaction between SiO<sub>2</sub>@POSS and polymer chains was performed by checking the filler adhesion and the formation of rigid rubber at the interface by SEM, AFM and NMR, also in comparison to the SBR/SiO<sub>2</sub>+POSS composites.

In the second part, the spectroscopic features of the SH-NBBs has been assessed by Solid State NMR, as well as the role of their architecture on the filler-polymer interactions.

**Chapter 5** reports the results of the comprehensive dynamic-mechanical investigation on the SBR nanocomposites obtained from SiO<sub>2</sub>@POSS.

Finally, **Chapter 6**, sums up the main results and reports the conclusion of the investigation.

The last part (i.e. **Appendix**) of this thesis describes the methods used during the preparation and characterization of SBR and PB nanocomposites.



**Chapter 1**  
**Introduction**

## **1.1 Hybrid materials and rubber nanocomposites for tires applications**

In the field of nanotechnology, hybrid materials have become a prominent area of current research and development and they have been defined as a promising new class of composites.

An hybrid material is defined as a formulate obtained by the combination of two or more parts. The material is phase separated, meaning that one or more components constitute the continuous phase (also called matrix) while one or more components constitute the dispersed phase (also called filler).

Obviously, final product properties are not only the sum of the individual contributions, but depend on the important role played by the interface between these two simple materials. Consequently, the change of the physical and chemical properties of the materials produced, is due to a suitable interface, which combines the advantages of the filler as the inorganic material (e.g rigidity, thermal stability) with the advantages of an organic polymer (e.g flexibility, dielectric, ductility and processability) <sup>1-3</sup>.

According to Sanchez et al.<sup>4</sup>, hybrid material can be divided in 2 classes according to the nature of bond that exists at the inorganic/organic (I/O) interface, which is highly predictive of the final material properties (Fig 1.1).

In detail, Class I hybrid materials are those showing weak interactions between the two phases, such as van der Waals, hydrogen bonding or weak electrostatic interactions; Class II hybrid materials are instead

those that show strong chemical interactions between the components.

As an example, blends are typical Class I hybrid materials, since they are formed if no relevant chemical interactions exist between the inorganic and organic building blocks. In this frame, a typical example is the combination of inorganic clusters or particles with organic polymers lacking of a covalent interaction between the components. If an inorganic and an organic network interpenetrate without strong chemical interactions, so-called interpenetrating networks (IPNs) are formed, which are for example the case of a sol-gel material (Fig 1.1 top)<sup>5</sup>. Class II hybrids are formed when the discrete inorganic building blocks, e.g. clusters, are covalently bonded to the organic polymers or inorganic and organic polymers are covalently connected with each other (Fig. 1.1, bottom)<sup>3</sup>.

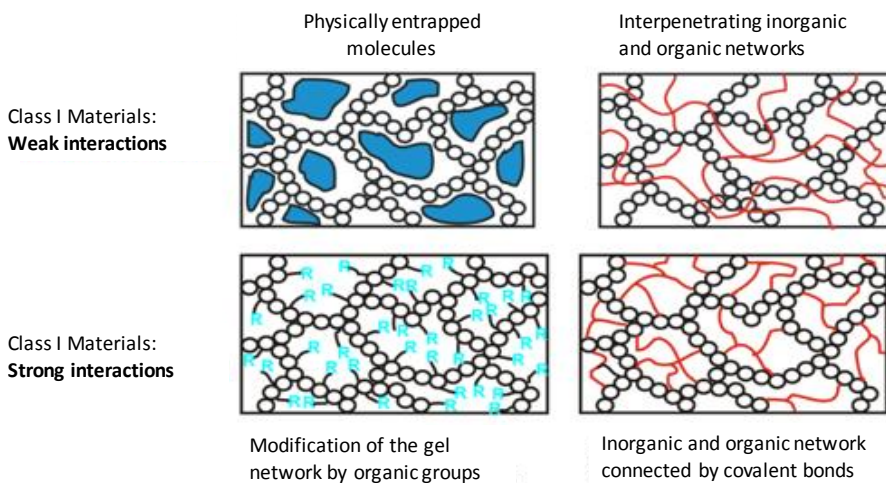


**Figure 1.1:** Main classes of organic-Inorganic hybrid materials<sup>3</sup>

If one of the structural units, either the organic or the inorganic, is in the range of 1-100 nm, hybrid materials are generally named nanocomposites. Examples of inorganic units for nanocomposites are nanoparticles (NPs), nanorods, carbon nanotubes and clay minerals. Usually a nanocomposite is formed by the incorporation of these building blocks by in organic polymers.

Since the tuning of properties at the interface can change dramatically the macroscopic properties of the whole material, nanocomposites are an attractive field of research for many applications ranging from biomedical, catalytic process, separation science, chemical sensing, fuel cell, solar energy accumulation, hydrogen storage, capacitors, micro/nano electronics devices, etc. (Fig. 1.2)<sup>1-3</sup>.

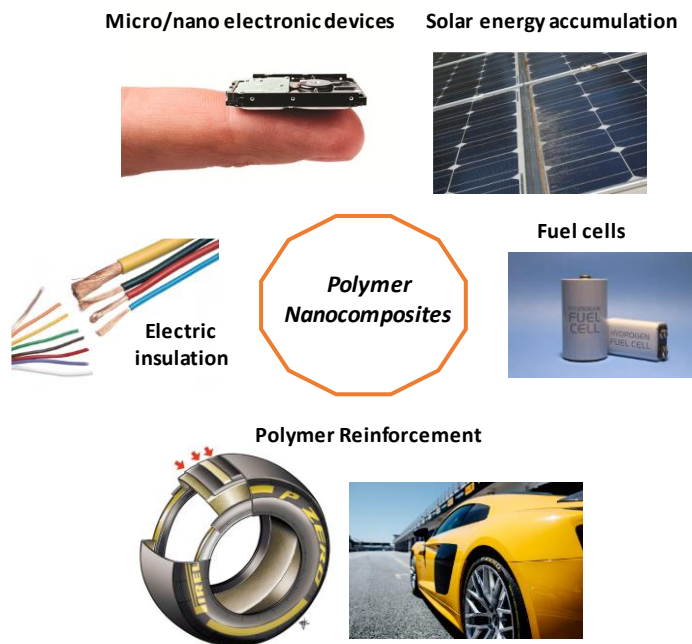


**Figure 1.2:** Application of polymer Nanocomposites

In recent years researchers of industry and universities have focused their interest in the properties of rubber nanocomposites, due to their wide applications in the manufacturing of tires, inner tubes belts, hoses, oil seals, gaskets and so on<sup>1-3</sup>.

A rubber nanocomposite is defined as a formulate obtained by the combination of an organic parts (e.g. NR Natural Rubber, IR Isoprene Rubber, BR Butadiene Rubber, SBR Styrene Butadiene Rubber, NBR Nitrile butadiene, Chloroprene rubber) and inorganic fillers which are fundamental for making them applicable in various fields<sup>1,2,5,6</sup>. Mineral fillers (e.g. micrometer carbon black and  $\text{CaCO}_3$ ) are known to improve the strength and stiffness of rubbers. Moreover, nanomaterials (e.g.  $\text{SiO}_2$ , silicates, bionanofibers, carbon nanotubes) are extremely useful polymeric reinforcing agents. Compared to traditional micrometric fillers, these particles can enhance the composite properties in relatively small concentrations<sup>7-12</sup>.

As concerns on tires application, rubber nanocomposites are the dominating materials due to their excellent mechanical properties, enhanced modulus and dimensional stability, flame retardancy, improved scratch and mar resistance, superior thermal and processing properties, reduced warpage of components and enhanced impact resistance<sup>1</sup>.

In particular, a challenging employ of these materials is in the development of the so-called "Green tire" i.e. energy efficient tire, which are able to reduce the rolling resistance without sacrificing grip and wear<sup>25-28</sup>. In fact, these three important properties form the so called "magic triangle" of tires (Fig. 1.3), which indicates that an ideal

compromise among these characteristics should be achieved for optimizing tires performance <sup>1</sup>.

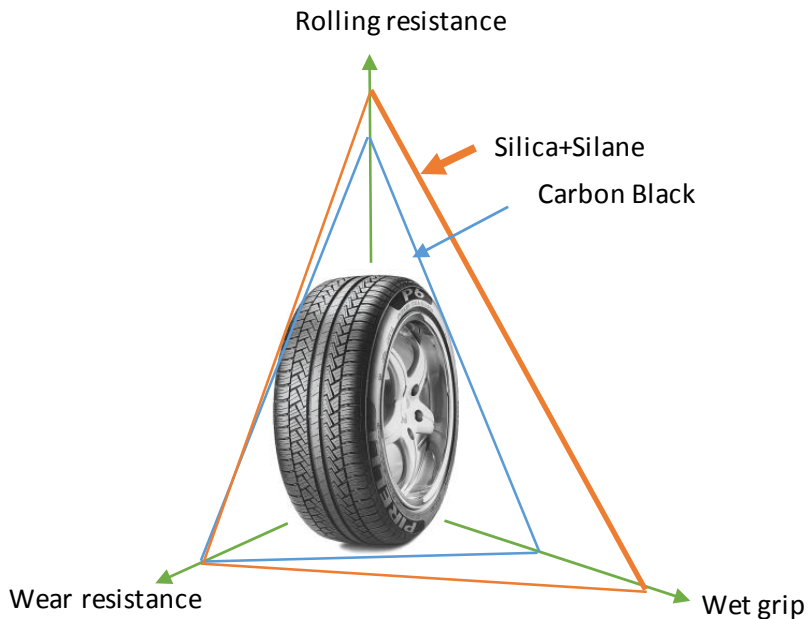


**Figure 1.3:** The “magic triangle” of tire’s properties

The extent of property enhancement strongly depends on the viscoelastic properties of the rubber composites utilized. These, in turn, rely on different parameters such as the filler typology and amount, size and shape of the filler particles (aspect ratio), the degree of dispersion and aggregation of particles in the matrix (filler-filler interaction) and the interfacial adhesion between filler and polymer chains (filler-rubber interaction) <sup>15-17</sup>.

Hence a deeper understanding of the influence of filler features on the reinforcing properties of rubber nanocomposites is required for upgrading their application in tires.

## 1.2 Filler in rubber nanocomposites for tires application

Many types of nanofillers can be incorporated in rubber for reinforcement issue. They can be generally classified on the basis of their chemical composition (e.g particle size, anisotropy) and influence on rubber properties. In detail they can be divided into categories: non-reinforcing, semi-reinforcing and reinforcing (Fig 1.4)<sup>1,2,6</sup>.

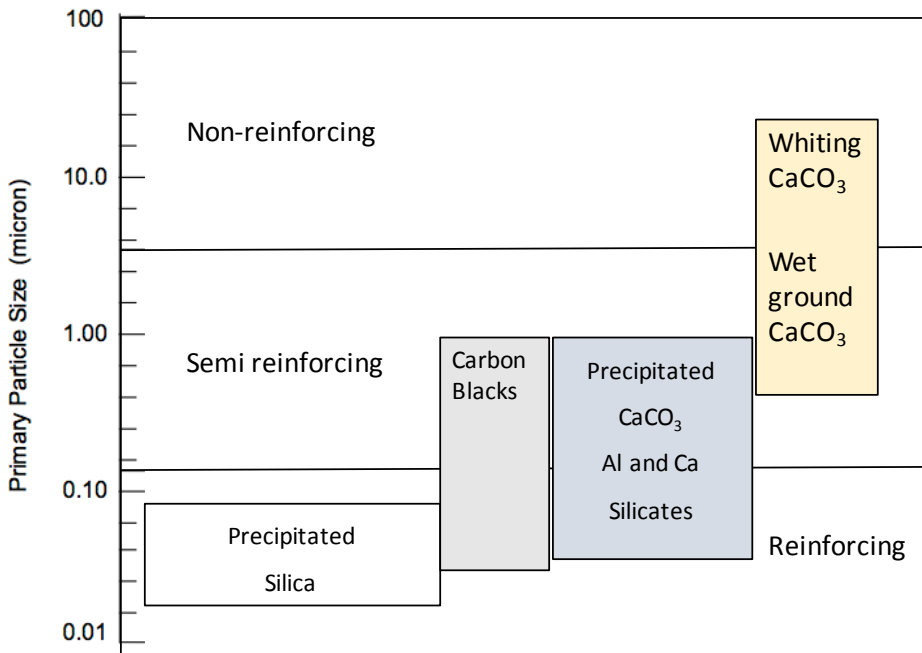


**Figure 1.4:** Classifications of filler reinforcing effect according to the particle size

Non reinforcing filler (or extruders) are generally bulky particulate materials like  $\text{CaCO}_3$  which are employed just to reduce the cost of the final material without any improvement of properties.

Instead carbon blacks and precipitated silica are the most common materials used as reinforcing nanofillers in elastomers. Recently the

research has also explored the possibility of utilize other carbon based materials (e.g carbon nanotubes, graphene), or natural layered silicates such as sepiolite, montmorillonite and halloysite<sup>1,2,6,18</sup>.

In the next section the most important characteristics of fillers and their influence on the final properties of composites will be summarized.

### **1.2.1 Filler features and their effect on composite properties**

#### **Particle size**

One of the first information generally considered about a filler is the average particle size. Particles produced for tire application must be nanometric to exert reinforcement on rubber. Bulky particulate materials like calcium carbonate can be employed just to reduce the cost of the final material without any improvement of properties<sup>1,2</sup>.

#### **Specific surface functionalities**

The nature of the filler surface determines the type of bonding with the matrix (covalent, Van der Waals, H-bond etc.) and as a consequence controls the nanocomposites homogeneity and the mechanical properties related (wear/abrasion resistance, properties at break). While carbon black surface chemistry can be controlled by simply its degree of oxidation, silica can be surface-modified with chemical compounds, in order to reduce the high hydrophilicity and to create a covalent bond with the matrix (vide infra)<sup>1,2,14</sup>.

## **Particle shape**

The shape of the particles has pronounced significance. In particular, it has been demonstrated that the reinforcing effect of the filler increases with the anisotropy of the particles, that is with the increase of the aspect ratio (average length/diameter ratio). For example, fillers with plate-like geometry like talc, mica, or layered silicates reinforce polymers more than spherical fillers<sup>1,2,16,17</sup>.

## **Filler aggregation and agglomeration**

Depending to the mutual affinity of the particles and to the type of bond existing at the filler-polymer interface, filler particles might not be homogeneously distributed inside the matrix forming aggregates and agglomerates. By definition the term aggregate is related to the undispersible clusters of NPs while agglomerate refers to particles clusters which can be redispersed by shearing forces.

A lot of evidences has shown that the probability of aggregation increases with decreasing particle size of the filler. Filler aggregation represents a problem because it induces a depletion of the properties of composites. It is well-known that tensile strength but also the fracture resistance of composites containing aggregated particles, drastically decrease with increasing number of aggregates. Aggregates may act therefore as fracture initiation sites and depending on aggregate strength they may break under the effect of external load, which results in the failure of the product<sup>1,2,19</sup>.

### 1.2.2 Filler networking and percolation threshold

The combination of filler particles and rubber matrix should result, in the simplest case, in a homogeneous distribution of filler particles in the matrix, provided that the filler particles have no tendency to agglomerate. The formation agglomerates generally takes place when the filler volume fraction in a nanocomposite is relatively high ( $\gg 0.05$ ), because the total interface area  $A$  is large, while the interparticle distance is short<sup>19</sup>.

At increasing filler content, a percolative threshold ( $f_c$ ) is attained and all the isolate, aggregated and agglomerated nanoparticles become part of a network extended through the whole matrix. The percolation threshold can be hence defined as the filler volume fraction at which all the particles are interconnected. From geometrical observations, Ostwald reported that a collection of spheres of equal radius closely packed fills 74% of the volume, while the remaining 26% is empty or corresponds to the outer phase. This value is the theoretical maximum filling volume in a polymer matrix. However, actual  $f_c$  values are much lower than the theoretical maximum filling volume as a consequence of the interactions occurring between particles (filler-filler interactions), between particle and matrix (filler-rubber interactions), and the formation of an interphase, which allow a continuous network to form even without close packing of particles<sup>1,2,6,19</sup>.

Nanocomposites properties (e.g electrical and mechanical) undergo dramatic changes upon filler percolation is reached (See Fig 1.5).

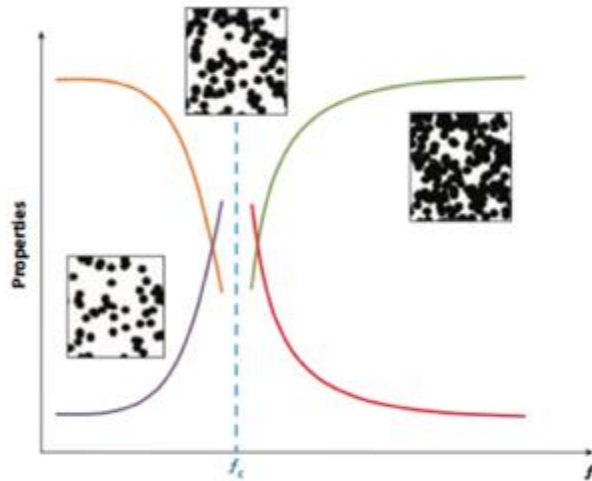


**Figure 1.5:** Schematic of mechanical and morphological properties of a rubber nanocomposite as a function of the filler volume fraction ( $f$ ).

$f_c$  indicates the percolation threshold<sup>19</sup>

For example, when an electrically conductive particulate (graphite, carbon nanotube, metal NPs) is dispersed in a non-conductive matrix (like most of the polymers), the resulting composite is not significantly conductive below  $f_c$  while become a good conductor above  $f_c$ . The same occurs for the reinforcing properties: below  $f_c$  the material exhibits mainly viscous character (similarly to the unfilled polymer), while above  $f_c$  the elastic modulus suddenly improve and the dissipation factor ( $\tan\delta$ ) decrease (see next section)<sup>1,2,20</sup>.

### 1.3 Reinforcing properties of rubber nanocomposites

The filler addition to a rubber matrix by either physical or chemical procedures usually leads to an improvement of properties of the material. Specifically, the effect of reinforcement is commonly represented by the complex modulus  $G^*$  (equation 1), which can be decomposed in an in phase elastic component ( $G'$ , storage modulus) and in a out-of-phase dissipative component ( $G''$ , loss modulus):

$$\mathbf{G^* = G' + iG''} \quad (1)$$

The  $G''/G'$  ratio is called  $\tan\delta$  (dissipation factor), and it indicates the ratio between energy lost and energy stored in a cyclic deformation. The contribution to the reinforcement exerted by the filler is mainly represented by  $G'$ .

In the literature, several models have been utilized for evaluating the structural and compositional contributions to the reinforcement in rubber nanocomposites in terms of  $G'$ ,  $G''$  and  $\tan\delta$ <sup>1,20,25</sup>.

One of the most employed approaches is based on the work of Payne, who studied the relation between the three dimensional filler aggregates and the dependence of the storage and loss moduli on the strain.

In detail, the model indicates that, for a viscoelastic material undergoing a relatively low oscillatory strain, a sigmoid decrease of the value of initial storage modulus ( $G'_0$ ) occurs until a plateau is reached at high strain ( $G'_\infty$ ). This behavior was explained referring to the breakage of the filler network which can occur at lower strain values compared to those necessary for the polymer chains rupture. In fact,

the filler particles are held together by relatively weak forces (e.g. H-bonds and Van der Waals interactions), while covalent bonds are present at the filler-polymer chains interface and in the rubber structure (crosslinks).

This effect is reversible when the strain is released and does not depend on the rubber type, while mainly on the filler characteristics.

The extent of the filler network breakdown can be evaluated as a difference between  $G'_0$  and  $G'_\infty$ , and it is associated with an energy-dissipative event (hysteresis), according to the following equation:

$$\Delta G' = G'_0 - G'_\infty \quad (2)$$

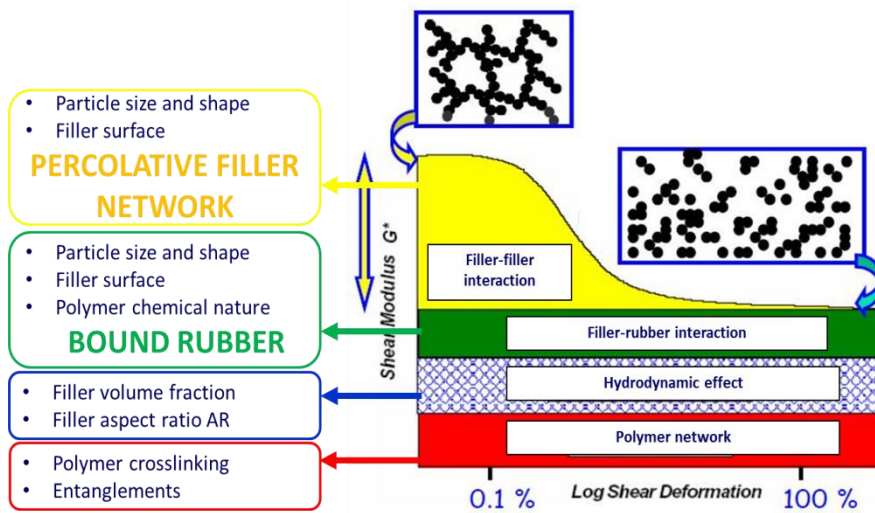


**Figure 1.6:** Scheme of a stress-strain curve for a rubber nanocomposite (right-side). The strain-dependent and strain-independent contributions to the Payne effect are indicated by different colors and briefly summarized (left-side).

In this way it is possible to separate two main distinct components contributing to the elastic modulus  $G'$  (Fig. 1.6): a strain-dependent component associated to the reinforcement brought by filler-filler interactions in the network and a strain-independent one mainly attributable to filler-rubber interactions<sup>20-27</sup>.

A rubber nanocomposite characterized by both a high value of modulus at low-strain (high  $G'_0$ ) and a low  $\Delta G'$  would demonstrate high reinforcement and low hysteresis.

These features have a great practical importance in tires applications since they reduce the rolling resistance and heat generation<sup>1,13</sup>.

However, other parameters must be considered for a comprehensive description of the rubber reinforcement. In particular, a key role is played by the interactions between filler and polymer at the interface.

In fact, when elastomers and reinforcing fillers are mixed, interactions occur and polymer chains are immobilized on the filler surface. This results in a thin layer of polymer (2–5 nm), which encapsulates filler particles and aggregates. These interactions can be so strong that even a good solvent for the polymer cannot extract it. The part of rubber that cannot be extracted is called bound rubber.

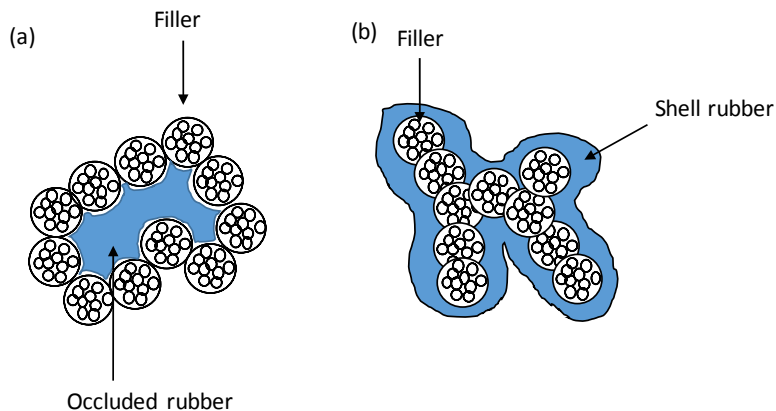


**Figure 1.7:** Scheme of a) occluded rubber and b) shell rubber

These concepts have been further refined through microscopic studies by Medalia et al<sup>28,29</sup>. In detail, they proposed the presence of two different types of rubber interacting with the filler aggregates: an “occluded rubber” trapped in the cavities of the filler network and a “shell rubber”, which is adsorbed onto the external surface of the aggregates (Fig 1.11).

A first relevant confirmation of these suggestions was given by Tsagaropoulos and Eisenberg in 1995<sup>30,31</sup>. They detected the presence of a well-defined fraction of rubber with higher glass transition temperature compared to the bulk rubber. This observation was validated for different filler/rubber systems and the amount of the rigid rubber increased as a function of the filler amount and surface area.

In 2003, Arrighi<sup>32</sup> proposed also a numerical method to calculate the exact amount of immobilized rubber from DMTA curves after appropriate deconvolution routines and integration. The interpretation

of this preliminary observation found opposition in literature, hence further investigations were necessary to clarify the issue.

For this reasons, more recent studies have been devoted to the detailed investigation of the interactions at the filler-rubber interface by NMR spectroscopy. The existence of polymer chains with lower mobility than those of pure elastomers has been revealed. In particular, three regions with different mobility have been identified: a mobile region far from the particles, an outer shell with lower mobility and an inner shell with very poor mobility<sup>33,34</sup>.

In summary, these studies have defined the formation of a polymer layer surrounding filler particles and connecting them in a percolative network diffuse thought the whole nanocomposite. According to this concept, the interpretation of the reinforcement based on the Payne effect model has to be reconsidered. As explained above, the network breakdown entails the rupture of the weak bonds between the filler particles. As the filler-filler contact must be mediated by the presence of interfacial rubber, the Payne effect can be associated to the disentanglement of the polymer chains which constitute the actual connections among filler particles forming the network.

This overview points out that the reinforcing properties of rubber nanocomposites strongly depend on the nature, loading and characteristic of the utilized fillers.

In the next paragraph, the influence of these parameters on the properties of rubber composites will be described focusing on silica, the most utilized inorganic filler in rubber nanocomposites for tires in alternative to carbon black.

## 1.4 Silica nanofillers in rubber nanocomposites for tires

Amorphous silica is the most widely utilized inorganic filler in rubber nanocomposites for tires. Three fundamental properties govern the influence of  $\text{SiO}_2$  on the rubber properties:

- specific surface area;
- concentration of silanol groups on the silica surface;
- particle size and shape.

In particular, the amount of the silanol groups on the silica surface plays an important role in determining its reinforcing capabilities in non-polar elastomers. These behave as polar acidic sites, resulting in a poor affinity of pure silica with the polymer matrix.

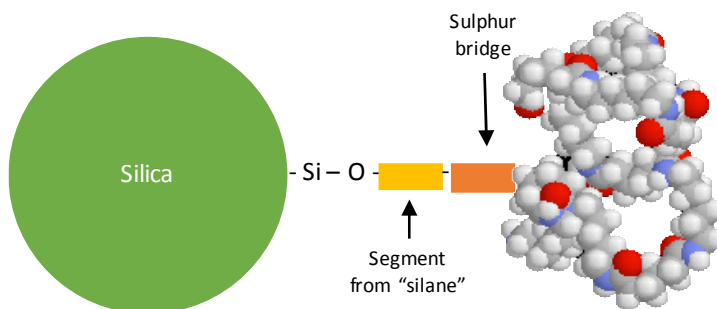


**Figure 1.8:** General approach for silica surface modification by silane coupling agents

This problem has been solved by functionalizing  $\text{SiO}_2$  particles with coupling agents, which favor the generation of bonding interactions at the interface between filler and polymer<sup>1,2,14,15</sup>.

Among them, bifunctional organic silanes are commonly utilized as coupling agents in silica-rubber nanocomposites for tires application. A scheme of the silica functionalization with silanes is reported in Figure 1.8<sup>1,7-9,55-59</sup>.

Our group<sup>14,15,37</sup> investigated and rationalized the effects induced by different functional groups of silane on the properties of rubber composites. In detail, we have examined both the morphology and the mechanical behavior of silica–natural rubber nanocomposites, obtained by in rubber sol–gel synthesis of silica NPs functionalized with trialkoxysilane having different functional groups.

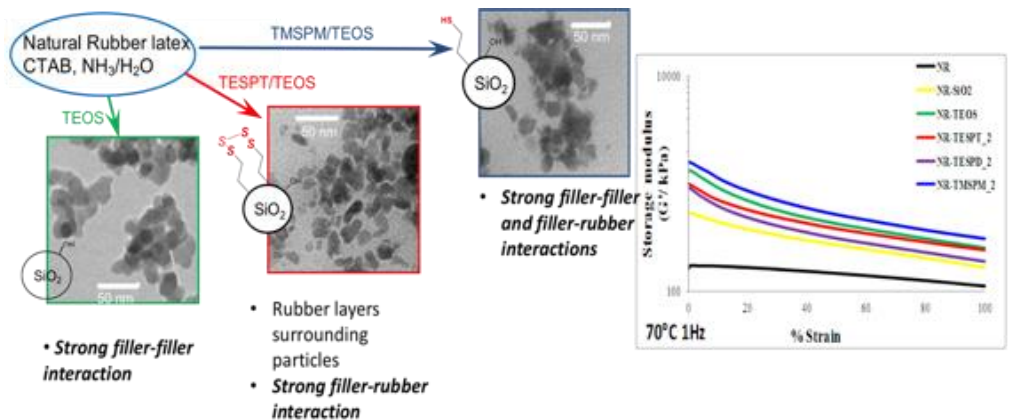


**Figure 1.9:** Effect of silica surface functionalization on the mechanical properties of natural rubber nanocomposites

These functionalities were selected among those which are suitable to promote the formation of differently shaped silica particles or to modulate the filler–filler and the filler–rubber interactions (Fig 1.9).

The results showed that the filler–rubber interaction due to substituents which chemically interact with the polymer, promotes the homogeneous distribution of the silica particles in the matrix, while the filler–filler interaction, favored by the shape induced physical interactions or by the chemical interaction among surface groups, mainly contribute to the filler networking and to the dynamic-mechanical properties of the composites.

This study demonstrated that the silica surface functionalization with suitable silane coupling agents plays a key role in tuning the filler-filler and the filler-rubber interactions, improving the functional properties of rubber nanocomposites.

Moreover, we have recently reported<sup>16,17</sup> a systematic discussion of the behavior of rubber composites in relation to the different shapes of silica NPs. In particular, shape controlled spherical and rod-like silica NPs with different aspect ratios (1–10) have been synthesized by a sol–gel method. NPs were used to prepare silica/SBR composites by blending method. The results revealed that particle anisotropy and alignment can provide, beside an increase of the filler-filler interactions, high percentage of immobilized rubber at the filler/ rubber interface, leading to a higher degree of reinforcement (Fig 1.10).

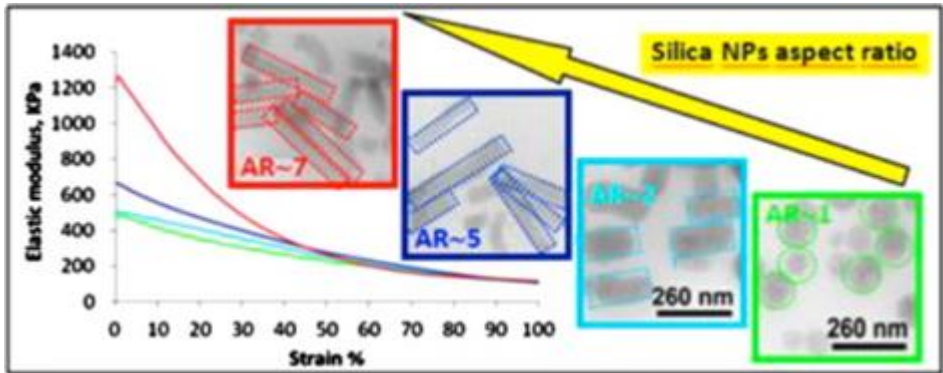


**Figure 1.10** Effect of Silica NPs with different aspect ratio on the reinforcement. Reprinted with permission from [16].

Copyright 2014, Elsevier

This strong interaction originates a significant reinforcement even if the anisotropic particle form a network less continuous than in samples containing spherical or near spherical particles.

These results confirm the possibility of tuning the formation of the filler network not only with the filler functionalization but also improving the filler-rubber interaction by using anisotropic fillers<sup>16,17</sup>.

In summary, the optimization of the filler morphology, including shape and specific surface area, surface chemistry, interfacial interactions with the polymer (filler-rubber interactions) or between the filler particles (filler-filler interactions) play a crucial role in determining the mechanical properties of the composites.

These outcomes suggest that the utilization of new fillers with tailored structure and functionalities able to simultaneously enhance the filler networking and the filler-rubber interaction, increasing the amount of

immobilized rubber, may to be a promising approach to effectively improve the mechanical properties of the composite and limit the silica amount in compounding.

In this context, emerging nanofillers which seems to be suitable candidates in this context are Polysilsesquioxanes<sup>38-43</sup>. Little is known about their effects in rubber nanocomposites for the tire applications.

However, great potentialities are expected, as witnessed by some recent researches.

### **1.5 Polysilsesquioxanes**

Polysilsesquioxanes (PSQs), constituted by the basic repeating unit of  $[\text{RSiO}_{1.5}]_n$ , represent a unique family of organic–inorganic hybrid materials which exhibit or impart, if included in composites, a number of beneficial properties, e.g. excellent thermal stability, low dielectric constant, good mechanical properties, chemical resistance, and even biocompatibility. These materials can assume many structural forms and serve manifold applications, due to the interaction of the siloxane bond networks with organic constituents. Three main classes of PSQs are generally reported: random branched sols, polyhedral oligomeric silsesquioxanes (POSS), and ladder-like (LPSQs) polysilsesquioxanes (Fig 1.12).

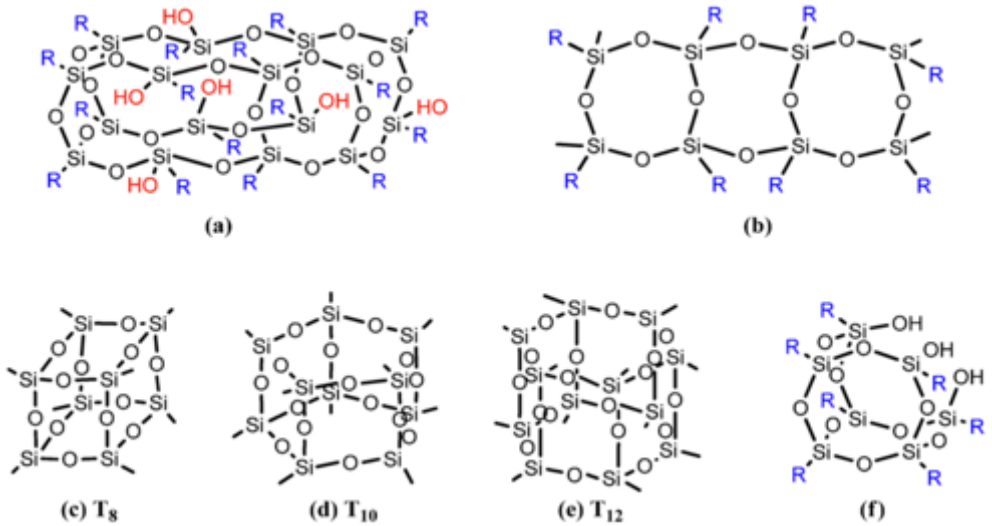


**Figure 1.11:** PSQs with different structures: a) random, b) ladder-like, c-e) cage with  $n = 8, 10, 12$ , f) open-cage

Reprinted with permission from [42]. Copyright 2011, Elsevier

### 1.5.1 Polyhedral Oligomeric Silsesquioxanes with cage structure

Generally, Polyhedral Oligomeric Silsesquioxanes correspond to cage structures of common formula  $(\text{RSiO}_{1.5})_n$ , with  $n$  ranging from 6 to 18 where  $R$  may be a hydrogen atom or an organic functional group, e.g., alkyl, alkylene, acrylate, hydroxyl or epoxide unit. POSS consists of both organic and inorganic matter with an inner core of inorganic silicon and oxygen and an outer layer of organic constituents, which could be either polar or nonpolar. POSS can be divided into molecular silica, monofunctional POSS and multifunctional POSS. When all the organic groups are non-reactive, they are labelled as molecular silica. If one of the organic groups is reactive, these POSS are called monofunctional

POSS or MonoPOSS. If more than one of the organic groups is reactive, they are known as multifunctional POSS.

The number of silicon atoms on each POSS molecules, which is usually 8, is not the only parameter characterizing the different POSS compounds. In fact, one of the most important features is the type of organic groups R which the POSS molecules bear. In Figure 1.12 are presented the most general chemical structure of a 8 silicon - POSS cubic cage.

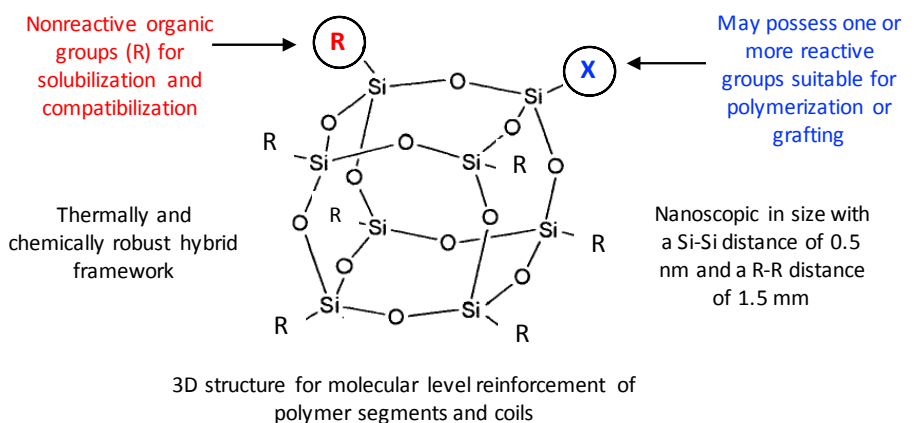


**Figure 1.12:** Structure and Properties of cage-like POSS

**R** generally indicates unreactive organic functionalities for solubilization and compatibilization of the POSS molecules with organic media, while **X** indicates reactive groups for grafting polymerization. These can be tailored with the synthetic chemistry tools, and nowadays a very wide array of chemical groups can be bonded to the inorganic core, both as **R** and as **X**, thus giving rise to the possibility of using the POSS in the most part of the polymeric systems. For example **R** can be

a cyclohexyl, cyclopentyl, phenyl or a methyl, while **X** can present a vinyl, a methacrylate or an epoxy ring and so on<sup>38-47</sup>.

### **1.5.2 Ladder-like polysilsesquioxanes**

Ladder-like polysilsesquioxanes (LPSQ), which are formed by inorganic double-chained backbone, have attracted considerable interest because they possess excellent thermo-resistant and mechanical properties, as do POSS. As already discussed, in nanocomposites the enhancement of properties depends largely on the shape and distribution of the nanofiller. Hence, tunable aspect ratio in LPSQs backbone, as well as enhanced mechanical properties and thermal stability compared to usual linear polysiloxane make ladder-like polysilsesquioxanes very strong competitors to POSS in nanocomposites applications.

Synthesis of ladder-structured polysilsesquioxanes was first reported in 1960 by Brown et al<sup>48</sup>. using a phenyltrichlorosilane monomer in the presence of potassium hydroxide (KOH) catalyst at high temperatures (~200 °C). While polymeric, highly condensed siloxane structures may have been obtained by Brown, the highly reactive trichlorosilanes used for hydrolysis and polycondensation most probably did not lead to linear siloxane structures as hinted by the broad <sup>29</sup>Si NMR peaks. As such, the structural feasibility of the obtained products by Brown has been widely debated. Most recently, Choi et al<sup>49-52</sup>, reinvestigated the synthetic feasibility of LPSQs by a facile synthetic method utilizing less reactive phenyltrimethoxysilane (PTMS) monomer coupled with a mild

base catalyst,  $K_2CO_3$ , in water/THF mixture solvent at room temperature to give either the preferential formation of Phenyl-POSS or ladderlike structured polyphenylsilsesquioxane (LPPSQ) depending on the initial concentrations of PTMS .

Changing the molecular precursor could be also possible to obtain cage or ladder PSQs with desired organic functions, lack of uncondensed silanols and tunable structural regularity. In this context, in 2001, Lee et al.<sup>53</sup> synthesized a novel high molecular weight ladder-like structured poly(methacryloxypropyl)silsesquioxane (LPMASQ) by using a in-situ polymerization of 3-(trimethoxysilyl)propyl methacrylate as silane precursor (Fig 1.13). The fully condensed LPMASQ revealed good thermal stability, good solubility in solvents with different polarities, and strong acid- resistance. A very low content of LPMASQ (2 wt%) was able to fully solidify an electrolyte solution to yield homogeneous gels with high ionic conductivity and stable wide electrochemical window.

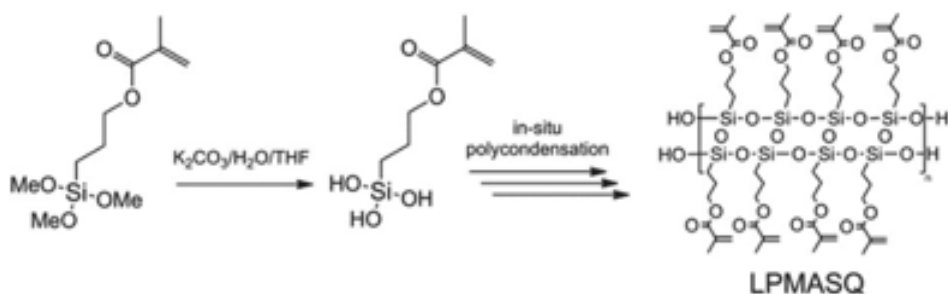


**Figure 1.13:** Syntheses of LPMASQ

Reprinted with permission from [53].

Copyright 2013 Royal Society of Chemistry

To sum up, these materials exhibited excellent physical and mechanical properties (e.g. high modulus, hardness) strongly dependent on the organic functional groups, as well facile synthetic procedure and high yields. For these reason, they may be used as novel nanofiller for industrial application in next generation of rubber nanocomposites.

## **1.6 PSQs-Polymer Nanocomposites: background and challenges**

The incorporation of PSQs into a polymeric material may result in dramatic improvements in the polymer's properties including greater temperature and oxidation resistance, surface hardening, and reduction in flammability. Therefore, research in PSQs-related polymers and copolymers has accelerated in recent years.

The properties of PSQs-containing polymer composites depend on the successful incorporation of PSQs particles in polymeric matrices. Two main approaches have been adopted to incorporate PSQs particles into polymer matrices: (i) *chemical cross-linking* and (ii) *physical blending*.

In the first approach, PSQs are bonded covalently with polymer, while in the second they are physically blended in the matrix by melt mixing or solvent casting methods<sup>38-47</sup>

Commonly, the first approach is widely utilized and POSS have been exploited as versatile nano-building blocks which, chemically bonded to the polymeric backbones through "grafting from" "grafting onto" or via (co)polymerization, act basically as cross-linking agents among the polymer chains (Fig 1.14).

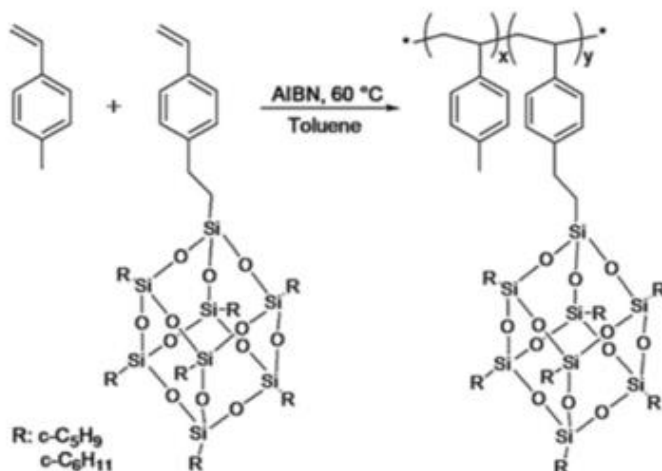


**Figure 1.14:** Polymerization of PS–POSS copolymers

Reprinted with permission from [42]. Copyright 2011, Elsevier

For instance, the in-situ copolymerization of POSS to produce hybrid organic–inorganic polymers with pendant POSS groups has been widely studied for both thermoplastics and thermosets, showing frequently improved thermal stability and physical properties. Haddan et al<sup>54,55</sup> prepared linear thermoplastic hybrid materials containing an organic PS backbone and large inorganic silsesquioxane groups pendant to the polymer backbone have been prepared through free radical copolymerization. The pendant inorganic groups drastically modify the thermal properties of the PS, interchain and/or intrachain POSS–POSS interactions affect the solubility and thermal properties.

Recently Matejka et al<sup>56</sup>, prepared rubbery epoxy-POSS hybrid composites by incorporating a novel diepoxy-POSS monomer in an epoxy network and then initiating the polymerization. By monitoring the hybrid formation by in-situ SAXS, they revealed that POSS units

self-assemble to form crystalline lamellae in the epoxy matrix, which serve as network physical junctions and severely restrict the polymer chains mobility, inducing a pronounced reinforcement compared to the neat polymer.

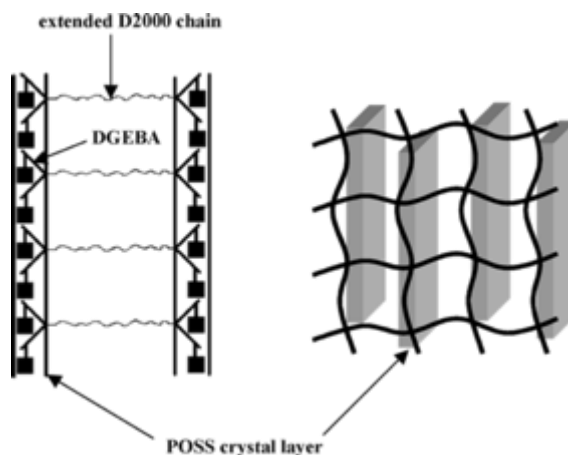


**Figure 1.15:** Organization of POSS nanounits In the epoxy matrix

Reprinted with permission from [56]. Copyright 2014, ACS Publications

They suggested that not only the loading of the nanofiller, but also the organization of the POSS nanounits in the polymer is fundamental for the nanocomposites performance. In fact, the structure of the studied networks was governed mainly by the POSS–POSS interaction within the organic matrix and it was controlled by the nature of the substituents of the POSS unit and by the topological location of the POSS in the network (Fig 1.15).

Similar results were obtained also with ladder-like polysilsesquioxanes. Recently Cho et al<sup>57</sup>, prepared a highly compatible inorganic-organic hybrid PVDF/UV-Curable polysilsesquioxane composites. The polysilsesquioxane (LPMASQ, cfr. 1.5.2) contained both phenyl and

methacryl groups which promoted hydrogen-bonding with the PVDF backbone and enhanced mechanical robustness after UV-curing (Fig. 1.16).

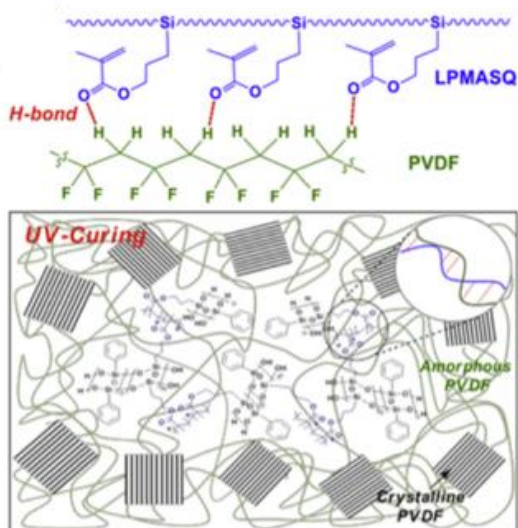


**Figure 1.16:** Schematic depiction of the hydrogen interaction between PVDF and LPMASQ and the formation of PVDF-LPMASQ composite  
Reprinted with permission from [57]. Copyright 2015, Elsevier

Many other studies<sup>58</sup> demonstrated the improved properties of polymer-PSQs hybrid nanocomposites by exploiting the covalent bonding between POSS or ladder-like PSQs functional groups and monomer/polymer chains.

However, these procedures often involve time-consuming syntheses, which restrict the large scale utilization and commercialization of the resulting composites, such as in tires applications.

Instead, in recent years, the possibility of preparing PSQs–polymer systems by *physical-blending* (i.e. *melt-blending*, *reactive-blending*, *mechanical blending*) have attracted great attention, and represents an appealing, cost-effective and environmentally friendly alternative for industrial development of hybrid nanocomposites with tailored properties<sup>104,105</sup>. Since the proper exploitation of the intrinsic PSQ properties is achieved only when these units are dispersed at molecular level or in nanosized clusters in the polymer, the key point of *physical-blending* lies in promoting the chemical–physical interaction between PSQ and matrix, by tuning the nature and chemical structure of the organic groups covalently attached to the Si–O framework<sup>59-62</sup>.

As concerns POSS nanounits, they are essentially utilized for the improvement of thermal, mechanical and functional properties of thermoplastic polymers (e.g. polyolefines, polyesters, polyamides, polycarbonates, PMMA and PS) and only few studies have been devoted to the inclusion of these nanounits in elastomeric composites commonly utilized in automotive industry.

In this context, Tanaka et al.<sup>63</sup>, described the mechanical properties of polymer composites based on polystyrene, poly(methyl methacrylate), ethylene-(vinyl acetate) incorporating POSS fillers with different structure and functionalities by melt mixing.

Results evidenced that unsaturated bonds at the side chains in POSS units favor an improvement of the thermal stability and the elasticity of polymer matrix (Fig. 1.17), thus suggesting the possibility to design effective POSS filled nanocomposites.

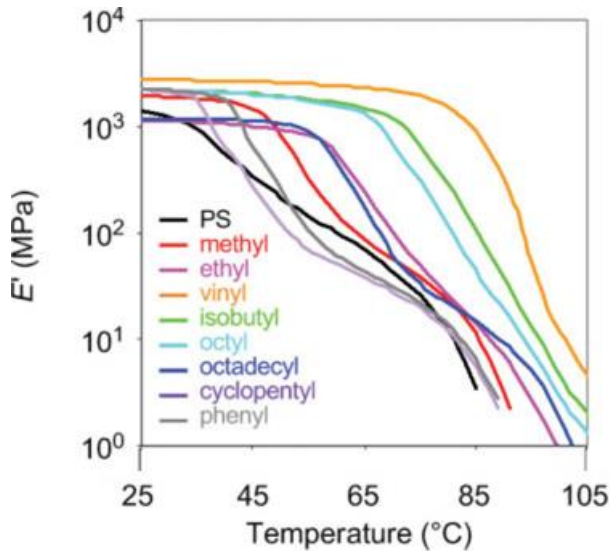


**Figure 1.17:** Dynamic mechanical curves of PS composites containing 5 wt. % of POSS fillers with different functional groups.

Reprinted with permission from [63]. Copyright 2009, Wiley

More recently, Frone et al.<sup>64</sup> have investigated the influence of both structure and concentration of POSS on the morphological, thermal and mechanical characteristics of polyethylene (PE)-based nanocomposites enclosing POSS nanounits with linear and branched substituents prepared by a melt mixing method. Beyond an increased thermal stability, the mechanical characterization of the composites showed significant improvement of tensile strength and elongation as compared to neat PE, which were more pronounced for nanocomposite containing branched POSS molecules, highlighting the influence of the molecular structure of polysilsesquioxanes on the final properties.

However, during blending, strong self-interaction between POSS cages often occurs, leading to aggregation, phase separation, and in turn to properties comparable or even worse than more conventionally filled polymers<sup>38,39</sup>.

This makes the use of POSS unjustified, due to their high cost., especially for large scale applications, like rubber nanocomposites utilized for tires

To face with this challenge, Kosmalka et al<sup>65</sup>. tried to improve the mechanical properties of butadiene-acrylonitrile rubber (HNBR) by using low percentage (2-10 wt. %) of POSS in the presence of a conventional filler, silica NPs (30 wt.%). They found that, after curing, the inclusion of POSS containing unsaturated reactive functionalities via ex-situ blending (i.e. vinylisobutyl, octavinyl, methacryloisobutyl and octamethacryl) increases the crosslink density and the aging resistance of the elastomeric matrix, and induces an enhancement of the mechanical properties with respect to reference nanoscaled silica. Thus mixing POSS with SiO<sub>2</sub> seems to be a promising approach. However, their synergistic effect could be compromised by poor control on either the action or the location/distribution of POSS units in the rubber matrix.

These issues prompted us to explore the possibility of benefit of both the POSS cross-linking action and the reinforcement mainly governed by silica, by utilizing SiO<sub>2</sub>-POSS “hybrid” systems, where silica NPs and POSS are not simply mixed together, but belong to the same functional structure.

In this context, several attempts have been recently carried out to obtain silica-POSS functional materials<sup>66,67</sup>. Recently Jesionowski et al.<sup>68,69</sup> proposed a method for preparing a SiO<sub>2</sub>/Silane/POSS hybrid filler by a new double-step functionalization method.

However, the mechanism proposed for the functionalization with POSS appears rather unclear and not convincing evidences about the anchoring of the nanocages onto the oxide surface have been provided. Moreover, despite all the above cited endeavours, there is hardly any investigation which reports on the synthesis and application of SiO<sub>2</sub>-POSS hybrids as functional nanofillers for rubber composites for tires application.

For this reason a new hybrid SiO<sub>2</sub>-POSS nanofiller, named SiO<sub>2</sub>@POSS, has been here developed. SiO<sub>2</sub>@POSS has been synthesized by silanization of commercial SiO<sub>2</sub> with methacrylsilane and successive grafting of small loadings of POSS via a surface reaction assisted by dicumylperoxide (DCP). The amount of peroxide was tailored in order to allow both the anchoring of the nanocages on the silica surface, under activation of the methacrylate groups<sup>70</sup> of silane and POSS units, and the preservation in the final hybrid structure of unreacted methacryl functionalities, still available for the interaction with the polymer host.

SiO<sub>2</sub>@POSS hybrid NPs were used to prepare by *ex-situ* blending styrene butadiene rubber (SBR) nanocomposites. The morphological and mechanical properties of SBR/SiO<sub>2</sub>@POSS nanocomposites, both uncured and cured by DCP, were investigated in detail and compared to those of nanocomposites obtained by physical mixing of SiO<sub>2</sub>,

methacrylsilane and OctaMethacrylPOSS in the polymer matrix. This allowed to outline connections among the peculiar hybrid structure of the novel filler, its efficacy in providing stronger interaction with rubber, and the enhancement of the mechanical properties.

Regarding ladder-like PSQs (LPSQs), though a lot of studies focused on the tailoring of their structure and functionalities, to the best of our knowledge no work has been reported on their application in rubber composites.

In fact, LPSQs containing reactive groups are mainly used as fillers in polymer composites applied in high-performance protecting coating, thermostable material, integrated circuit, semiconductor devices and for hybrid polymer electrolytes for lithium ion batteries<sup>50-53</sup>.

Thus, it seems to us very innovative exploring the possibility to produce rubber nanocomposites enclosing LPSQs bearing specific and fixed functional groups, and with tunable molecular structure. This may allow to gather useful information about the influence of LPSQs on polymer chains mobility and mechanical properties.

However, as mentioned above (see section 1.5.2) the preparation of such systems is usually a delicate process, which requires a strict control and understanding of synthetic details in order to avoid possible side reactions (cross-linking, cyclization and gelation).

In this context, Dirè et al.<sup>71,72</sup> have recently reported a relatively simple synthesis of thiol-functionalized PSQs (SH-NBBs) with tunable POSS-like or LPSQ-like structure, by using an in-situ water production (ISWP) sol-gel strategy. These species may represent therefore suitable

candidates for the preparation of rubber nanocomposites with defined properties.

In order to substantiate this possibility, low loadings of SH-NBBs with different molecular structure, have been incorporated in polybutadiene (PB) by a simple and rapid *solution-blending* (swelling) technique.

A comprehensive investigation of the interactions between SH-NBBs units and polymer host has been performed by solid-state NMR spectroscopy, focusing on the effects of loading and architecture on the molecular structure and mobility of the polymeric chains.

## **1.7 Aim of the thesis**

The principal aim of the present work is to investigate the effect of PSQs with different structure and functionalities as innovative nanofillers on the dynamic-mechanical behaviour of rubber nanocomposites (StyreneButadieneRubber and PolyButadiene) potentially relevant for tires application.

The activity has been divided into two main parts:

1. Effect of POSS cage nanostructures with highly reactive groups as innovative filler on the mechanical properties of SBR nanocomposites;
2. Effect of SH-functionalized silsequioxanes (SH-NBBs) with tunable and controlled ladder and cage structures as filler in PB-nanocomposites.

In detail, the first part of the work has been dedicated on:

- Synthesis and characterization of the novel “hybrid” SiO<sub>2</sub>@POSS nanofiller;
- Incorporation in styrene butadiene rubber (SBR) by *ex-situ blending* of SiO<sub>2</sub>@POSS hybrid NPs and complete structural and morphological characterization of both uncured and cured nanocomposites;
- Investigation of the filler-polymer interactions by spectroscopic and microscopic examination of rigidity of the polymer layers in contact with the filler;

- Comprehensive Investigation of the mechanical, thermal and rheological properties of the SBR/SiO<sub>2</sub>@POSS nanocomposites comparing to those of nanocomposites obtained by simple addition of mixtures of SiO<sub>2</sub> and OctaMethacrylPOSS in the polymer matrix.

Concerning on the SH-functionalized silsesquioxanes (SH-NBBs), the activity has been directed toward the:

- Synthesis of SH-functionalized silsesquioxanes (SH-NBBs) (in collaboration with the group of Prof. Dirè of University of Trento);
- Incorporation in PolyButadiene rubber by *in-situ blending* of SH-NBBs with different cage/ladder ratios;
- Comprehensive investigation on the interactions between SH-NBBs units and polymer host by solid-state NMR spectroscopy, focusing on the effects of loading and architecture on the molecular structure and mobility of the polymeric chains



## **Chapter 2**

# **Fundamentals of rubber compounding**

Chapter 2 illustrates the types and the characteristics of rubbers, fillers, vulcanization ingredients and the others chemicals used for the preparation of the nanocomposites.

## 2.1 Formulation of rubber compounds

The heart of the rubber compounding is the formulation, usually referred in the industry as a recipe. A generalized rubber formula is given in Table 2.1<sup>73</sup>.

**Table 2.1:** General tire formulation

<i>Ingredient</i>	<i>phr</i>
Crude rubber	100
Filler	50
Softener	5
Antioxidant	1
Stearic acid	1
Zinc oxide	5
Accelerator	1
Sulphur	2
<i>Total</i>	<i>165</i>

Rubber compounds are generally based on only one rubber or on a blend of two or more raw rubbers to achieve the best balance properties. The total of the crude rubber in a given recipe is generally defined as 100 parts. All other non-rubber ingredients are rationed against the 100 parts of rubber (phr).

Each ingredient has a specific function, either in processing, vulcanization or end use of the product. The various ingredients may

be classified according to their specific function in the following groups:

fillers (carbon blacks and non-black fillers); plasticizers and softeners (extenders, processing aids, special plasticizers); age resistors or antidegradants (antioxidants, antiozonants, special age resistors, protective waxes); vulcanizing and curing ingredients (vulcanizing agents, accelerators, activators); special-purpose ingredients (colouring pigments, blowing agents, flame retardants, odorants, antistatic agents, retarders).

However, many ingredients are capable of acting in more than one manner<sup>1,6,73,74</sup> (Fig 2.1).



**Figure 2.1:** Ingredients commonly used in tire industry

## 2.2 Rubbers

Crude rubbers are typically categorized as amorphous polymers with very high molecular weight ( $M_n > 100,000$ ), having a random-coil arrangement. They can be cross-linked to form a tridimensional network. Whose glass transition temperature is sub-ambient and, amongst other properties, rubbers have the ability to be extensively and on release of stress, return to their original length.

The main characteristics of elastomers, which make these materials essential in several industrial sectors, are their elasticity, flexibility, and toughness. Beyond these common features, each rubber has its own unique properties. Although the processing and final properties of rubber articles are highly dependent on the base elastomer, the properties can be extensively manipulated by appropriate choice of compounding ingredients.

Rubbers can be divided in two main types: natural and synthetic. Natural rubber (NR) belongs to the first group, it is known also as cis-1,4 polyisoprene and is produced from the latex of a large variety of plants in many regions of the world. However, the most widely exploited commercial source of NR is the *Hevea brasiliensis* tree. Natural rubber latex is a colloid where the dispersed phase is mainly rubber and the dispersion medium is water. In addition, latex contains small quantities of proteins, resins including fats, fatty acids, other lipids, sterol and sterol esters, carbohydrates and mineral matter <sup>1,6</sup>.

The second group constituted by synthetic rubbers is very broad so only some kinds of elastomers will be introduced subsequently.

The first to be mentioned is synthetic polyisoprene rubber (IR) which, depending on the polymerization conditions, can exist as different isomeric forms. 1,4-IR can exist in *cis* or *trans* forms depending on the orientation of the substituents across the enchainment double bond.

These isomers are the most important while the other forms, 1,2-IR and 3,4- IR, are of less importance. After vulcanization, polyisoprene shows aging properties and resistance to chemicals similar to those of natural rubber, while the physical properties are not as good as those of NR.

Other general-purpose elastomers, such as NR and IR, are styrene-butadiene rubber (SBR) and butadiene rubber (BR).

SBR denotes a copolymer of styrene and butadiene, typically containing about 23% styrene. It does not develop high tensile strengths without the aid of reinforcing fillers. The tread-wear and heat-ageing properties of SBR are superior to those of NR, but the resilience and low-temperature behavior are inferior. This kind of rubber is generally used in many applications, particularly the principal end uses are passenger car tires (45% of the worldwide capacity), truck and bus tires (9%), retread tires (16%), other automotive (6%) and mechanical goods (16%)<sup>1,6</sup>.

## **2.3 Fillers**

Fillers are compounding ingredients, usually in powder form, added to crude rubber in large proportions (typically 30 phr). They can be classified in two major groups: carbon black and non-black fillers.

Carbon black consists essentially of elemental carbon in the form of near-spherical particles coalesced in aggregates of colloidal size, obtained by incomplete combustion or thermal decomposition of hydrocarbons. The carbon black grades differ from one another regarding their particle size, aggregate form and shape.

A wide variety of non-black fillers for rubbers exists. Today, the principal non-black fillers are silicas and calcium carbonates. Other major fillers are mica, talc, zinc oxide, magnesium carbonate, magnesium oxide, titanium oxide, barites and many others. Short fibres of aramid, carbon, glass, nylon or polyester, are also widely used in rubber compounds.

Fillers are added for purposes either economical or technical. Some are incorporated in the polymer matrix as extenders and therefore in order to make the final product less expensive. Others act mainly as reinforcing agent. Consequently, fillers may be also classified into two categories: reinforcing and non-reinforcing.

## **2.4 Antidegradants**

Elastomer-based products suffer irreversible changes to their required design properties during service. In particular, a loss in mechanical properties and alterations in surface aspect can occur.

These changes, brought about by a number of agents such as oxygen, ozone, heat, light, high energy radiation and high humidity, are collectively referred to as ageing.

In order to prevent these changes, additives (i.e. antidegradants or age resistors), are employed with typical loading levels in the range of 1- 4 phr.

The most common antidegradants are the antioxidants, which protect the elastomer against oxidation, and the antiozonants, which retard or hinder the appearance of surface cracks caused by ozone. Age resistors may be divided into two main groups: staining and non-staining. While the former are strong protective agents but discolour and stain to various degree, the latter are less effective but can be used in white and coloured rubber compounds <sup>73,74</sup>.

## 2.5 Vulcanizing ingredients

### 2.5.1 Vulcanization with sulfur

Vulcanization is a chemical process discovered by Charles Goodyear in 1839 for converting natural rubber or related polymers into more durable materials via the addition of sulfur or other equivalent curatives and accelerators. Vulcanized materials are less sticky and have superior mechanical properties.

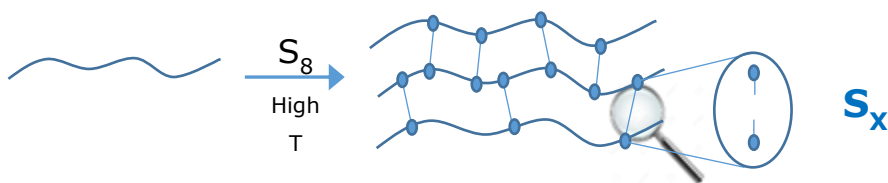


**Figure 2.2:** Vulcanization process

This process modifies the polymer by forming cross-links (bridges) between individual polymer chains. (Fig 2.2). However, the reaction of rubber with sulphur is slow even at high temperatures, in fact usually

requires several hours. In order to increase the rate of vulcanization, it is necessary to add accelerators and activators. By adding accelerators, the vulcanization time can be reduced to minutes or seconds and in most cases the physical properties of the final product are also improved <sup>1,6</sup>

Accelerators are classified as primary or secondary: the primary ones provide considerable scorch delay (i.e the time during which it is possible to manipulate the rubber composite before curing), medium fast curing, and good modulus development; the secondary are usually scorchy and provide very fast curing regime. There are a wide variety of accelerators (more than 100), hence they are classified as their generic chemical structure: class 1 sulfenamide (CBS), class 2 thiazole (MBT), class 3 guanidines, class 4 thiurams, class 5 dithiocarbamates and class 6 dithiophosphates. Inorganic and organic activators are used to activate the accelerators <sup>75,76</sup>. Zinc oxide is the most important inorganic activator. As reported by Heideman<sup>8</sup>, the addition of zinc oxide increases the vulcanization rate and the cross-linking efficiency. However, only the zinc oxide action is not enough to activate the vulcanization process<sup>77</sup>. In fact, ZnO is best used in combination with other organic activators able to increase the effectiveness of accelerators: fatty acids, although weak amines, guanidines, ureas, thioureas, amides, polyalcohols. The most important and popular type of organic activators is stearic acid <sup>78</sup>.

## 2.5.2 Vulcanization with Peroxide

Peroxides are capable of vulcanizing most polymer types, including standard unsaturated and saturated elastomer grades, fluoroelastomers and silicones. The use of coagents synergistically with peroxides helps to expand the utility of this vulcanization process<sup>79-82</sup>.

Peroxide vulcanization consists of a radical process initiated by peroxide decomposition that leads to the crosslinking of rubber. Peroxide vulcanization is typically used in rubber applications such as automotive, construction and building, wire and cable which require good ageing resistance, high processing temperature, good compression set at elevated temperature or colour stability<sup>79-83</sup>.

A wide range of peroxides for crosslinking of rubber is available on the market. Some of the typically used peroxides are shown in Figure 2.3.

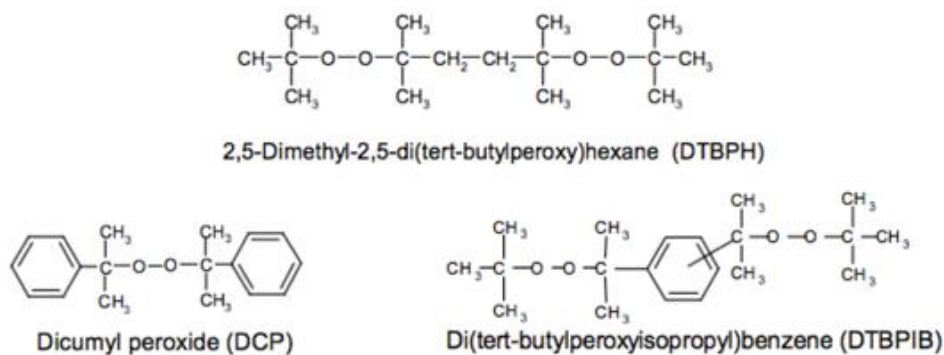


**Figure 2.3:** Structure of the typically peroxide used in the tire industry

Normally, for rubber vulcanization relatively stable peroxides are selected, since they should be stable at storage temperature and also at compounding temperature, which can be rather high. However, they should be labile enough to quickly yield the radical species at the

vulcanization temperature yet providing proper scorch safety. The reactivity of the peroxide is mainly determined by its molecular structure<sup>83</sup>.

A very important factor to consider in peroxide selection is the nature of the radicals formed by their decomposition. Depending on the reactivity of these radicals, subsequent rearranging reactions take place leading to new radical species. These are sometimes reactive but in other cases their reactivity is lower compared to the initial species, thus hindering the peroxide efficiency.

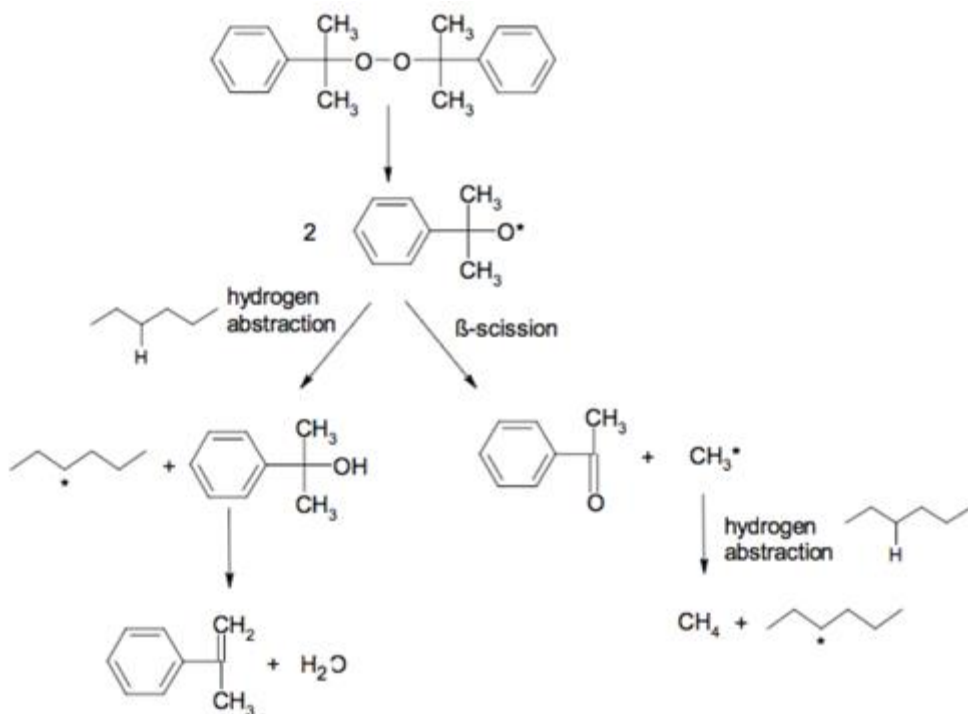


**Figure 2.4:** Vulcanization mechanism with dicumylperoxide (DCP)

For instance, when using DCP, one of the most used crosslinking peroxides<sup>84</sup>, its decomposition yields methyl radicals, (Fig 2.4). These

radicals are still very reactive and at the same time they are less sterically hindered than the initial cumyloxy radicals. Therefore, they will easily react further and provide good crosslink efficiency. The best radicals for peroxide crosslinking are those which are good abstractors, like for instance methyl and cumyloxy radicals, and poor in addition to double bonds.

As a result of peroxide vulcanization the crosslinks formed consist of carbon-carbon bonds between the polymer chains, while in Sulphur vulcanization the crosslinks between the chains consist of Sulphur bridges: carbon-Sulphur and Sulphur-Sulphur bonds. The carbon-carbon bond is more rigid and stable (351 kJ/mol bond energy) than the carbon-Sulphur (285 kJ/mol) and Sulphur-Sulphur (267 kJ/mol) bonds. This difference in network structure produces two vulcanization systems with different characteristic properties, since the lower the bond energy the easier the bonds break under influence of mechanical or thermal energy. This will reflect, for instance, in ageing properties: peroxide vulcanization has much better heat ageing characteristics than Sulphur cured elastomers, due to the fact that the carbon-carbon bonds are more stable than the Sulphur bridges <sup>84,85</sup>.



## **Chapter 3**

### **Experimental: Preparation of fillers and nanocomposites**

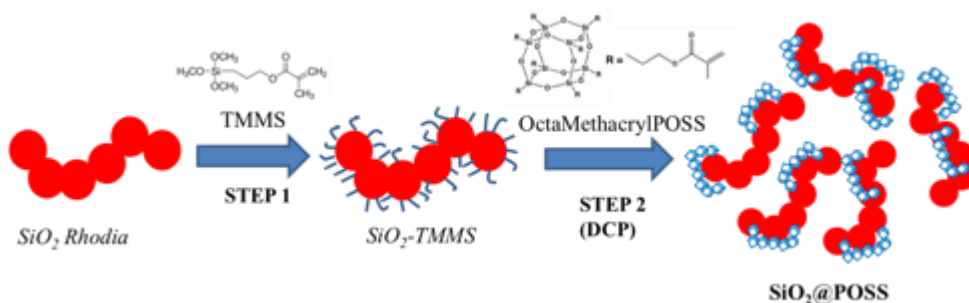
This Chapter is divided into two main parts. In the first part, the synthesis method for obtaining the novel SiO<sub>2</sub>@POSS hybrid filler is described as well as the preparation of the related SBR/SiO<sub>2</sub>@POSS nanocomposites. In the second part, the preparation of Thiol-Nano Building Blocks (SH-NBBs) and of PB/SH-NBBs nanocomposites are discussed.

### 3.1 Synthesis of SiO<sub>2</sub>@POSS hybrid filler

**Materials:** Silica Rhodia Zeosil MP 1165; OctaMethacrylPOSS (POSS) and MethacrylEthyl POSS (MonoPOSS) from Hybrid Plastics; 3-(Trimethoxysilyl)propylmethacrylate 98% (TMMS) and dicumylperoxide (DCP) from Sigma-Aldrich.

#### Experimental procedure

SiO<sub>2</sub>@POSS hybrid filler was prepared by the novel double-step functionalization procedure described in Scheme 3.1.



**Scheme 3.1:** Experimental procedure for the preparation of SiO<sub>2</sub>@POSS hybrid filler

In the first step (STEP 1), 3-(Trimethoxysilyl)propyl methacrylate (TMMS) was at first dispersed by ultrasound in a methanol/water solution (4/1 v/v) and then hydrolyzed at room temperature for 2 h in the presence of a suitable amount of SiO<sub>2</sub>. In a typical procedure, 15g of TMMS and 50g of SiO<sub>2</sub> were dispersed in 150ml of methanol/water solution (4/1 v/v).

After 2 h, the silane functionalized NPs (SiO<sub>2</sub>-TMMS) were washed with MeOH, collected by centrifugation and the powders were dried in oven at 60 °C for 12h.

This protocol affords about of 60g of SiO<sub>2</sub>-TMMS ready for the next step.

In STEP 2, 15g of SiO<sub>2</sub>-TMMS were suspended in toluene (150 mL) and then OctaMethacrylPOSS nanounits (3, 5 or 10 wt. % respect SiO<sub>2</sub>) were introduced in the solution. Successively, a suitable amount of DCP (2 wt. %, molar ratio POSS/DCP = 20/1) was added and the suspension was refluxed for 2h. The peroxide promotes the activation of the methacrylate groups of both silane and POSS units, favoring the anchoring of the nanocages onto the silica surface and their partial condensation to form, possibly, nanometric networks (see Scheme , STEP 2)<sup>70</sup>.

Finally, the obtained SiO<sub>2</sub>@POSS powders were filtered, washed several times with toluene and dried in oven at 120 °C in air for 12 h.

Hereafter the different SiO<sub>2</sub>@POSS fillers will be labeled as SiO<sub>2</sub>@POSS-X where X refers to the different loadings of MethacrylPOSS (X = 0, 3, 5 or 10 wt. %).

In order to better understand the action exerted by POSS reactive groups in SiO<sub>2</sub>@POSS hybrid filler in promoting the cross-linking, the networking and, in turn, the reinforcement, the same synthesis was performed using MethacrylEthyl POSS (10 wt. %) instead of OctaMethacrylPOSS. MethacrylEthyl POSS (Figure 3.1) possesses only one Methacryl group able to interact in principle with TMMS and seven unreactive Ethyl groups.

This hybrid filler will be labeled as SiO<sub>2</sub>@MonoPOSS-10, which indicates that that 10 wt. % of MethacrylEthylPOSS are nominally grafted onto silica.

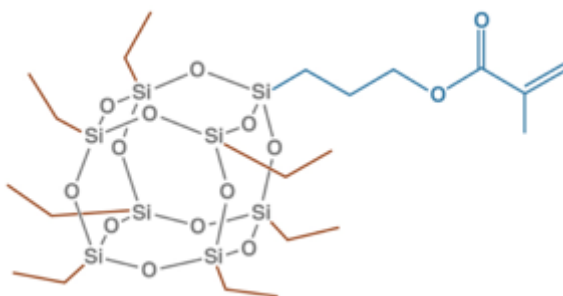


**Figure 3.1:** Structure of MethacrylEthyl POSS

## 3.2 Preparation of SBR nanocomposites

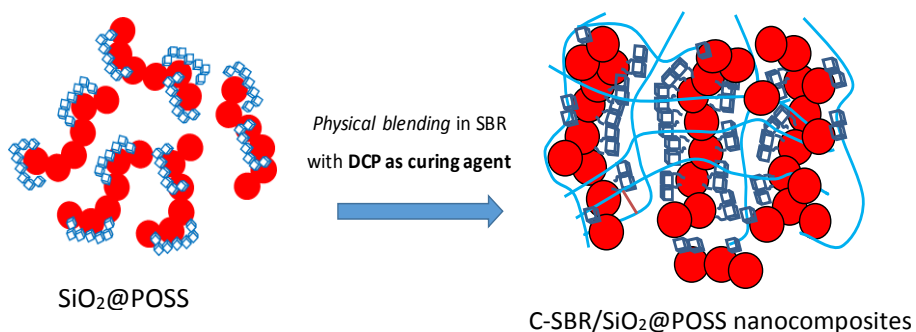
### 3.2.1 Preparation of SBR/SiO<sub>2</sub>@POSS and SBR/SiO<sub>2</sub>@MonoPOSS

**Materials:** SBR styrene butadiene rubber SLR 4630 from Styron Europe; SiO<sub>2</sub>-TMMS, SiO<sub>2</sub>@POSS and SiO<sub>2</sub>@MonoPOSS earlier synthesized, Silica Rhodia Zeosil MP 1165; OctaMethacrylPOSS (OctaPOSS) and MethacrylEthyl POSS (MonoPOSS) from Hybrid Plastics; 3-

(Trimethoxysilyl)propylmethacrylate 98% (TMMS) from Sigma Aldrich; *N*-(1,3-dimethylbutyl)-*N'*-phenyl-*p*-phenyldiamine Santoflex-6PPD from Flexsys was used as antioxidant; ZnO was from Zincol Ossidi; stearic acid Stearina TP8 from Undesa and dicumylperoxide (DCP) from Sigma Aldrich.

### Experimental procedure

In order to prepare uncured rubber nanocomposites, SiO<sub>2</sub>-TMMS and SiO<sub>2</sub>@POSS hybrid filler were mixed by ex-situ blending technique in an internal mixer with Styrene Butadiene rubber in a Brabender Plastimeter lab station (mixing chamber of 50 mL, filling factor of 0.7) following the procedure summarized in Scheme 3.2.



**Scheme 3.2:** Experimental procedure for the preparation of C-SBR/SiO<sub>2</sub>@POSS nanocomposites by ex-situ blending

The whole procedure is separated in three mixing steps at different temperature, according to the thermal stability of the ingredient: for example, silane coupling agents and silica fillers are mixed in the high temperature step, in order to obtain complete silica surface

functionalization, while curatives must be added in the low temperature step to avoid premature vulcanization. Two minutes after the last filler addition 6PPD, Zinc oxide and stearic acid were added; this lag time avoids secondary reaction between ZnO with silica silanols. The mixture was maintained in this mixing condition (145°C, 60 rpm) for 7 minutes.

In the second step, the material obtained in stage 1 is reloaded in the internal mixer operating at 90°C at 60 rpm. Dicumylperoxide was then added and mixed for 2 minutes. The mixture is finally processed in a two rolling mill as a third step at 50°C for 3 minutes to improve filler distribution in the sample. The amounts of compounding ingredients are listed in table 2.1 and expressed in phr (parts for hundred rubber); the silane amount depends on the silica amounts, while the loading of all the other ingredients is relative to rubber, i.e it the same for all the silica concentrations. Finally, composites were further molded in a two-roll mill for 2 minutes to produce sheets suitable for the vulcanization process.

In detail,  $32.0\text{g} \pm 0.5\text{phr}$  of SBR polymer was first introduced in the mixer and plasticized for 30 seconds at 60 RPM at 145°C, then the filler (33 phr  $\text{SiO}_2$ @POSS hybrid fillers or 30 phr  $\text{SiO}_2$ -TMMS) was introduced, mixed for about 4 minutes and then discharged.

Vulcanization chemicals were then added to the obtained composites in two further steps. Firstly, stearic acid (2 phr), zinc oxide (3.5 phr) and 6-PPD (2 phr) were mixed with the obtained composites at 60 rpm for 5 min at 145 °C. Successively, DCP (1.5 phr) was introduced at a working temperature of 90 °C and by mixing at 60 rpm for 3 min.

The ensuing composites were further milled for 2 min. in a two open roll-mill to produce sheets of about 0.5 cm thick, suitable for the vulcanization process. Curing profiles were measured with a Moving Die Rheometer (RPA 2000, Alpha Technological). The optimum curing was achieved under the following conditions:  $\pm 1^\circ$  oscillation angle, 170 °C temperature, and 10 min running time. However, since both the filler networking and distribution are related to the DCP during the curing process, SBR/SBR/SiO<sub>2</sub>@POSS nanocomposites have been cured also at 155°C and 185°C for 10 min. Hereafter, uncured nanocomposites are labelled as SBR/SiO<sub>2</sub>@POSS-X, where X refers to the different amounts of OctaMethacrylPOSS (X = 0, 3, 5, or 10 wt. %); accordingly, SBR/SiO<sub>2</sub>@POSS-0 corresponds to a composite containing exclusively SiO<sub>2</sub> (30 phr) functionalized with TMMS (i.e. SiO<sub>2</sub>-TMMS NPs). The different cured nanocomposites are analogously labelled as C-SBR/SiO<sub>2</sub>@POSS-X\_Y, where Y indicates the curing temperature (Y = 155, 170 and 185°C).

SiO<sub>2</sub>@MonoPOSS hybrid nanofiller was used to prepare C-SBR/SiO<sub>2</sub>@MonoPOSS nanocomposites by using the same procedure and chemicals reported above (Scheme 3.2). The MonoPOSS is constituted by only one reactive group (Methacryl), while the other seven functionalities are basically poorly reactive (i.e alkyl groups). After grafting onto SiO<sub>2</sub>-TMMS by condensation between the methacryl group of silane and that of the MonoPOSS, no more functional groups should be available in SiO<sub>2</sub>@MonoPOSS for POSS-POSS interaction or reaction with the polymer. Therefore, after curing,

this hybrid system could be useful for a deeper understanding of the effect of Methacryl POSS functionalities on the mechanical properties of the SBR/SiO<sub>2</sub>@POSS nanocomposites. The MonoPOSS cured nanocomposite is labelled as C-SBR/SiO<sub>2</sub>@MonoPOSS.

**Table 3.1:** Compounding ingredients for SBR/SiO<sub>2</sub>@POSS-X and SBR/SiO<sub>2</sub>+POSS-X nanocomposites

Ingredients	SBR/SiO <sub>2</sub> @POSS-X (%)	SBR/SiO <sub>2</sub> +POSS-X (phr)
Styrene Butadiene Rubber	100	100
SiO <sub>2</sub> Rhodia	-	30
SiO <sub>2</sub> -TMMS	30	-
SiO <sub>2</sub> @POSS hybrid filler	33	-
SiO <sub>2</sub> @MonoPOSS hybrid filler	33	-
TMMS	-	0,96/2
OctaMethacryl POSS	-	0-3-5-10
6PPD	1	1
ZnO	2,7	2,7
Stearic Acid	0,85	0,85
DCP	2	2

### 3.2.2 Preparation of SBR/SiO<sub>2</sub>+POSS and SBR/SiO<sub>2</sub>+MonoPOSS

In order to find a relation between the peculiar structure of the SiO<sub>2</sub>@POSS hybrid filler and the features of the resulting composites, the properties of SBR/SiO<sub>2</sub>@POSS-X, both uncured and cured, were compared to those of nanocomposites prepared by simply mixing SiO<sub>2</sub>, TMMS and OctaMethacrylPOSS (SBR/SiO<sub>2</sub>+POSS). In detail, the compounds were fed into the same polymer matrix under the same experimental conditions (i.e. curing chemicals, temperature, rotor speed) described above for SBR/SiO<sub>2</sub>@POSS.

Uncured and cured SBR/SiO<sub>2</sub>+POSS composites were prepared by blending SBR with a filler mixture composed by SiO<sub>2</sub> Rhodia (30 phr), TMMS coupling agent (2 phr) and different loading of MethacrylPOSS. These composites before or after curing were labelled as SBR/SiO<sub>2</sub>+POSS-X or C-SBR/SiO<sub>2</sub>+POSS-X\_Y, respectively. X refers to the different amounts of OctaMethacrylPOSS (X = 0, 3, 5, or 10 phr) while Y indicates the curing temperature (Y = 155, 170 and 185°C). C-SBR/SiO<sub>2</sub>+POSS-0 corresponds thus to a composite prepared by mixing only SiO<sub>2</sub> and TMMS at 170°C.

Finally, the same procedure was adopted for the preparation of SBR/SiO<sub>2</sub>+MonoPOSS and C-SBR/SiO<sub>2</sub>+MonoPOSS, by mixing SiO<sub>2</sub>, TMMS and 10 phr of MethacrylEthylPOSS (MonoPOSS).

### **3.3 Synthesis of Thiol Functionalized Nano Building Blocks (SH-NBBs)**

**Materials:** (3-Mercaptopropyl)trimethoxysilane (McPTMS) and dibutyltindilaurate (DBTL) were purchased from ABCR and used without any further purification. Chloroacetic acid (CIAA) and 1-propanol (PrOH), were purchased from Sigma Aldrich and used as received.

#### **Experimental procedure**

The preparation of the thiol-functionalized nanobuilding blocks (SH-NBBs) was performed by following the procedure reported by Dirè et al<sup>71,72,86</sup>, and described in Scheme 3.3. In detail, thiol-functionalized nanobuilding blocks were synthesized from 3-mercaptopropyltrimethoxysilane by using the in-situ water production (ISWP) process in which the water needed to hydrolyze the precursor was provided by an esterification reaction between 1-propanol and chloroacetic acid. The water provided through the esterification reaction of chloroacetic acid (CIAA) and 1-propanol enabled the hydrolysis-condensation of (3-Mercaptopropyl)trimethoxysilane (McPTMS). In detail, the synthesis was carried out under a nitrogen atmosphere using Schlenk technique. All the solvents were dried before use by following standard procedures. All the glassware used for reactions was dried in oven at 80 °C for 24 h prior to use. McPTMS (465  $\mu$ L, 2.5 mmol) was diluted in PrOH (3.36 mL) in a self-condensing Schlenk flask. CIAA (1.417 g) and

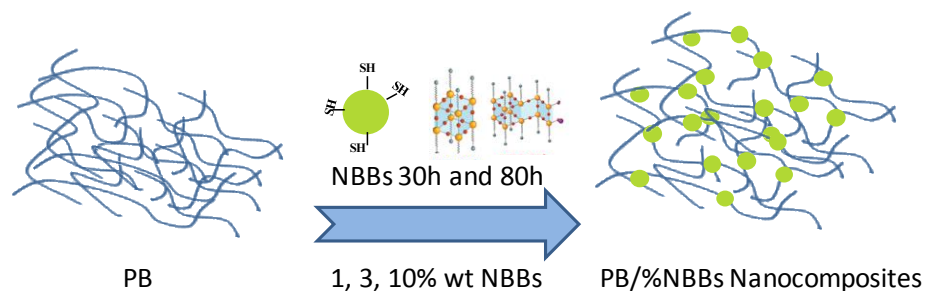


### 3.4 Preparation of PB/%NBBs Nanocomposites

**Materials:** Polybutadiene, cis average  $M_w$  200,000-300,000 and toluene were purchased from Sigma–Aldrich and used as received; SH-NBB\_30h and SH-NBB\_80h earlier synthesized.

#### Experimental procedure

SH-NBBs synthesized at different reaction times (30 and 80h) have been incorporated in swollen polybutadiene (PB) to produce nanocomposites, according to the procedure showed in Scheme 3.4.



**Scheme 3.4:** Experimental procedure for the preparation of PB/%NBBs nanocomposites

Pre-dried PB was swollen for 1 night in toluene. The resulting solutions were split into different flasks for the addition of different amounts of SH-NBBs solutions. In a typical procedure, 2g of PB was dissolved in 40 mL of anhydrous toluene. Then, different loadings of SH-NBBs (0,5, 1, 3, 10, 20 and 30 wt. %) were added to the swollen polymer and stirred for 2h under  $N_2$  flow. The obtained solution was cast in a Petri dish and

the volatiles were removed overnight by maintaining the system under an aspiration hood. Finally, the complete elimination of the by-products from the composites was achieved by heating the samples at 70°C for 1 hour under vacuum.

Hereafter the different nanocomposites will be labeled PB/Y%NBB\_Xh where Y refers to the different percentage of SH-NBBs (Y = 0,5, 1, 3, 10, 20 and 30 wt. %), while X denotes the different reaction times (Xh = 30 or 80h).



## Chapter 4

### Results: Morphological and physico-chemical characterization of fillers and related nanocomposites

In analogy with Chapter 3, this Chapter is divided into two main parts. In the first part, the spectroscopic and morphological characterization of the SiO<sub>2</sub>@POSS hybrid is discussed. Then, the morphology and the topography of the SBR/SiO<sub>2</sub>@POSS nanocomposites are investigated by SEM, TEM and AFM. Crosslinking density is obtained by swelling experiments while the rigidity of the polymer chains is evaluated by <sup>1</sup>H NMR. In the second part, after IR and NMR characterization of pure SH-NBBs, the efficacy of the SH-NBB functionalization with the polymer has been assessed by FT-IR and TGA. Finally, the filler-polymer interaction and the role of the SH-NBBs architecture was studied in detail with Solid State NMR and by swelling.

Technical information about all characterization methods are reported in the Appendix A1.

## **4.1 Spectroscopic and morphological characterization of the hybrid SiO<sub>2</sub>@POSS nanofiller**

### **4.1.1 FT-IR spectroscopy**

The efficacy of the silica functionalization with TMMS and, successively, with POSS nanounits was checked by FT-IR spectroscopy.

Figure 4.1 reports reports the comparison among the spectra of pure TMMS, bare SiO<sub>2</sub> and SiO<sub>2</sub>-TMMS.

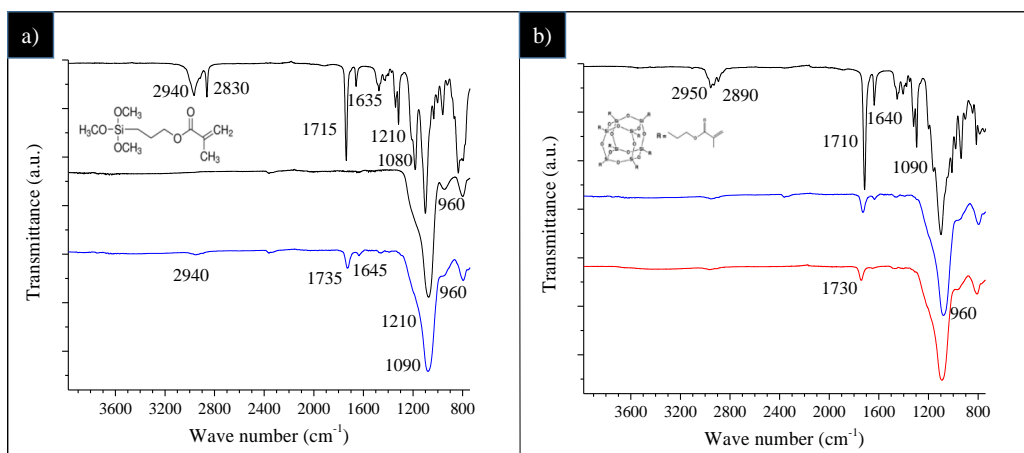


**Figure 4.1:** FT-IR spectra of: a) pristine TMMS (top, bold black line), SiO<sub>2</sub> (black line) and SiO<sub>2</sub>-TMMS (blue line); b) pure POSS (top, bold black line), SiO<sub>2</sub>-TMMS (blue line) and SiO<sub>2</sub>@POSS-10 (red line).

As reported in several previous studies<sup>87-89</sup>, the spectrum of TMMS shows the following main bands (Fig. 1a, bold black-line): the silane C–H stretching at 2940 and 2830 cm<sup>-1</sup>; the methylene C–H bending at 1454 cm<sup>-1</sup>; the –C–CO–O– skeletal vibration from the methacryloxy group at 1320 and 1210 cm<sup>-1</sup>; the band of  $\nu$  Si–O–C at 1080 cm<sup>-1</sup>; the intense carbonyl vibration of non-hydrolyzed TMMS at 1715 cm<sup>-1</sup> and the weak stretching of C=C bond at 1635 cm<sup>-1</sup>.

For unmodified SiO<sub>2</sub> (Fig.4.1a, black line), the very broad absorption between 3600–3200 cm<sup>-1</sup> attributable to the stretching of OH groups from physically absorbed water, the band of the Si–O–Si stretching vibrations at 1090 cm<sup>-1</sup>, and the band at 960 cm<sup>-1</sup> due to Si–OH stretching are noticeable.

The spectrum of SiO<sub>2</sub>-TMMS (Fig. 4.1a, blue line) displays the characteristic absorption bands at 1735 cm<sup>-1</sup> and 1645 cm<sup>-1</sup> (very weak) deriving from C=O and C=C stretching of the TMMS methacryl group. Moreover, a weak shoulder at 1210 cm<sup>-1</sup> related to the -C-CO-O- skeletal vibration from the methacryloxy group of the silane is detectable<sup>87-89</sup>. It can be also observed that the -Si-OH stretching at 960 cm<sup>-1</sup> gradually decreases in intensity compared to SiO<sub>2</sub>, probably due to the formation of Si-O-Si bonds resulting from the condensation reactions between the alkoxy groups of TMMS and the surface hydroxyl groups of silica.

These results suggest the effective silanization of SiO<sub>2</sub> particles by TMMS.

To obtain SiO<sub>2</sub>@POSS, SiO<sub>2</sub>-TMMS NPs were then reacted with POSS assisted by DCP, which should promote the activation of the methacrylate groups of both silane and POSS units, favoring the POSS anchoring on the oxide surface.

The FT-IR spectra of pristine POSS, SiO<sub>2</sub>-TMMS and of the obtained SiO<sub>2</sub>@POSS-10 hybrid filler are reported in Fig.4.1b. For pure POSS (Fig.4.1b, bold black-line), the observed bands have been attributed to the C-H stretching vibration of methyl and methylene groups at 2950 and 2890 cm<sup>-1</sup>; to C=O and C=C stretching of POSS methacryl groups at 1710 and 1640 cm<sup>-1</sup>, respectively; to Si-O stretching vibrations typical of the POSS cage at 1090 cm<sup>-1</sup>. As expected, since the typical absorption bands of the POSS cages overlap the stretching and bending vibrations of silica and TMMS, the spectra of SiO<sub>2</sub>@POSS-10 hybrid filler and SiO<sub>2</sub>-TMMS result very similar (Fig. 4.1b, red and blue line

respectively), in spite of the functionalization with POSS. Analogous results have been attained for SiO<sub>2</sub>@POSS-3 and SiO<sub>2</sub>@POSS-5 hybrid nanofillers.

However, these results are not conclusive and have to be confirmed in order to prove the efficacy of the POSS functionalization procedure.

From these results it appeared highly questionable proving the efficacy of the POSS functionalization procedure.

Thus, in order to assess the anchoring of POSS units on filler surface, STEP 1 and STEP 2 were repeated by selecting a different oxide substrate, which does not display IR-absorption bands in the same spectral region of silane and POSS. We utilized commercial crystalline ZnO NPs <sup>91</sup>, since it has been demonstrated that TMMS can be efficiently bonded to ZnO through the hydrolysis and condensation reactions similar to those occurring in silica.

The FT-IR spectra of pure ZnO, ZnO-TMMS and ZnO@POSS-10 NPs are reported and described in Figure 4.2.

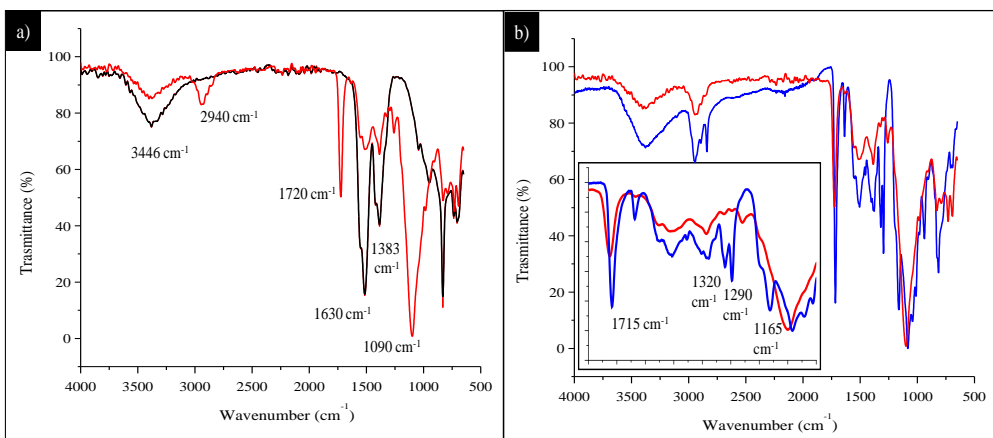


**Figure 4.2.** FT-IR spectra of: a) pristine ZnO (black line) and ZnO functionalized with TMMS (ZnO-TMMS, red line); b) ZnO-TMMS (red line) and ZnO@POSS-10 (blue line).

Pristine ZnO (Fig. 4.2a, black line) showed broad absorption bands at  $3380\text{ cm}^{-1}$  and  $1550\text{ cm}^{-1}$  assigned to the stretching and bending vibration modes of water most likely adsorbed through H-bonding to OH groups on the surface of ZnO NPs. The other band at  $1383\text{ cm}^{-1}$  in the ZnO sample was considered an impurity. After reacting ZnO with TMMS, the spectrum (Fig. 4.2a, red line) revealed the characteristic absorption bands of the silane. In detail, the weak band at  $2940\text{ cm}^{-1}$  was assigned to the stretching of C–H vibration, while those at  $1725$  and at  $1085\text{ cm}^{-1}$  were associated to the vibration of C=O and Si–O–C bonds of TMMS.

In Figure 4.2b the spectra of ZnO-TMMS (red line) and ZnO@POSS-10 (blue line) are compared. ZnO@POSS-10 NPs show the bands at  $2950$  and  $2890\text{ cm}^{-1}$  attributable to the C–H stretching vibrations of methyl and methylene groups of POSS terminations. The vibrations typical of

methacryloxy groups ( $\nu$  C=O,  $\nu$  C=C,  $\nu$  -C-CO-O-) and the Si-O-C stretching increase in intensity if compared to those observed in ZnO-TMMS (see inset Fig. 4.2b). These results, beyond indicating the effective POSS functionalization of the ZnO NPs, can be considered an indirect probe of the efficacy of the functionalization route in providing the anchoring of POSS nanounits on oxide surfaces.

#### 4.1.2 Nitrogen adsorption-desorption experiments

Nitrogen physisorption experiments were performed on bare SiO<sub>2</sub>, SiO<sub>2</sub>-TMMS and SiO<sub>2</sub>@POSS NPs, in order to highlight the effect on functionalization on the aggregation/porosity of the fillers.

In particular, the adsorption-desorption isotherms of pristine silica and SiO<sub>2</sub>@POSS-10 samples are reported in Figure 4.3.

SiO<sub>2</sub> NPs display a type IV Brunauer isotherm, typical of mesoporous materials, and a relatively high specific surface area ( $SSA_{BET}$ ) of  $168.6 \pm 3.4 \text{ m}^2 \text{ g}^{-1}$  <sup>92-94</sup>.

Conversely, SiO<sub>2</sub>@POSS shows a Type II isotherm with H3 hysteresis loop, characteristic of particle agglomerates giving rise to slit-shaped pores. Accordingly, a remarkable reduction of the surface area is detected for this sample ( $SSA_{BET} = 8.2 \pm 0.2 \text{ m}^2 \text{ g}^{-1}$ ). A similar behavior was observed for SiO<sub>2</sub>-TMMS NPs with  $SSA_{BET} = 29.0 \pm 0.6 \text{ m}^2 \text{ g}^{-1}$  (isotherm not shown).

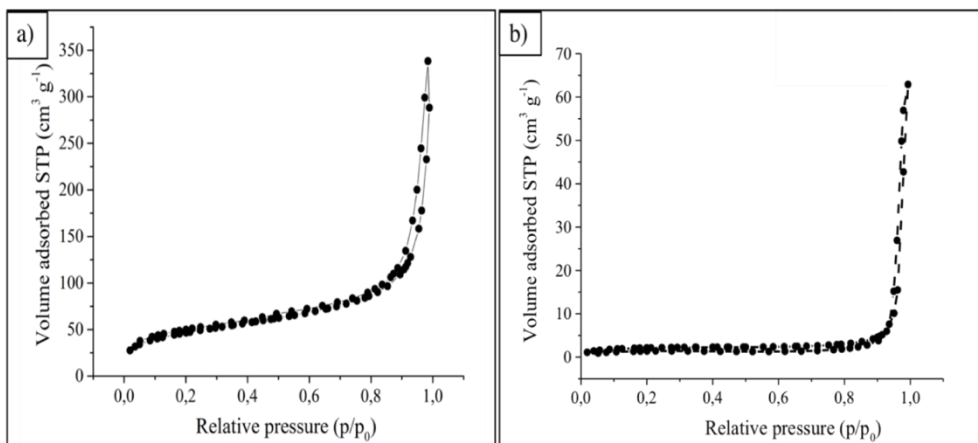


**Figure 4.3.** Adsorption–desorption isotherm at liquid nitrogen temperature of: a) pristine SiO<sub>2</sub> and b) SiO<sub>2</sub>@POSS hybrid nanofiller.

These results may be explained referring to the outgassing treatment at 150°C undergone by the samples before the measurements. This thermal activation may promote the reactivity among the methacryl functionalities of POSS units in SiO<sub>2</sub>@POSS, thus increasing the aggregation and leading to large filler agglomerates.

#### 4.1.3 Thermogravimetric analysis (TGA)

To quantitatively assess the silica functionalization, TGA analysis was performed on SiO<sub>2</sub>-TMMS, SiO<sub>2</sub>@POSS-10 and on naked silica NPs and showed in Figure 4.4. In detail, the total amount of TMMS grafted onto SiO<sub>2</sub> was evaluated by the net weight loss of SiO<sub>2</sub>-TMMS between 180°C and 980 °C, i.e. considering the total weight loss with exclusion of that associated to bare SiO<sub>2</sub> (i.e. 3.860 wt. %). The quantity of POSS

units in SiO<sub>2</sub>@POSS-10 was similarly calculated subtracting the contributions of both SiO<sub>2</sub> and TMMS from the total weight loss<sup>92-94</sup>.

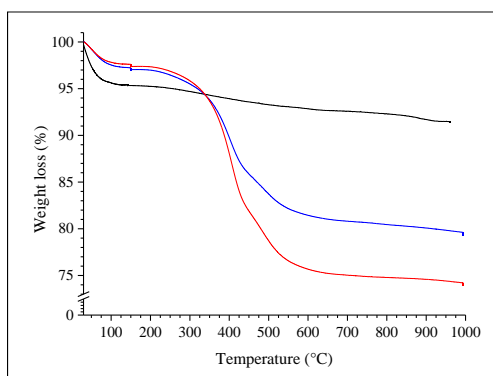


**Figure 4.4.** TGA curves of pristine SiO<sub>2</sub> Rhodia (black line), SiO<sub>2</sub>-TMMS (blue line) and SiO<sub>2</sub>@POSS-10 (red line) NPs.

Moreover, assuming that the functionalizing agents were equally distributed on the silica surface and referring to the BET surface area of SiO<sub>2</sub> ( $SSA_{BET} = 168.6 \pm 3.4 \text{ m}^2 \text{ g}^{-1}$ ), the number of functionalizing molecules per nm<sup>2</sup> ( $\Sigma = \text{molecules nm}^{-2}$ ) was also estimated (Table 4.1). The obtained results confirm the functionalization of silica with silane in SiO<sub>2</sub>-TMMS and, though to a lower extent, with POSS nanounits in SiO<sub>2</sub>@POSS NPs (Table 4.1)<sup>92-94</sup>.

**Table 4.1.** Surface density of functional molecules on SiO<sub>2</sub>-TMMS and SiO<sub>2</sub>@POSS-10 NPs.

Compound	Functionalizing agent	MW (g mol <sup>-1</sup> )	Net weight loss (wt. %)	Grafted amount (mmol g <sup>-1</sup> )	$\Sigma$ (molecules nm <sup>-2</sup> )
SiO <sub>2</sub> -TMMS	TMMS	248.4	13.398	0.539	1.927
SiO <sub>2</sub> @POSS-10	POSS	1434.0	5.807	0.041	0.154

To more effectively assess the silica functionalization by POSS,  $^{29}\text{Si}$  NMR experiments were performed on  $\text{SiO}_2$ @POSS hybrid fillers in collaboration with Prof S. Dirè and Dr E. Callone of University of Trento.

#### 4.1.4 Solid state NMR investigation of $\text{SiO}_2$ @POSS hybrid filler

Figure 4.5 presents the  $^{29}\text{Si}$  CPMAS spectra (see Appendix for details) recorded on  $\text{SiO}_2$ -TMMS,  $\text{SiO}_2$ @POSS-3 and  $\text{SiO}_2$ @POSS-10.

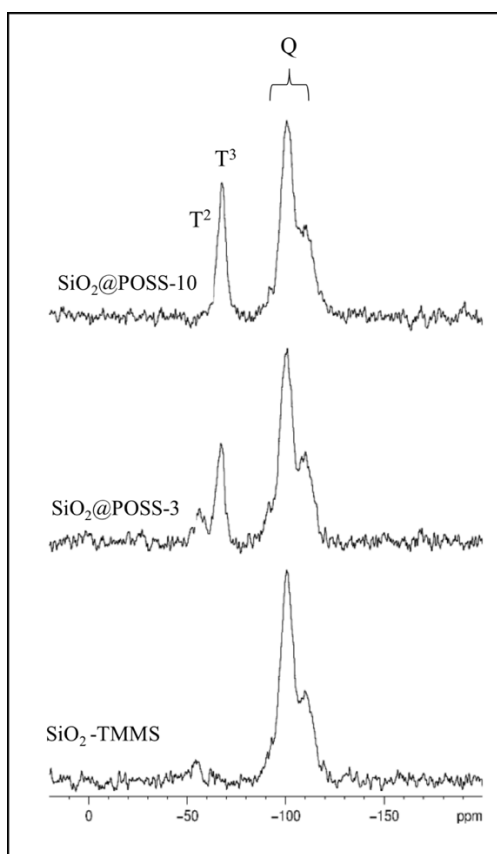


**Figure 4.5.**  $^{29}\text{Si}$  CPMAS of  $\text{SiO}_2$ -TMMS and  $\text{SiO}_2$ @POSS-X (X= 3, 10 % of POSS)

The Q-units region of the CPMAS spectrum of SiO<sub>2</sub>-TMMS sample (Fig. 4.5 bottom) displays the complex resonance of the SiO<sub>2</sub> phase, resulting from the overlapping of three components at -92.2 (Q<sup>2</sup>), -100.5 (Q<sup>3</sup>) and -110.1 (Q<sup>4</sup>) ppm, respectively. The TMMS functionalization of the SiO<sub>2</sub> particles is proved by the resonance at -55.7 ppm due to the T<sup>2</sup> units and the very weak signal at -66.5 ppm assigned to the T<sup>3</sup> units.

In the CPMAS spectra of SiO<sub>2</sub>@POSS-3 and SiO<sub>2</sub>@POSS-10 (Fig. 4.5), the features of the Q units appear unchanged whereas the signals of T units strongly increase in intensity compared to SiO<sub>2</sub>-TMMS.

It is not possible to distinguish the T units of TMMS from those of POSS since they present the same chemical shift<sup>95,96</sup>. However, the POSS molecules contribute in particular to the T<sup>3</sup> resonance, in agreement with their structure. Therefore, the increase of T<sup>3</sup>/T<sup>2</sup> ratio in SiO<sub>2</sub>@POSS-10 in comparison to SiO<sub>2</sub>@POSS-3 and, in particular, to SiO<sub>2</sub>-TMMS is a clear indication of the effective POSS grafting onto the surface of the functionalized silica NPs.

In order to get information on the interactions among the acrylate functions of TMMS and POSS in the final hybrid nanofillers, <sup>13</sup>C CPMAS NMR investigation was performed on SiO<sub>2</sub>@POSS-X NPs. In particular, the spectrum of SiO<sub>2</sub>@POSS-10 is shown in Fig. 4.6. The liquid NMR spectrum of the pristine TMMS is also reported for comparison (Fig. 4.6, top).

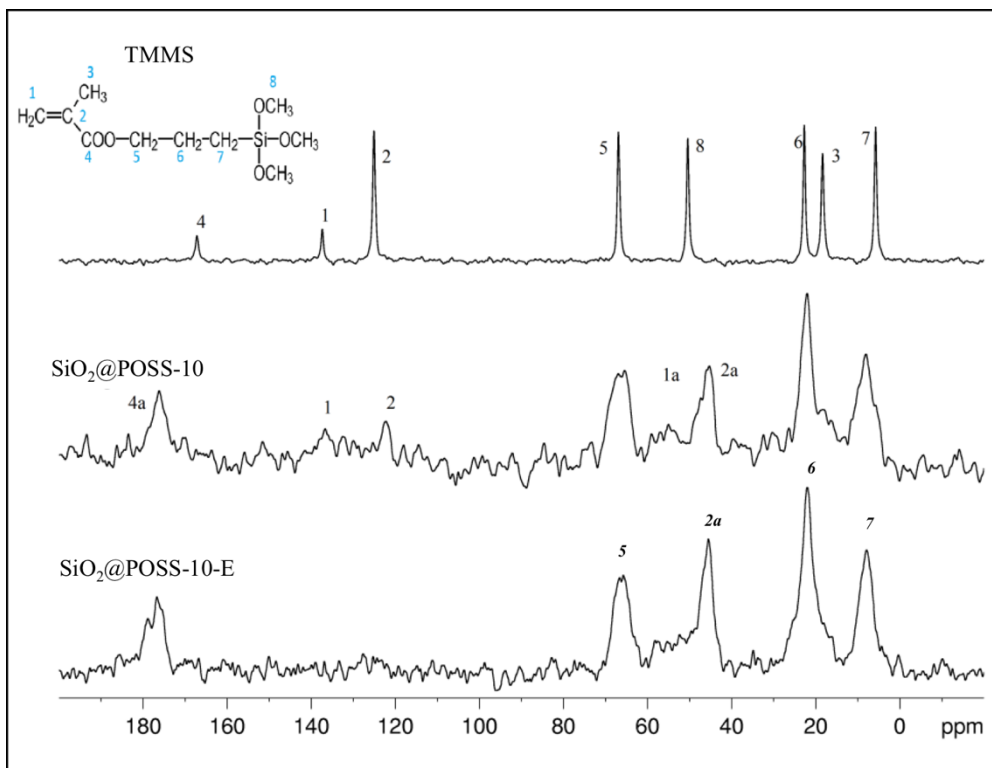


**Figure 4.6:**  $^{13}\text{C}$  CPMAS spectra of silica functionalized with TMMS and POSS.

The polymerization among the acrylate functionalities of TMMS and POSS, activated by DCP, leads to the appearance in the  $\text{SiO}_2@POSS-10$  spectrum of the peak *2a* at 45 ppm and to a broad signal in the range 52-56 ppm (*1a*), both attributable to  $-\text{CH}_2-$ -based chains formed through polymerization. Moreover, the downfield shift (of about 8 ppm) of the carbonyl peak *4*, compared to the resonance found at 167.2 ppm in the unreacted acrylate chain, such as in pristine TMMS, further confirms the successful reaction between organosilane and

nanocages. These results further substantiate the POSS anchoring onto functionalized silica surfaces.

Despite the poor S/N ratio, in SiO<sub>2</sub>@POSS-10 residual weak signals in the range 110-150 ppm may suggest the presence of residual C=C bonds (signals at 125.1 and 137.4 ppm, respectively), which could be available for the cross-linking reactions with rubber chains during the curing of the composites. In order to prove this hypothesis, a SiO<sub>2</sub>@POSS-10 sample prepared by using an excess of DCP, for improving the condensation of the methacrylate functions was investigated (SiO<sub>2</sub>@POSS-10-E, Fig. 4.6 bottom). The obtained spectrum displays an almost flat profile in the C=C region, supporting the idea that in SiO<sub>2</sub>@POSS-10 hybrid sample unreacted methacrylate functionalities are still present.

In summary, the NMR study points out the effective grafting of POSS molecules on SiO<sub>2</sub>-TMMS NPs and the expected presence of residual methacrylate groups available for the interaction with rubber.

#### **4.1.5 TEM investigation of SiO<sub>2</sub>@POSS hybrid filler**

The morphology of SiO<sub>2</sub>@POSS NPs was investigated by TEM (in collaboration with Prof S. Polizzi of University Ca' Foscari of Venice) and compared to that of bare silica (Figure 4.7). Images show that pure SiO<sub>2</sub> is constituted by large agglomerates where the NPs are highly aggregated, due to their polar surfaces (Fig. 4.7a). At higher magnifications, the NPs assume almost elongated shape and average diameter ranging between 15 and 20 nm (Fig. 4.7 c, e).

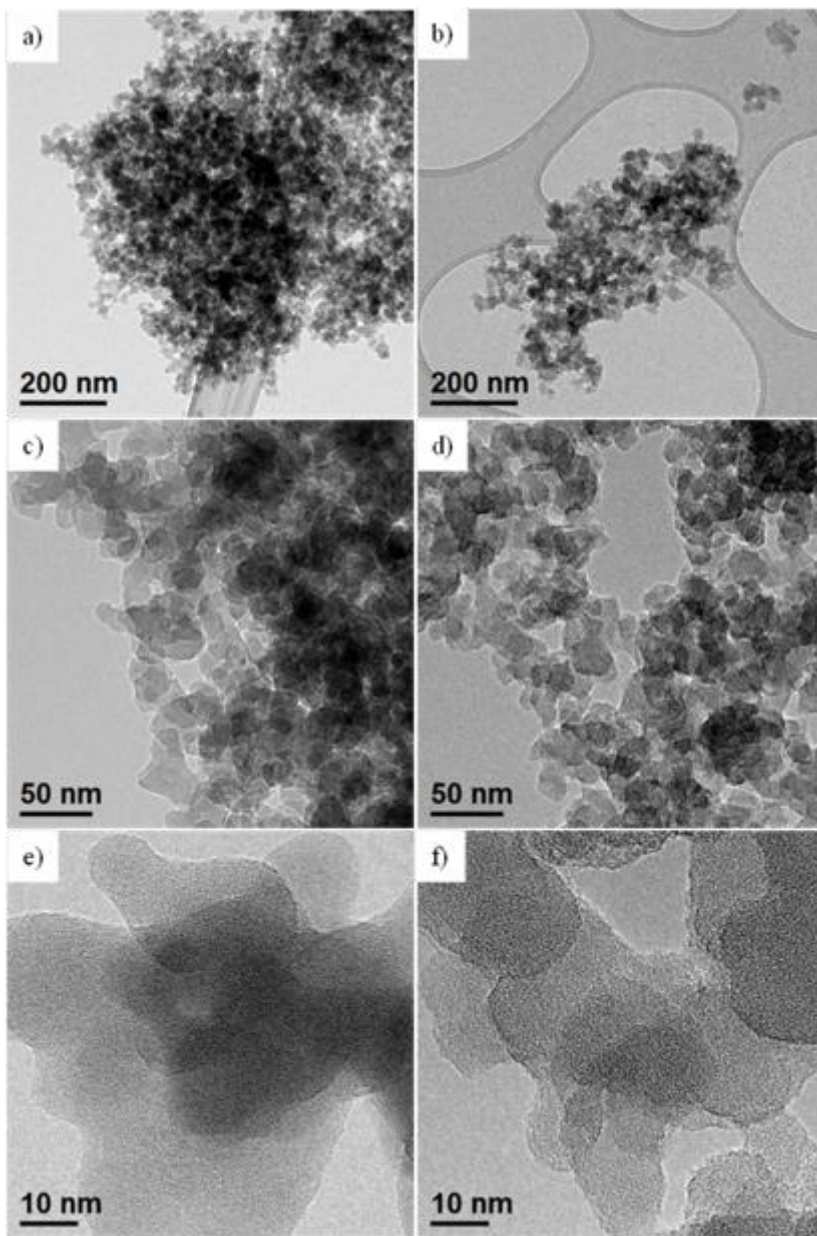


**Figure 4.7:** TEM images at different magnifications of: a), c) and e) bare SiO<sub>2</sub> NPs; b), d) and f) SiO<sub>2</sub>@POSS-10 nanofiller.

After functionalization with POSS units ( $\text{SiO}_2@\text{POSS-10}$ , as representative example), the silica NPs morphology does not significantly change (Fig. 4.7b). However, going more in depth into the images observation, the NPs boundaries appear less defined than in pure silica (Fig. 4-7 d and f). These effects may be related to the presence of POSS domains, which create a surface shell on the particles surface, hindering the aggregation.

Since both  $\text{SiO}_2$  and POSS are amorphous, it is tricky to associate the less defined boundaries of the  $\text{SiO}_2@\text{POSS-10}$  images, to the presence of POSS nanounits. Thus, in order to observe the effect of the functionalization on the filler surface features, in analogy with the IR investigation, the TEM analysis was carried out also on  $\text{ZnO}@\text{POSS-10}$  sample, constituted by highly crystalline ZnO NPs (Fig. 4.8a) functionalized with POSS nanocages.

In this case, TEM images of  $\text{ZnO}@\text{POSS-10}$  NPs (Fig. 4.8b) revealed thin and irregular amorphous layers surrounding and partially connecting the nanocrystals, attributable to the presence of nanometric aggregates of POSS units. This again supports the efficacy of the functionalization procedure in favoring the anchoring of POSS on oxide surface.

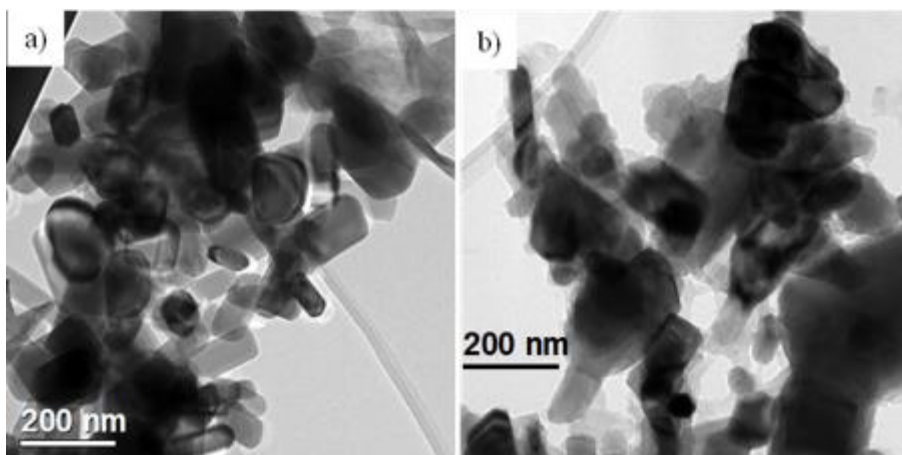


**Figure 4.8:** TEM images of a) pure ZnO and b) ZnO@POSS-10 NPs

## **4.2 Characterization of SBR/SiO<sub>2</sub>@POSS and SBR/SiO<sub>2</sub>+POSS nanocomposites**

### **4.2.1 TEM investigation of the nanocomposites**

The morphology of the nanocomposites and the filler dispersion were investigated by TEM (in collaboration with L. Conzatti of ISMAC of Genova) for both cured and uncured samples obtained by incorporating in SBR the hybrid filler SBR/SiO<sub>2</sub>@POSS-X or the mixture of SiO<sub>2</sub>, TMMS and POSS (i.e. SBR/SiO<sub>2</sub>+POSS-X). The images collected for uncured SBR/SiO<sub>2</sub>@POSS-10 and SBR/SiO<sub>2</sub>+POSS-10 samples are reported in Figure 4.9.

SBR/SiO<sub>2</sub>@POSS-10 is constituted by very compact and large NPs agglomerates, which have micrometric dimensions and are inhomogeneously distributed through the rubbery matrix (Fig. 4.9a). This irregular organization generates regions in which the rubber is

constrained (inset Fig. 4.9a). However, the presence of wide areas lacking in filler particles can be detected (Fig. 4.9b).

Conversely, in SBR/SiO<sub>2</sub>+POSS-10, the filler distribution is rather continuous and homogeneous (Fig. 4.9c), with silica NPs organized in sub-micrometric or even nanometric agglomerates (Fig. 4.9d).

The better dispersion may be tentatively ascribed to the larger amounts of either TMMS or POSS nanounits present during the mixing procedure, in comparison to those effectively grafted onto the surface of silica in SiO<sub>2</sub>@POSS filler after functionalization, as assessed by NMR investigation.

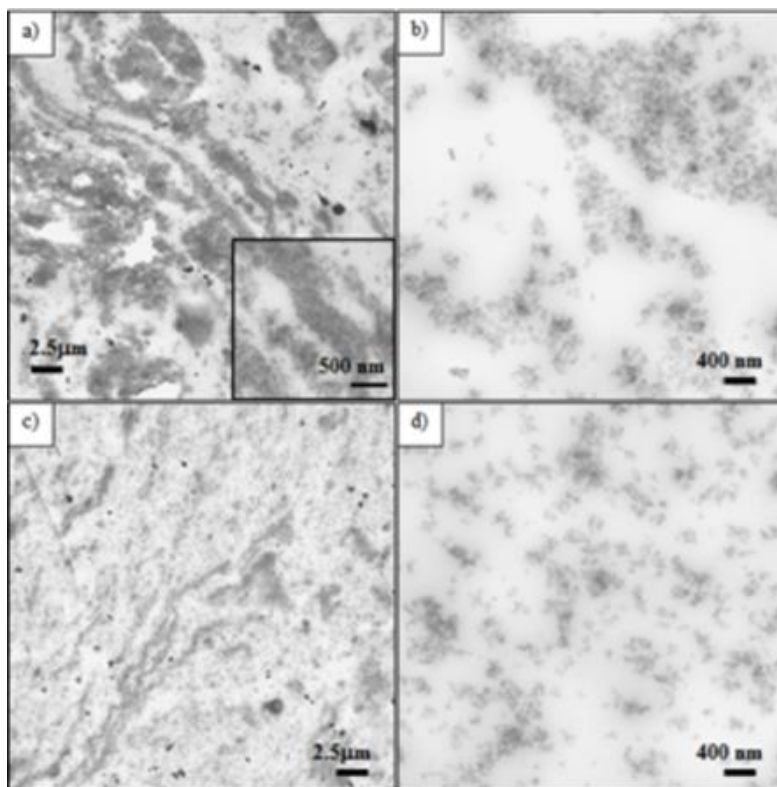


**Figure 4.9** TEM images at different magnifications of uncured: a) and b) SBR/SiO<sub>2</sub>@POSS-10; c) and d) SBR/SiO<sub>2</sub>+POSS-10 nanocomposites.

After curing (170°C, 10min), a more continuous and homogeneous filler network was generally observed compared to the crude composites (Fig. 4.10). This is particularly evident for C-SBR/SiO<sub>2</sub>+POSS-10, where silica NPs form small nanometric aggregates (Fig. 4.10c), which are very uniformly dispersed in the matrix and only partially interconnected (Fig. 4.10d). Although an improved particle distribution is detectable also for C-SBR/SiO<sub>2</sub>@POSS-10, the sample still exhibits micrometric NPs agglomerates and filler-free zones (Fig. 4.10a, b). However, these agglomerates appear less dense than those showed by the uncured composite (see Fig. 4.9a), and some thin rubbery regions separating the NPs aggregates are noticeable (inset Fig. 4.10a and Fig. 4.10b).

After curing the enhancement of the filler dispersion may be related to the further mixing steps and to the DCP action<sup>9</sup>, which activates the reaction between the methacryl groups of both TMMS and POSS and the rubber vinyl functionalities, leading to an increased cross-linking and, probably, to the immobilization of rubber among NPs aggregates.

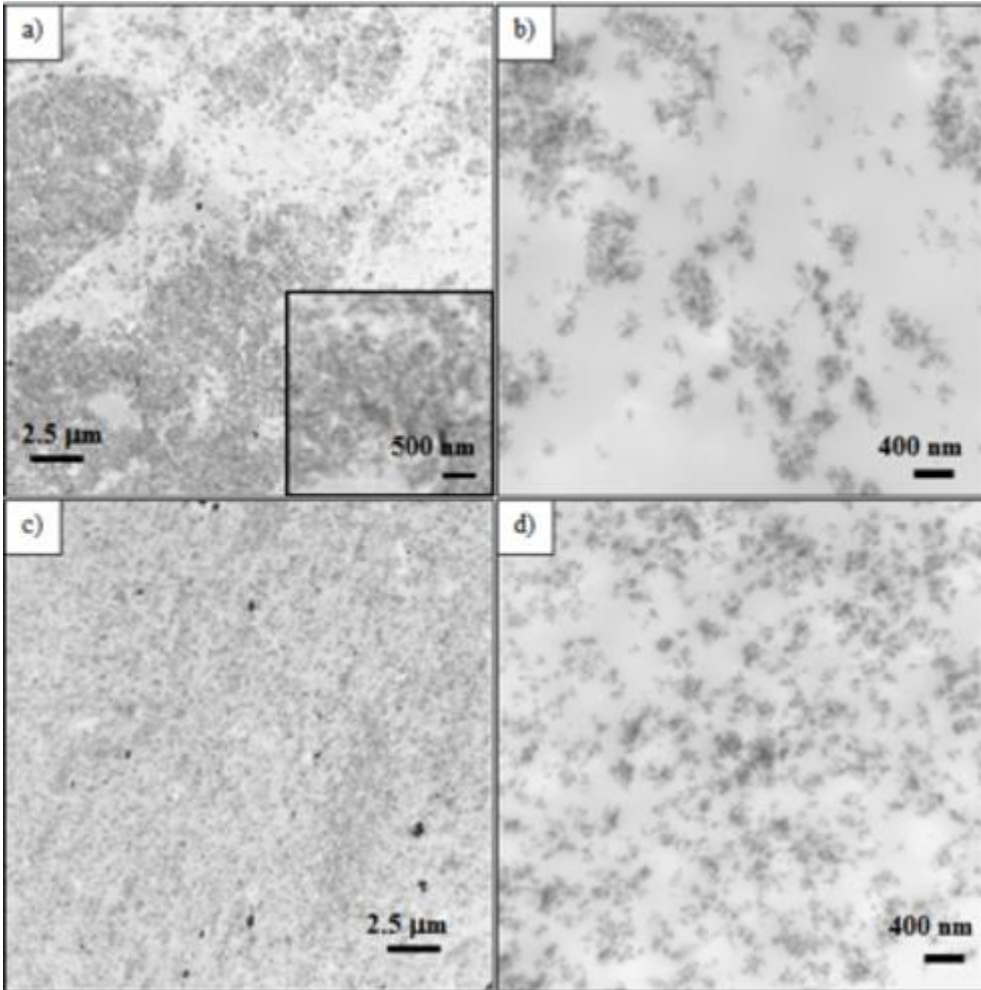


**Figure 4.10:** TEM images at different magnifications of: a) and b) C-SBR/SiO<sub>2</sub>@POSS-10; c) and d) C-SBR/SiO<sub>2</sub>+POSS-10 nanocomposites.

#### 4.2.2 Morphology of SBR nanocomposites by SEM

Polymeric surfaces in nanocomposites present inhomogeneities at the microscopic scale, which can affect their properties of adhesion, wettability, abrasion and degradation in the environment. Therefore,

the identification of in-homogeneities and its mapping have great importance in science and technology<sup>1,6,97,98</sup>.

In particular, the interfacial interaction (adhesion) between filler and polymer represents an important factor which influences the mechanical properties of the composites.

Some evidences<sup>99-103</sup> demonstrated that composite strength and toughness are very much dependent on the adhesion quality. For poorly bonded particles, the strength at the particle/polymer interface is weak due to a non-adherence of particles to polymer. Thus, the composite cannot tolerate any amount of particles and its strength decreases with increasing the filler loading. Instead, for composites containing well-bonded particles, further addition of particles to the polymer will lead to an increase in strength.

In this study, the adhesion between SiO<sub>2</sub>@POSS hybrid nanofiller and SBR in the cured nanocomposites was evaluated by SEM microscopy and compared with C-SBR/SiO<sub>2</sub>+POSS composites. The samples were fractured in liquid nitrogen in order to understand the surface structure of the sample along the fracture. Then, after sputtering with a thin platinum layer, they were observed at the accelerating voltage 30 kV using both secondary electrons detector (SE) and backscattered electrons (BSE) detector (See Appendix for details).

Figure 4.11 reports the SEM images at different magnification obtained for C-SBR/SiO<sub>2</sub>+POSS-10 and C-SBR/SiO<sub>2</sub>@POSS-10 nanocomposites. C-SBR/SiO<sub>2</sub>+POSS-10 samples show a sharper interface with significant boundaries between the two phases (Fig. 4.11a and 4.11b), while C-SBR/SiO<sub>2</sub>@POSS-10 exhibited continuous surfaces (Fig. 4.11 c and

4.11d). Moreover,  $\text{SiO}_2$ @POSS hybrid NPs appear to be covered by the polymer on the fractured surface and the interfacial adhesion between the filler and the polymer seems to be enhanced.

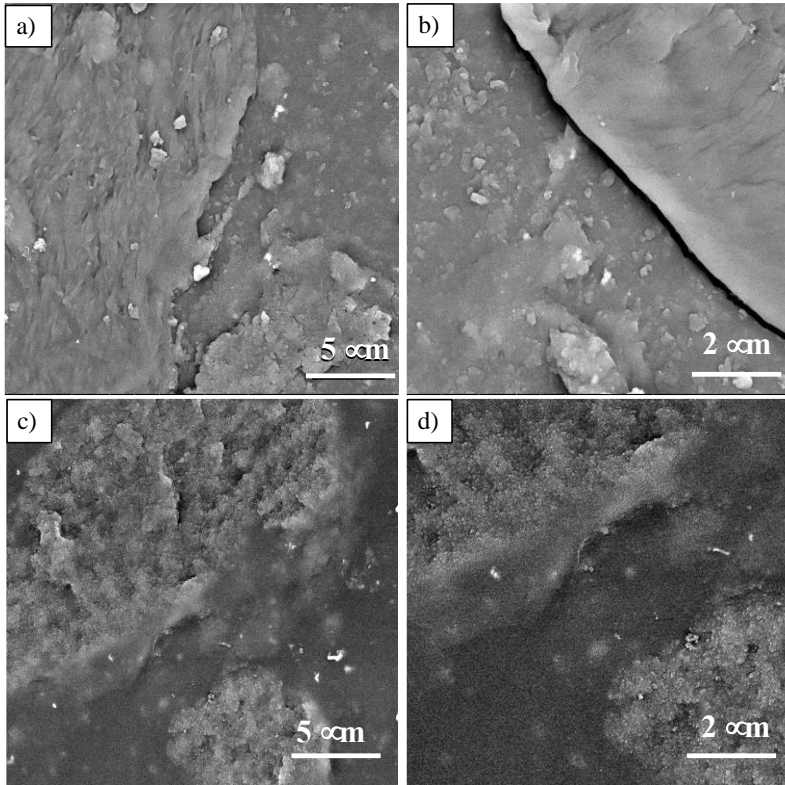


**Figure 4.11:** SEM images at different magnifications of:  
a) and b) C-SBR/SiO<sub>2</sub>+POSS-10; c) and d) C-SBR/SiO<sub>2</sub>@POSS-10  
nanocomposites

Since both the filler networking and distribution in these nanocomposites are clearly influenced by the curing with DCP (see TEM investigation), the interfacial adhesion between filler and rubber was evaluated for the sample cured with the same curing time (10 min) but at different temperature : i) 155°C, where dicumylperoxide is in

principle less reactive and the curing is at the early stages ii) 170 °C, i.e. the optimum temperature for DCP activation and curing; iii) 185°C, a temperature at which the peroxide is surely reacted and the curing is rather complete<sup>70,104,105</sup>.

As reported before, the samples cured at different temperatures for 10 min are labelled as SBR/SiO<sub>2</sub>@POSS-10\_Y and C-SBR/SiO<sub>2</sub>+POSS-10\_Y (Y = 155°C, 170°C, 185°C), respectively.

Figure 4.12 shows the SEM micrographs of C-SBR/SiO<sub>2</sub>+POSS-10 and C-SBR/SiO<sub>2</sub>@POSS-10 nanocomposites at increasing curing temperature. In detail, C-SBR/SiO<sub>2</sub>+POSS-10\_155°C and C-SBR/SiO<sub>2</sub>@POSS-10\_155°C nanocomposites (Fig 4.12 a, d) show sharp interfaces with significant boundaries between the two phases. Moreover, the filler surface appears poorly penetrated by the rubber matrix, indicating weak adhesion between particles and polymer chains. This behaviour may be explained considering that, under these curing conditions, DCP is in principle poorly active and thus methacryl functionalities of both POSS and TMMS should be not able to interact with the vinyl groups of SBR, leading to weak filler-rubber interactions.

At 170°C, i.e. the optimum activation temperature for DCP, the C-SBR/SiO<sub>2</sub>+POSS-10\_170°C nanocomposite seems to show again phase separation and poor adhesion between filler and polymer (Fig 4.12 b). Instead, the C-SBR/SiO<sub>2</sub>@POSS-10\_170°C sample exhibits continuous surfaces where the SiO<sub>2</sub>@POSS hybrid nanofiller appears to be homogeneously covered by rubber, with remarkable interfacial adhesion (Fig 4.12 e). This behaviour is more clearly detectable in the SEM images collected after curing at 185°C (Fig. 4.12 f)

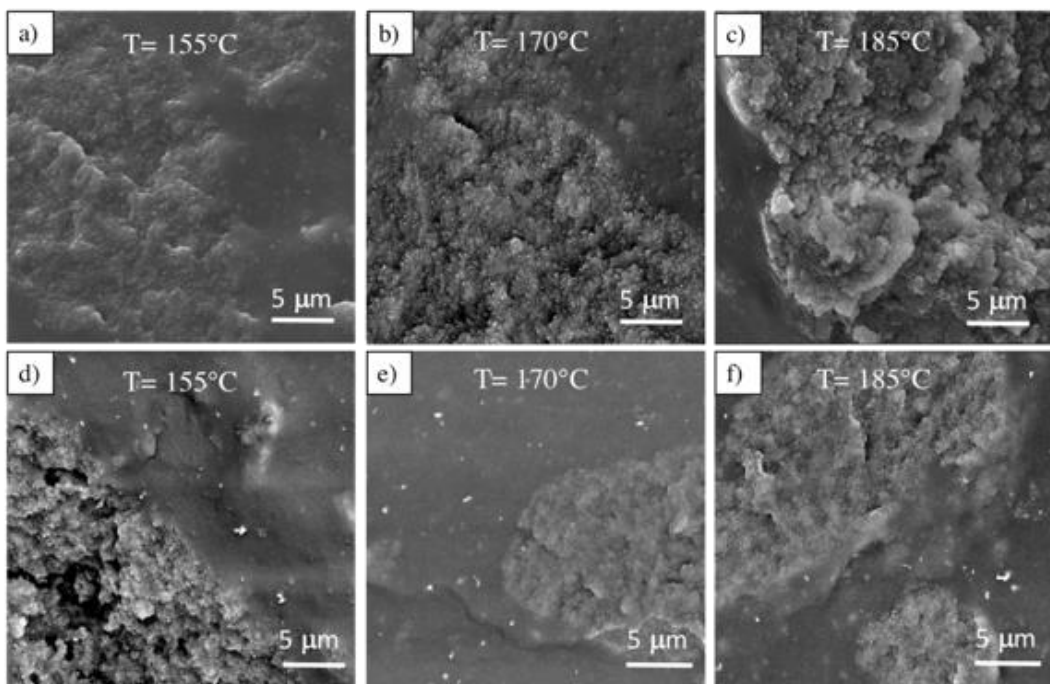


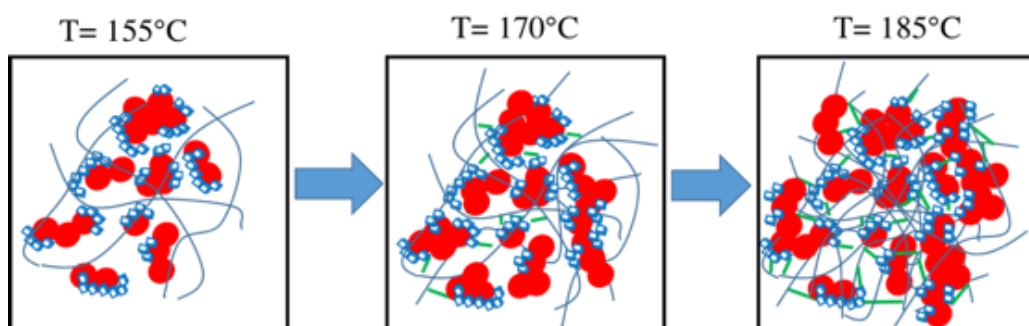
**Figure 4.12:** SEM images of a), b) and c) C-SBR/SiO<sub>2</sub>+POSS-10 and d), e) and f) C-SBR/SiO<sub>2</sub>+POSS-10 nanocomposites cured at different temperatures (155, 170 and 185°C) for 10 min

The overall SEM results on SBR composites seem to highlight a peculiar filler networking induced by the presence of the POSS nanounits, especially when they are grafted to silica in SiO<sub>2</sub>@POSS, and mediated by DCP activation.

In detail, in the hybrid filler the POSS nanocages anchored to the SiO<sub>2</sub> NPs, thanks to the high number of reactive functionalities, may provide after curing with DCP a relevant cross-linking action at the surface or even inside these aggregates. This results in better adhesion properties and, according to TEM investigation, in the formation of a tight filler network, in which thin rubbery regions separate the NPs aggregates.

Instead, when POSS is mixed with silica within the rubber matrix (e.g. C-SBR/SiO<sub>2</sub>+POSS-10 sample), the synergism between POSS and filler NPs in providing immobilized rubber seems partially hindered, since better lower adhesion and more dispersed and only partially interconnected aggregates are detectable.

The above outcomes allowed us to propose a mechanism for the network formation in SBR/SiO<sub>2</sub>@POSS nanocomposites during the curing reaction (Scheme 4.3).



**Scheme 4.1:** Mechanism for the network formation in SBR/SiO<sub>2</sub>@POSS nanocomposites during the curing process.

At low temperatures (e.g. at 155°C), the peroxide reactivity is only partially activated, and therefore the crosslinking between SiO<sub>2</sub>@POSS hybrid filler functionalities and rubber chains is weak. As a consequence, the network formation proceeds slowly and very poor interfacial adhesion between filler and rubber is achieved. At 170°C and 185°C, the full activation of DCP promotes the crosslinking reactions involving methacryl functionalities of POSS and TMMS. This leads to the generation of a tight network constituted by compact

agglomerates, distributed inhomogeneously through the rubbery matrix and highly covered by the polymer phase.

In order to further highlight the role of the MethacrylPOSS grafted onto  $\text{SiO}_2$  in promoting the network formation, the adhesion properties of C-SBR/ $\text{SiO}_2$ @MonoPOSS-10 composites were also studied and compared to those of C-SBR/ $\text{SiO}_2$ @POSS-10 sample.

In fact, the MonoPOSS is constituted by only one reactive methacryl group, while the other seven alkyl functionalities are basically poorly reactive. Therefore, after grafting onto  $\text{SiO}_2$ -TMMS by condensation between the methacryl group of silane and that of the MonoPOSS, no more functional groups should be available in  $\text{SiO}_2$ @MonoPOSS for filler-filler interaction or reaction with the polymer chains.

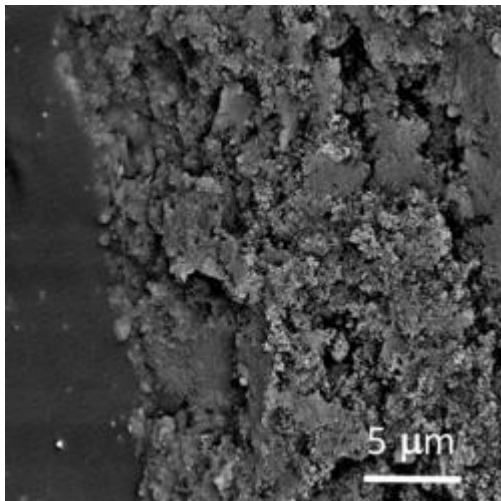


**Figure 4.13:** SEM images of SBR/ $\text{SiO}_2$ @MonoPOSS-10

In agreement with this hypothesis, the SEM micrograph of C-SBR/ $\text{SiO}_2$ @MonoPOSS-10 (Fig. 4.13) reveals that the filler-polymer

interfacial interaction is weak, as demonstrated by the clear phase separation.

This result further supports the key role of MethacrylPOSS units decorating silica NPs aggregates in SiO<sub>2</sub>@POSS in providing high cross-linking at the surface or even inside these aggregates, and fostering the formation of a tight filler network which immobilizes filler and rubber.

The experiments have been performed in the laboratory of Institute of Macromolecular Chemistry of Prague in collaboration with Prof. Miroslav Slouf and Prof. Libor Matejka.

#### **4.2.3 Atomic Force Microscopy (AFM) investigation of the nanocomposites**

The nanocomposites morphology was also investigated by AFM operating in tapping mode in air. The analysis was performed on fresh surfaces after freeze-fracturing the materials for obtaining of “cross-sectional images”. In this conditions it is possible the investigation of the topography and heterogeneity of the composite from the nano to micrometer level<sup>97</sup>.

Surfaces of filler and rubber were measured and evaluated as height images (information about material topography) and as phase images (information about the material heterogeneity).

In detail, in this analysis the phase signal is related to the energy dissipated by the tapping tip while scanning the surface, and gives information at the nanometric scale about the size and the shape of

local rubber heterogeneities, identifying regions with different stiffness.

In analogy to SEM investigation, the AFM images of C-SBR/SiO<sub>2</sub>@POSS and C-SBR/SiO<sub>2</sub>+POSS were collected for composites subjected to different curing temperatures with the same curing time.

The results are summarized in Figure 4.14.

For C-SBR/SiO<sub>2</sub>@POSS-10\_155°C (Fig. 4.14 top), AFM images collected at the lowest curing temperature show an inhomogeneous dispersion of filler particles with small contact zone between the neighbour particles.

In according with SEM and TEM characterization, for composites cured at 170°C (conventional curing temperature) SiO<sub>2</sub>@POSS particles appear more aggregated and a better covering of the filler (bright part) by rubber layers (dark part) is observed. Finally, in C-SBR/SiO<sub>2</sub>@POSS-10\_185°C cured at higher temperature, the interface adhesion between SiO<sub>2</sub>@POSS and rubber matrix appears remarkably increased. In fact, most of the filler particles are completely aggregated in micrometric agglomerates without rubber lacking zones.

The AFM images of C-SBR/SiO<sub>2</sub>+POSS-10 are reported in Figure 4.14 (bottom). As observed by TEM, in these composites silica NPs form small nanometric aggregates (Fig. 4.7c), which are very uniformly dispersed in the matrix and only partially interconnected. This behaviour is clearly detectable in the images collected after curing at the highest temperatures (i.e. 170°C and 185°C). Moreover, by comparing the interfacial adhesion in C-SBR/SiO<sub>2</sub>+POSS-10 with that in C-SBR/SiO<sub>2</sub>@POSS-10, it is evident a lower interaction between the

filler and the rubber matrix for the composite obtained by simply mixing SiO<sub>2</sub>, TMMS and POSS, as assessed by the prevalence of the bright spots in the images.

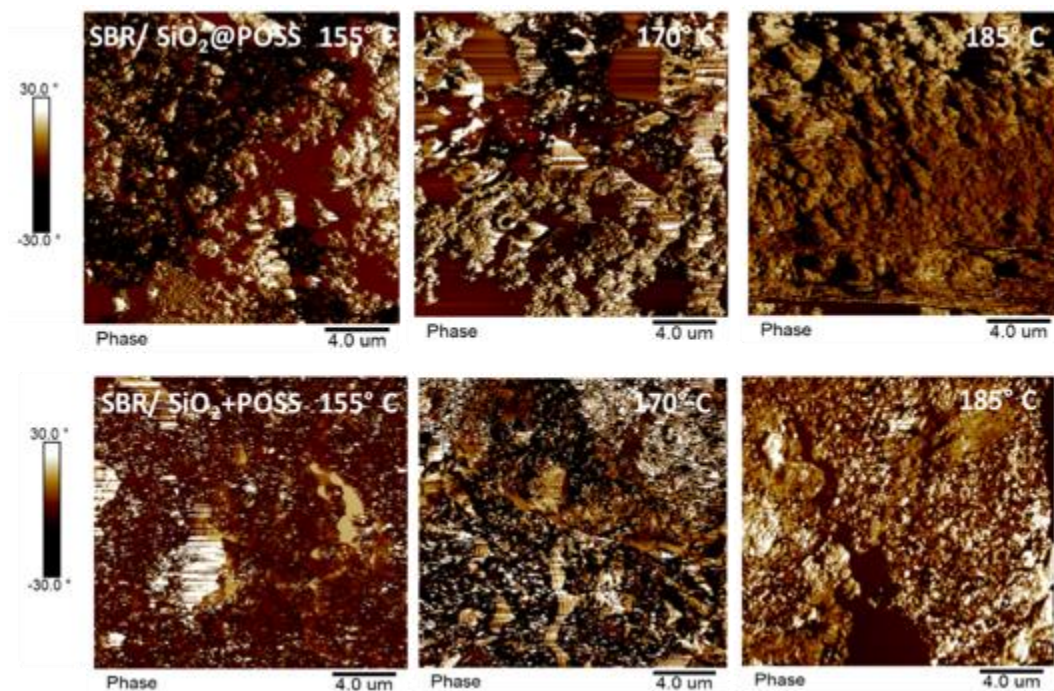


**Figure 4.14:** AFM images of C-SBR/SiO<sub>2</sub>@POSS-10 (top) and C/SBR/SiO<sub>2</sub>+POSS-10 (bottom) nanocomposites cured at different temperatures

This is in agreement with SEM results (Fig 4.11 and 4.12), further confirming the better adhesion between the two phases in SBR/SiO<sub>2</sub>@POSS compared to SBR/SiO<sub>2</sub>+POSS nanocomposites and in turn, the key role of SiO<sub>2</sub>@POSS NPs promoting a cross-linking action at the surface or even inside these aggregates, immobilizing rubber. In order to assess the immobilization of rubber in proximity to the NPs

surface, resulting in relevant interfacial adhesion, swelling experiments were performed.

The experiments have been performed in the laboratory of Institute of Macromolecular Chemistry of Prague in collaboration with Prof. Milena Spirkova and Prof. Libor Matejka.

#### **4.2.4 Swelling experiments**

Swelling experiments were performed on C-SBR/SiO<sub>2</sub>@POSS-X and C-SBR/SiO<sub>2</sub>+POSS-X composites cured at 170°C for 10min, in order to evaluate the effect induced by the introduction of POSS nanocages.

The  $\nu$  value was determined according the Flory-Rehner equation<sup>106,107</sup> and the results are summarized in Figure 4.15. For C-SBR/SiO<sub>2</sub>@POSS-X samples, the reticulation degree generally increases with the POSS loading, becoming remarkable for C-SBR/SiO<sub>2</sub>@POSS-10. Conversely, the  $\nu$  values for C-SBR/SiO<sub>2</sub>+POSS-X nanocomposites for X=5 and 10 are only slightly higher than those calculated for the reference sample (C-SBR/SiO<sub>2</sub>+POSS-0, not including POSS), while definitively lower than those of C-SBR/SiO<sub>2</sub>@POSS-X.

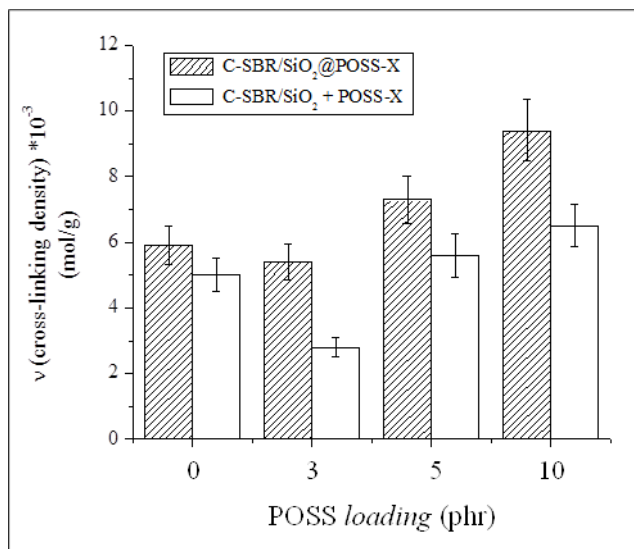


**Figure 4.15:** Trend of the  $\nu$  values for C-SBR/SiO<sub>2</sub>@POSS-X and C-SBR/SiO<sub>2</sub>+POSS-X nanocomposites.

These outcomes may be explained referring to the peculiar morphological properties of the composites. In C-SBR/SiO<sub>2</sub>@POSS-X nanocomposites, POSS nanocages are anchored to the SiO<sub>2</sub> NPs inducing the formation of a tight filler network, in which thin rubbery regions separate the NPs aggregates (see Fig. 4.7a, b). This may favor an enhanced immobilization of rubber in proximity to the NPs surface, resulting in a high cross-linking density and relevant interfacial adhesion.

Instead, when POSS is simply mixed with silica within the rubber matrix (i.e C-SBR/SiO<sub>2</sub>+POSS-X samples), the synergism between POSS and filler NPs in providing immobilized rubber seems partially hindered, since more dispersed and only partially interconnected aggregates are

detected (see Fig. 4.7c, d). Accordingly, lower cross-linking density values are obtained for these composites.

#### **4.2.5 $^1\text{H}$ MAS NMR investigation on SBR nanocomposites**

High Resolution Solid State NMR is known as a powerful technique in structural characterization, but it also finds large application in the study of interfaces in nanocomposites. As this technique can provide clear information about the changes in polymer chains structure and dynamics, its application in the study of rubber nanocomposites can afford an in depth knowledge on the nature strength of the interfacial interaction between the elastomer blocks and filler nanounits and the filler networking in the final materials. In particular, the solid state NMR investigation of rubber composites allows to determine the fraction of rubber chains having slower dynamics and to on unraveling useful correlations with the filler-rubber interaction and the mechanical properties of the composites.

The variation of segmental dynamics of polymer chains are clearly reflected by the broadening/narrowing of  $^1\text{H}$  NMR signals measured under static conditions <sup>108-110</sup>.

In the present study,  $^1\text{H}$  MAS NMR spectra have been recorded for SBR/SiO<sub>2</sub>@POSS-10 and SBR/SiO<sub>2</sub>+POSS-10 nanocomposites, in order to clarify the effect of the POSS in enhancing the filler-rubber interaction, the networking and the cross-link density.

The experiments have been performed in the laboratory of Institute of Macromolecular Chemistry of Prague in collaboration with Prof. Jiri Brus and Prof. Libor Matejka.

Figure 4.16 summarizes the  $^1\text{H}$  MAS NMR spectra collected for SBR/SiO<sub>2</sub>@POSS-10, SBR/SiO<sub>2</sub>+POSS-10, SBR/SiO<sub>2</sub>-TMMS composites and for pure SBR cured at 170°C. Moreover, the spectra of SBR/SiO<sub>2</sub>@POSS-10, cured at 155°C (i.e. SBR/SiO<sub>2</sub>@POSS-10\_155°C sample) has been also included.

A preliminary inspection of the spectra reveals differences in the line-widths of the signals recorded for the different samples (Fig. 4.16, right-side). This is particularly evident as concerns on the splitting of the signal resonating at ca. 7 ppm, which is clearly observable for the C-SBR pure. This splitting almost disappears in the spectra of C-SBR/SiO<sub>2</sub>-TMMS and, more markedly, for C-SBR/SiO<sub>2</sub>@POSS-10 and C-SBR/SiO<sub>2</sub>+POSS-10 nanocomposites.

These results suggest the polymer chains rigidity increases from SBR pure (Fig. 4.16, blue line), i.e the sample with most flexible chains, to C-SBR/SiO<sub>2</sub>+POSS-10 and C-SBR/SiO<sub>2</sub>@POSS-10 (green and violet lines, respectively), i.e the composites with the highest fraction of rigid chains.

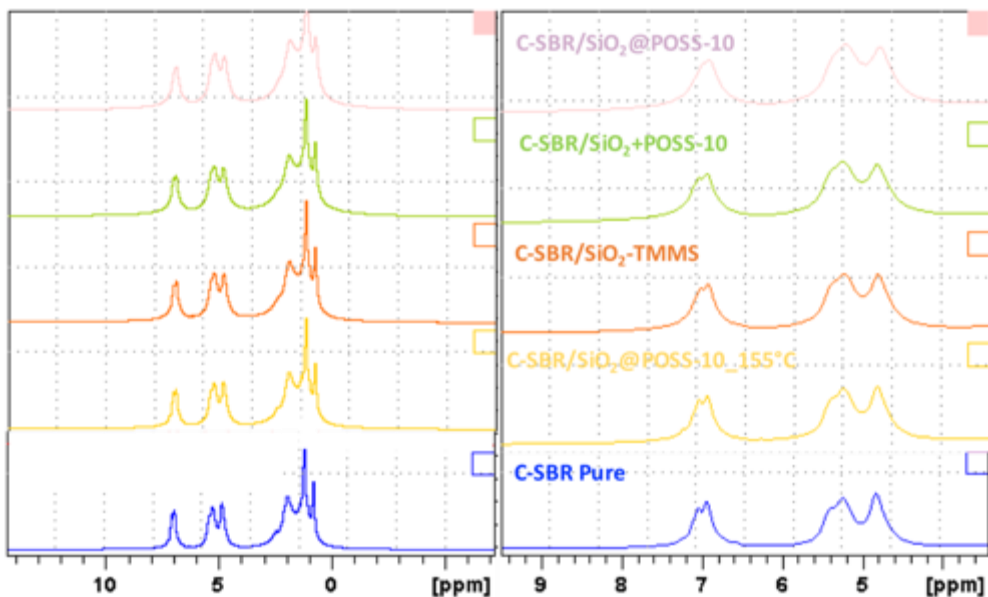


**Figure 4.16:** Full-range (left-side) and expanded  $^1\text{H}$  MAS NMR spectra of cured SBR and SBR nanocomposites recorded at 15 kHz (right-side).

To obtain more precise data about segmental dynamics and to estimate the fraction of immobilized polymer segments in the prepared systems, static  $^1\text{H}$  NMR spectra were inspected in detail and were simulated by four lines: three narrow lines at 7.0, 5.4, and 1.2 ppm, which represent the flexible fractions, whereas a single broad component at 4.6 ppm corresponding to rigid domains and surface confined polymer chains (Figure 4.17). The relative areas calculated by the integration of these lines are summarized in Table 2.

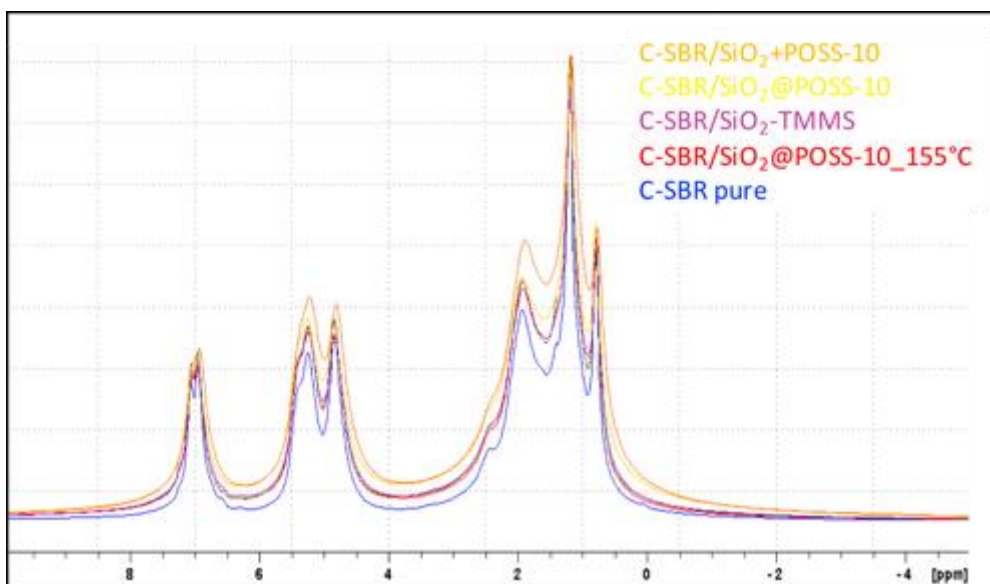


**Figure 4.17:** Magnification of  $^1\text{H}$  MAS NMR spectra of cured SBR and SBR nanocomposites

**Table 4.2:** Line-widths and areas obtained by simulation of  $^1\text{H}$  NMR spectra of SBR nanocomposites

Sample	7.1 ppm		5.4 ppm		1.3 ppm		4.6 ppm	
	linewidth	Area%	linewidth	Area%	linewidth	Area%	linewidth	Area%
C-SBR pure	800	0.14	1000	0.27	1200	0.44	12000	0.15
C-SBR/SiO <sub>2</sub> @POSS_155°C	800	0.04	1500	0.21	1600	0.39	13500	0.36
C-SBR/SiO <sub>2</sub> -TMMS	900	0.04	1600	0.20	1600	0.38	13500	0.38
C-SBR/SiO <sub>2</sub> @POSS-10	1000	0.03	1800	0.17	1800	0.31	19000	0.48
C-SBR/SiO <sub>2</sub> +POSS-10	1300	0.03	2200	0.16	2300	0.31	19000	0.50

The results confirm that SBR pure represents the most mobile system, since polymer segments with restricted mobility represent less than 15% (see area of the signal at 4.6 ppm).

By adding SiO<sub>2</sub>-TMMS to SBR (i.e. C-SBR/SiO<sub>2</sub>-TMMS composite), the fraction of rigid fraction considerably increases up to 38%, indicating the presence of surface confined polymer chains.

C-SBR/SiO<sub>2</sub>+POSS-10 and C-SBR/SiO<sub>2</sub>@POSS-10 nanocomposites exhibit the most extensive immobilization of polymer chains. This is reflected by the broadening of all the signals (see Fig. 4.17) as well as by the highest fraction of completely immobilized segments (relative area of ~ 50 %, Table 4.2).

The above outcomes are in agreement with the morphological and cross-link density properties of the composites.

In particular, C-SBR/SiO<sub>2</sub>@POSS-10 sample exhibits a tight filler network in which thin rubbery regions connect the NPs aggregates (cfr. TEM investigation in section 4.7). This may favor an enhanced immobilization of rubber chains in proximity to the NPs surface, as assessed by NMR, inducing a high degree of cross-linking density.

For C-SBR/SiO<sub>2</sub>+POSS-10, it must be observed that, though the results of crosslinking density show a lower reticulation degree for this sample compared to C-SBR/SiO<sub>2</sub>@POSS-10 nanocomposites, <sup>1</sup>H NMR reveals the highest fraction of immobilized polymer chains (see Table 1). This controversial result may be explained considering that the amount of POSS nanounits effectively grafted onto the silica surface in SiO<sub>2</sub>@POSS (see Solid State NMR investigation of fillers) is lower in comparison to that present during the mixing procedure for preparing C-SBR/SiO<sub>2</sub>+POSS-10 sample. It can be inferred that actually in C-SBR/SiO<sub>2</sub>@POSS-10 a remarkable fraction of polymer chains with restricted mobility can be achieved by using very low loadings of POSS,

thus envisaging promising mechanical properties for this nanocomposite (see Chapter 5).

Finally, a lower restricted mobility (i.e low polymer chains rigidity) has been determined for SBR/SiO<sub>2</sub>@POSS-10 sample cured at 155°C for 10 min compared to that cured at the conventional temperature of 170°C. This is in agreement with the mechanism proposed for the network formation in SBR/SiO<sub>2</sub>@POSS nanocomposites (see Scheme 4.1).

In fact, at 155°C (i.e before DCP temperature activation), the crosslinking between the methacryl groups of Octa POSS in SiO<sub>2</sub>@POSS hybrid filler and rubber chains is weak, due to the ineffective activation of dicumylperoxide. As a consequence, the network formation is hindered and very poor interfacial adhesion is detected (cfr. SEM and AFM investigations). As a consequence, a lower rubber chains immobilization is observed for these samples.

## 4.3 Characterization of SH-NBBs

### 4.3.1 FT-IR spectroscopy

The different structure of the SH-NBBs in terms of fraction of cage and ladder-like units, was evaluated by FT-IR and reports in Figure 4.18.

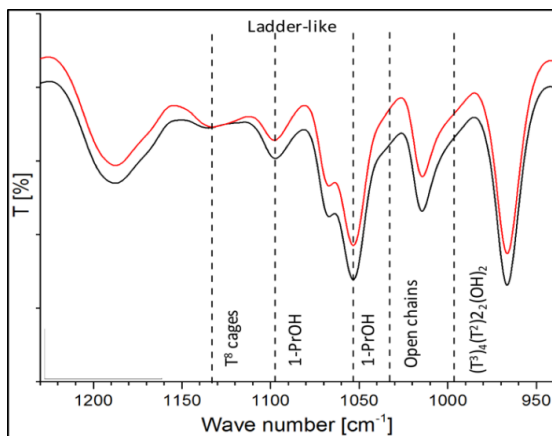


**Figure 4.18:** FT-IR spectra of a) Pure SH-NBB\_30h (black line) and 80h (red line)

As reported by Borovin et al<sup>71,72,86</sup>, the spectra of pure SH-NBBs (Figure 4.18) display intense and broad bands in the region between 950 and 1200  $\text{cm}^{-1}$  attributable to the Si–O–Si stretching vibrations. In detail, the band at 1033  $\text{cm}^{-1}$  is assigned to open chains while those between 1040 and 1140  $\text{cm}^{-1}$  can be attributed to  $(\text{T}^1)_2(\text{OH})^4$  and ladder-like species, respectively. The band at 996  $\text{cm}^{-1}$  is instead attributable to  $(\text{T}^3)_4(\text{T}^2)_2(\text{OH})^2$  open cages. Finally, the band centered at 1135  $\text{cm}^{-1}$  can be attributed to  $\text{T}^8$  cage-like species. Unfortunately, the presence of intense bands at 1097 and 1053  $\text{cm}^{-1}$  associated to 1-propanol (reaction solvent) makes complicate a careful spectra analysis.

However, despite weak difference in terms of intensity, the spectra of SH-NBBs\_30h and SH-NBBs\_80h are quite similar and it is difficult to observe a preferential formation of cage-like compared to ladder-like structures. The only significant differences were the slight increase in intensity of the T<sup>8</sup> cage band in the SH-NBBs\_80h in comparison with SH-NBBs\_30h which included a higher fractions of cages units.

To sup up, these results are not conclusive and have to be confirmed in order to prove the different structure of SH-NBBs\_30h compared to SH-NBBs\_80h.

For this reason, in order to follow the evolution of the pristine McPTMS and SH-NBBs growth along the reaction time, <sup>29</sup>Si NMR spectra were acquired.

#### **4.3.2 NMR investigation of pure SH-NBBs**

As reported by Borovin et al<sup>71,72,86</sup>. the Si network structural features can be tuned by simply controlling the duration of the reaction. The number of different Si-based monomer species that theoretically can be formed due to both transalcoholysis and hydrolysis reactions is ten, and all of them may be identified by the high resolution <sup>29</sup>Si NMR. The main problems in silicon nucleus observations with NMR are that the natural abundance of <sup>29</sup>Si isotope is only 4,67%, and the T<sup>1</sup> relaxation times in liquid are quite long (starting from 5s); thus the experimental time needed for reasonable S/N ratio spectra acquisition can exceed the time after which the subjected system changes. So, the in depth analysis of fast reacting system by means of <sup>29</sup>Si NMR is possible only if

polarization transfer from abundant nucleus as proton to less receptive silicon is exploited.

Distortionless Enhancement by Polarization Transfer (DEPT) is an experiment that utilizes a polarization transfer from one nucleus to another to increase the signal strength of the second nucleus. The polarization transfer occurs from a nucleus with a relatively larger gyromagnetic ratio  $\gamma$  ( $^1\text{H}$ ) than the one of the analyzed nucleus ( $^{13}\text{C}$  or  $^{29}\text{Si}$ ). DEPT is much more sensitive than a regular pulse experiment. Furthermore, the repetition rate is governed by the relaxation times of the protons and not by those of the second nuclei. Since proton relaxation times are the shortest, the period of time to allow magnetic equilibration (recycle delay) is much shorter than in Single Pulse sequence. This translates to an improved signal-to-noise (S/N) per unit time for DEPT over a regular Single Pulse NMR experiment.

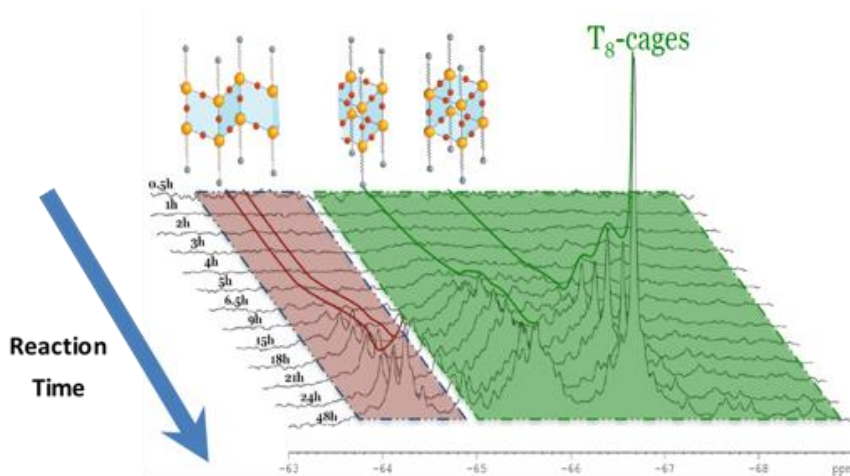


**Figure 4.19:**  $^{29}\text{Si}$  DEPT spectra of SH-NBBs versus reaction time at  $100^\circ\text{C}$ <sup>27</sup>

Figure 4.19 showed the T signals of  $^{29}\text{Si}$  DEPT spectra of SH-NBBs versus reaction time at  $100^\circ\text{C}$ . The  $\text{T}^3$  region, presented on the Figure 4.19 can be divided into 3 separated groups of peaks. The most high-field shifted, centered at  $-66.7$  ppm (green line) starts to rapidly develop after 6.5 hours of reaction. This signal sharpened dramatically around 15 hours of reaction, suggesting that amount of closed  $\text{T}^8$  cages rapidly increased. The two sharp peaks at  $-64.1$  ppm and  $-64.25$  ppm (red lines) are attributed to the ladder-like species, made of different number of cycles. They begin to appear on the spectra at the same time with  $\text{T}^8$  cages (15 hours), but do not demonstrated similar rapid growth<sup>86</sup>.

Finally, figure 4.20 showed the possible architecture of SH-NBBs after 48 and 72 hours of reaction.

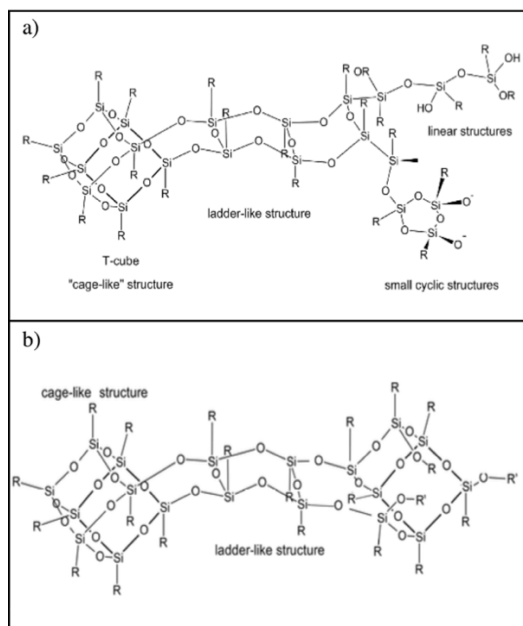


**Figure 4.20:** Possible architectures of SH-NBBs<sup>27</sup>, reacted more than a) 48 hours and b) 72 hours;  $\text{R}=(\text{CH}_2)_3\text{SH}$

NMR spectroscopy results confirmed a preferential formation of cage-like compared to ladder-like structures and the narrowing of the species distribution over long reaction times. In the next paragraph, the effect of different structure (ladder/cage) of the SH-NBBs on the thermal properties of the nanocomposites will be evaluated by IR and TGA. Moreover, the filler-polymer interaction and the role of the different SH-NBBs architecture will be studied in detail with Solid State NMR and compared with the crosslinking density results.

## **4.4 Characterization of PB/SH-NBBs Nanocomposites**

### **4.4.1 FT-IR spectroscopy**

The effective incorporation of SH-NBBs (Scheme 4) in the polymer matrix was preliminary checked by FT-IR spectroscopy.

Figure 4.21a shows the IR spectra after the incorporation of the SH-NBB\_80h with different loading in the polymer matrix. In the region between 900-1200  $\text{cm}^{-1}$  has been observed a general increasing of typical bands of n Si-O-Si improving the SH-NBBs loading, suggesting a possible interactions between SH-NBBs units and polymer chains. Moreover, the characteristic stretching vibration of C=C double bonds band in SH-NBBs was identified by a broad band centered at 1656  $\text{cm}^{-1}$  (Inset Figure 4.21a). This absorption decreases in intensity in the PB/%NBB nanocomposites, confirming an effective functionalization of the SH-NBBs with the polymer matrix. A similar FT-IR investigation has been performed for PB/1%NBB\_30h and PB/3%NBB\_30h (spectra not shown)<sup>26</sup>.

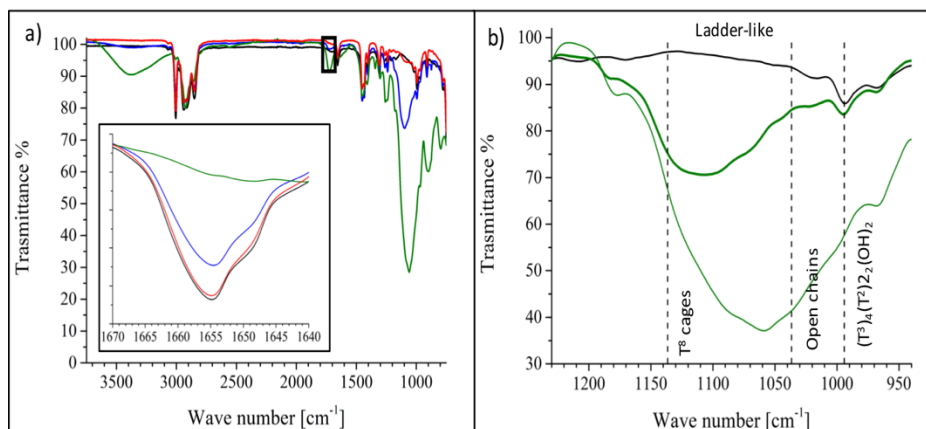


**Figure 4.21.** FT-IR spectra of a) Pure Polybutadiene (black solid line), PB/1%NBB\_80h (red line), PB/3%NBB\_80h (blue line) and PB/10%NBB\_80h (green line). Inset: magnification of C=C double bonds band and b) Pure Polybutadiene (black solid line), PB/10%NBB\_80h (green line) and PB/10%NBB\_30h (light green line)

Figure 4.21b reports the FT-IR spectra of PB nanocomposites loaded with 10wt. % of SH-NBBs synthesized with different reaction times (30h and 80 h). Small differences may be observed in the region between 1050 and 1150  $\text{cm}^{-1}$ . In particular, it seems that PB/NBB\_30h (light green line) display more intense signals in the region of ladder-like structures (1150-1050  $\text{cm}^{-1}$ ) compared to PB/NBB\_80h (green line)<sup>86</sup>. Moreover, in the PB/NBBs\_80h (Fig 4.21b green line) nanocomposites may be observed a slight increase and shift of the peak centered at 1135  $\text{cm}^{-1}$  attributable to the T<sup>8</sup> cage band in comparison with PB/NBBs\_30h<sup>26</sup>.

The results, beyond indicating the effective incorporation of the SH-NBBs within the polymer matrix, suggest a different interaction of these nanounits with the polymer chains.

These outcomes seem to envisage an effect of the SH-NBBs architecture on the composites properties, i.e. a better filler-polymer interaction achievable by incorporating SH-NBBs units in polybutadiene with a higher cages/ladder-like ratio.

However, further investigation on the properties of the composites are mandatory to support this hypothesis (see NMR investigation), and in particular to evaluate the role of the SH-NBBs structure in upgrading their mechanical properties.

#### **4.4.2 Thermogravimetric analysis (TGA)**

The effect of SH-NBBs incorporation in PB on the thermal stability of the resulting nanocomposites has been investigated by thermogravimetric analysis (TGA).

Figure 4.22a shows the weight loss curves obtained for pure PB and for PB/%NBB\_80h nanocomposites. All the samples show an initial weight loss beginning at nearly 350°C and continuing until 400°C. From 400°C to 500°C, a second and more evident weight loss occurs, which is less remarkable as the loading of SH-NBBs in the composites increases and become maximum for the composite enclosing 10 wt.% of filler. This indicates an increased thermal stability of the polymer matrix after the incorporation of the SH-NBBs. Similar results were obtained for PB/%NBB\_30h nanocomposites.

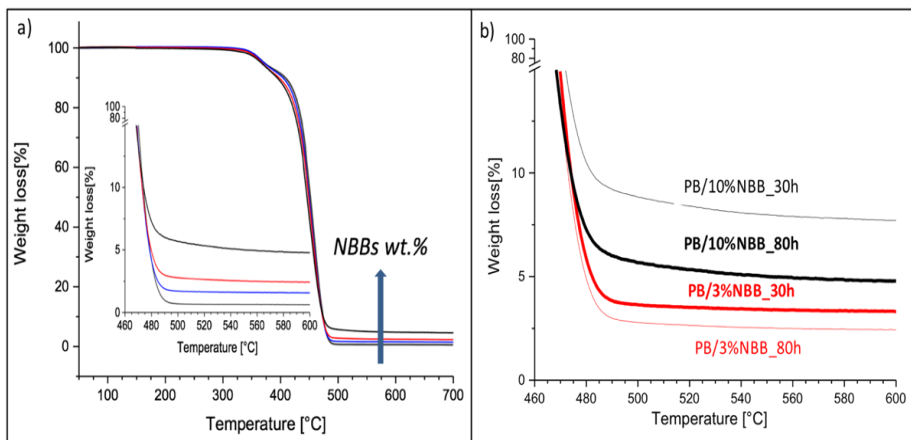


**Figure 4.22:** TGA curves of a) pure PB (light black line), PB/1%NBB\_80h (blue line) and PB/3%NBB\_80h (red line) and PB/10%NBB\_80h (black line) and b) effect of the SH-NBBs structure on the thermal properties on the nanocomposites

Figure 4.22b reports the TGA curves of PB nanocomposites loaded with 3 and 10wt. % of SH-NBBs synthesized with different reaction times (30h and 80 h). Although the curves of PB/3%NBB\_30h and PB/3%NBB\_80h samples appear superimposable until 500°C, small differences can be observed at higher temperatures. However, no clear indications about the role of the SH-NBBs architecture can be inferred from the TGA curves.

### 4.4.3 Swelling experiments

Swelling experiments were performed on PB/%NBB nanocomposites, in order to evaluate the cross-linking induced by the introduction of SH-NBBs nanounits. In detail, cross-linking density ( $\nu$ ) values were determined according to the Flory-Rehner equation<sup>106,107</sup> and the results are summarized in Figure 4.23.

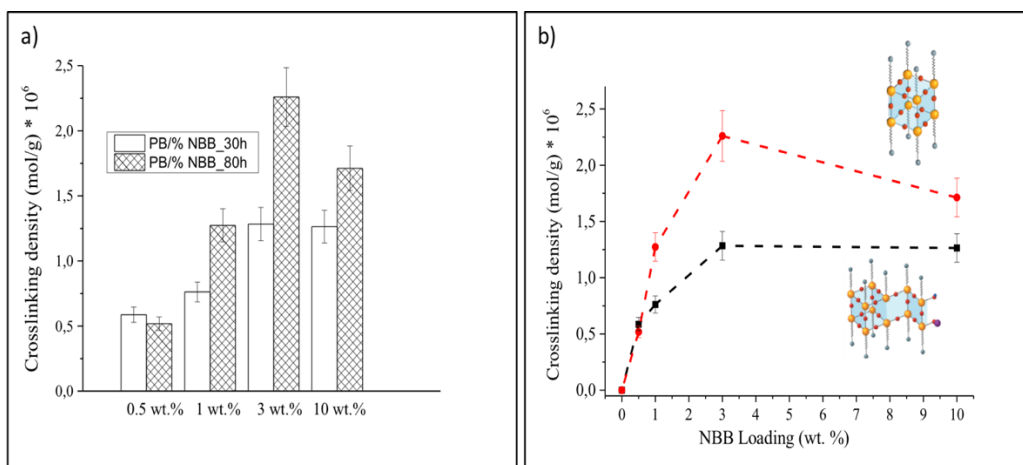


**Figure 4.23:** a) Comparison between the cross-linking density values of PB/%NBB nanocomposites synthesized with different reaction times; b) Trend of the cross-linking density as a function of SH-NBBs loadings for PB/%NBB\_30h (black line) and PB/%NBB\_80h (red line). Insets in b) show the molecular architecture corresponding to NBB\_30h (bottom) and NBB-80h (top), respectively.

For both PB/%NBB\_30h and PB/%NBB\_80h nanocomposites the  $\nu$  values generally increase with the SH-NBBs amount and are very similar at the lowest filler loadings (i.e. for 0.5 and 1 wt. %, see Fig. 4.23a), Interestingly, the reticulation degree becomes remarkably

different for PB/3%NBB\_30h and PB/3%NBB\_80h nanocomposites (Fig. 4.23).

In fact, as clearly showed by Fig. 4.23b, the crosslink density is significantly higher and reach a maximum for the sample enclosing 3 wt.% of SH-NBB\_80h units which possess a larger fraction of cages in their molecular structure (see inset in Fig. 4.23b). At higher loading (i.e. 10wt.%) PB/NBB\_30h and PB/NBB\_80h nanocomposites show a depletion of the cross-linking density values. This effect may be correlated to aggregation among the SH-NBBs units which generally takes place when the filler volume fraction in a nanocomposite becomes relatively high.

These results again suggest a key role of the SH-NBBs architecture in influencing the filler-polymer interactions and seem to indicate that nanocages, thanks to their high number of tunable functionalities concentrated on the same small unit, may provide improved chemical or physical interactions at the polymer-NBBs interface, thus enhancing the nanocomposite performances.

#### **4.4.4 NMR investigation of PB/%NBBs nanocomposites**

In order to get deeper insights into the nature of polymer-filler interactions, and clarify the importance of cage/ladder structures on the polymer chain dynamics, preliminary  $^1\text{H}$  MAS NMR spectra were collected for nanocomposites enclosing SH-NBBs synthesized with different reaction times (20h, 30h and 80h) and therefore with different molecular architecture. The experiments have been

performed in the laboratory “Klaus Müller” in the University of Trento in collaboration with Dr. Emanuela Callone and Prof. Sandra Dirè.

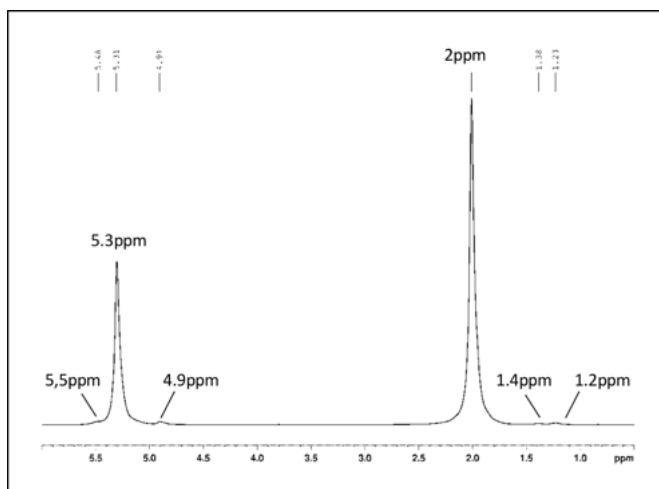
### **<sup>1</sup>H MAS NMR results**

Figure 4.24 shows the pure polybutadiene proton spectrum. It presents two intense signals due to olefinic (5.3 ppm) and aliphatic protons (2 ppm). They are the fingerprint of a bulk PB without crystalline fractions. It is possible to identify other minor resonance at 5.5, 4.9, 1.4 and 1.2 ppm attributable to non-terminal 1,2 olefinic, terminal 1,2 olefinic and 1,2 methylene protons, respectively. The width of the signals in the solid state is too large for allowing identification and quantification of the *cis* and *trans* protons ( $\Delta\delta = 0.05$  ppm in the liquid state)<sup>24-27</sup>.

These features have been observed also for PB/%NBB nanocomposites. Interestingly, an in depth inspection on the spectra reveals differences in the line-widths of the signals recorded for the different samples. In particular, increasing either the loading or the reaction times of SH-NBBs, a small up-field shift and a right shoulder gradually arise in the signals of both olefinic and aliphatic protons (Fig. 4.25). Although, the peaks of PB/3%NBB\_20h and PB/3%NBB\_30h (green and red lines, respectively) appear essentially superimposed, displaying only a small variation in the shoulder intensity, the differences become remarkable comparing the spectral features of these composites to those of PB/3%NBB\_80h (blue line).

This suggests the occurrence of conformational changes in the PB, e.g. different packing and reduced mobility of rubber chains, as different

loadings of SH-NBBs with different molecular architecture are introduced in the polymer matrix.



**Figure 4.24.**  $^1\text{H}$  MAS NMR spectrum of pure polybutadiene

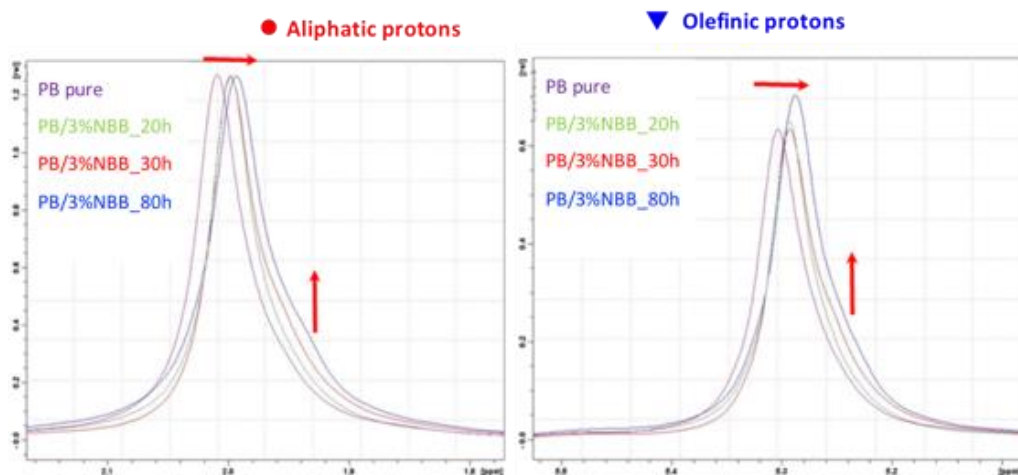


**Figure 4.25:**  $^1\text{H}$  MAS NMR spectra of PB pure, PB/3%NBB\_20h, PB/3%NBB\_30h and PB/3%NBB\_80h. Magnification of aliphatic protons (left-side) and olefinic protons (right-side).

To obtain more precise data about segmental dynamics and to estimate the fraction of immobilized polymer segments in the prepared systems, spectra were analyzed in detail and both olefinic and aliphatic protons signals were simulated by: two narrow lines at, 5.31 and 2.01 ppm, which represent the flexible fractions, whereas two broader components (i.e. the weak shoulder observed in the signals) at 5.27 and 1.97 ppm probably corresponding to rigid domains. The relative areas calculated by the integration of these lines are summarized in Table 4.2.

A trend of the signals area not only related to the SH-NBBs loading but, more interestingly, also to their reaction times has been obtained (Fig. 4.25). This envisages an effect of the different molecular architecture of SH-NBBs (cage/ladder ratio) on the polymer chain dynamics.

In particular, increasing the cages/ladder ratio in SH-NBBs the shoulder area in the signals increases (Fig. 4.26), becoming highest for PB/1%NBB\_80h and PB/3%NBB\_80h enclosing SH-NBBs with a prevalence of cage units in their molecular structure. These results suggest that nanocages, may really provide effective chemical or physical interactions at the polymer-SH-NBBs interface, resulting in a restricted polymer chains mobility.

This is in agreement with the swelling experiments, showing crosslink density values significantly higher for PB/3%NBB\_80h containing fillers which possess a larger fraction of cages in their molecular structure.

However, further investigation (e.g. Time Domain NMR) are necessary in order to define clear relations among SH-NBB architecture,

molecular structure and restricted chains mobility of the polymeric host.

**Table 4.3:** Areas obtained by simulation of  $^1\text{H}$  NMR spectra of olefinic and aliphatic protons in PB/%NBB nanocomposites

$\delta$ (ppm)	olefinic		aliphatic	
	5.31	5.27	2.01	1.97
sample	Rel.Area%	Rel.Area%	Rel.Area%	Rel.Area%
PB	81.9	18.1	81.1	18.9
PB/1%NBB_30h	82.7	17.3	81.9	18.1
PB/1%NBB_80h	77.3	22.7	77.4	22.6
PB/3%NBB_30h	77.6	22.4	80.3	19.7
PB/3%NBB_80h	75.4	24.6	74.0	26.0

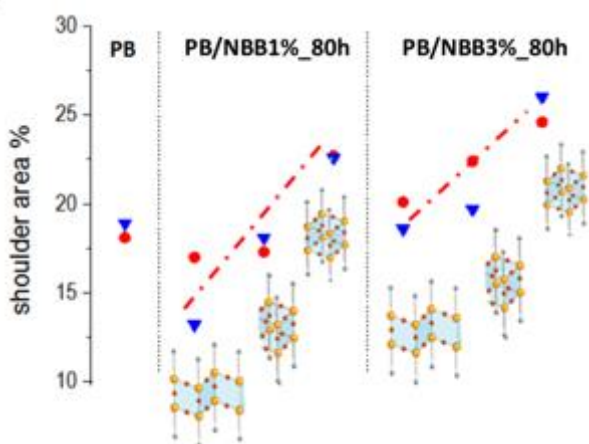


**Figure 4.26:** Effect of the different molecular architecture of SH-NBBs (cage/ladder ratio) on the polymer chain dynamics

In conclusion, the experimental data achieved confirm the importance of the SH-NBBs molecular architecture in determining the properties of the resulting nanocomposites.



## Chapter 5

### Results: dynamic-mechanical properties of SBR nanocomposites

This chapter is dedicated to the discussion of the dynamic-mechanical properties of nanocomposites whose preparation, morphology and chemical properties are described in Chapter 3 and 4. In the first part, the mechanical properties of both cured and uncured SBR/SiO<sub>2</sub>@POSS and SBR/SiO<sub>2</sub>+POSS nanocomposites have been firstly evaluated with an Oscillating Disk Rheometer (ODR) operating in shear mode. Successively, dynamo-mechanical thermal analysis (DMTA) have been also performed on the cured samples. Finally, an in depth investigation of the tensile properties of nanocomposites has been reported, in order to further shed light on the effects of the POSS incorporation on rubber nanocomposites properties, by evaluating their behaviour also under high deformation conditions.

## **Dynamic-mechanical properties of SBR nanocomposites**

### **5.1 Evaluation of the rheological properties of rubber nanocomposites by ODR (Oscillating Disk Rheometry)**

A forced oscillating-disk rheometer can measure both the low and high frequency dynamic properties of a rubber specimen throughout vulcanization. It may be used also to measure the rheological properties of unvulcanized polymers. The instrument consists of a cone-shaped disk which is embedded in the rubber specimen and oscillated through a small angle while the specimen is heated under pressure. Both stress and strain in terms of torque and displacement, respectively, are measured by appropriate transducers and recorded on an oscillograph. Provisions are made for changing both frequency

and strain. At low frequency, the instrument is a convenient tool for determining all of the curing parameters of a rubber specimen. At high frequencies, the change in the dynamic properties of a rubber specimen throughout vulcanization may be continuously followed<sup>97</sup>.

In the present study, the mechanical performance of all uncured and cured composites in terms of reinforcement were determined by ODR and compared to those of the composites prepared without POSS (i.e. SBR/SiO<sub>2</sub>@POSS-0 and SBR/SiO<sub>2</sub>+ POSS-0 samples), in order to evaluate the effect of POSS nanocages on the final materials properties.

The trends of the storage modulus ( $G'$ ) as a function of strain, for uncured SBR/SiO<sub>2</sub>@POSS-X and C-SBR/SiO<sub>2</sub>@POSS-X rubber composites (Curing:170°C for 10 min), are reported in Figure 5.1.

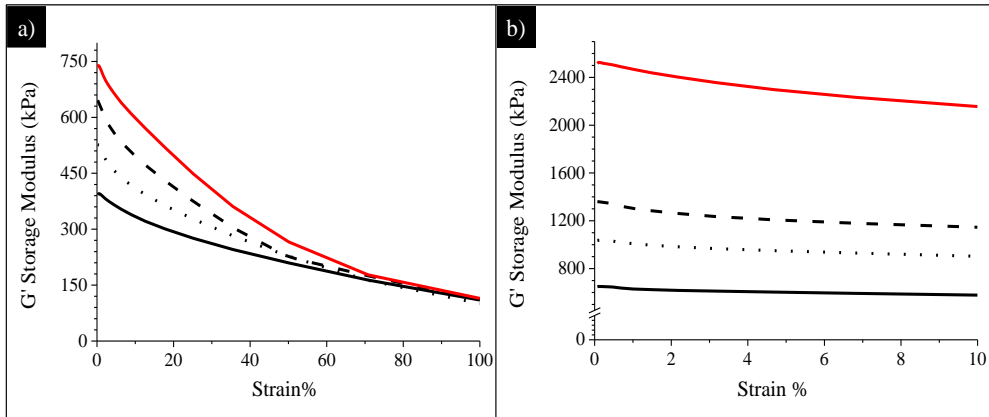


**Figure 5.1.** Storage modulus  $G'$  vs strain of a) SBR-SiO<sub>2</sub>@POSS-X and b) C-SBR-SiO<sub>2</sub>@POSS-X composites: X = 0 (i.e. SiO<sub>2</sub> 30 phr, black line), X = 3 (dotted line), X = 5 (dashed-line) and X = 10 (red line).

Before curing (Fig. 5.1a), the anchoring of POSS nanounits onto SiO<sub>2</sub> NPs, even in low amount (3 phr), leads to a significant increase of the

modulus at low strain ( $G'_0$ ) if compared to SBR/SiO<sub>2</sub>@POSS-0. Following the widely accepted mechanistic interpretation that the Payne effect is related to the breakdown of filler network upon oscillatory shear<sup>16</sup>, the higher  $G'_0$  values obtained in the presence of SiO<sub>2</sub>@POSS hybrid particles point out a greater reinforcing effect. This behavior may be connected to the peculiar filler networking in SBR/SiO<sub>2</sub>@POSS composites, where compact micrometric agglomerates are inhomogeneously distributed within the rubbery matrix, generating regions in which rubber is constrained (see Chapter 4, Fig 4.2). These features provide on one hand remarkable filler-filler interactions (i.e. high  $G'_0$  values) and, on the other, may favor the interaction between polymer and filler albeit weak before curing.

At the highest deformation, the modulus ( $G'_\infty$ ) resulted very similar for all the composites (Fig. 5.1a), regardless the POSS loading. This means that the differences in reinforcement are less effective once the network is broken down. Usually, at high strain, only a particular surface reactivity can originate different mechanical characteristics of the samples, as the particles are supposed to be not mutually interacting. In the present case, the trend observed for SBR/SiO<sub>2</sub>@POSS-X samples may be connected to the presence of POSS methacryl functionalities which, before the DCP curing activation, are not able to chemically interact with the polymer chains.

The impact of POSS introduction on the mechanical properties of uncured SBR/SiO<sub>2</sub>@POSS-X and SBR/SiO<sub>2</sub>+POSS-X composites was also

studied by monitoring the dependence of the loss modulus ( $G''$ ) on the strain (Fig 5.2) <sup>111,112</sup>.

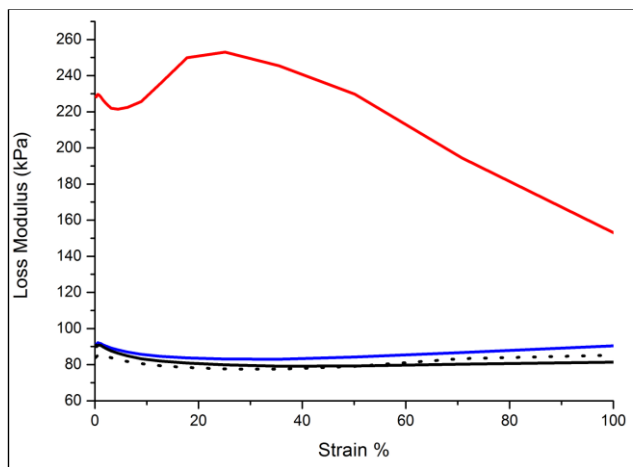


**Figure 5.2:** Loss modulus  $G''$  vs strain of uncured a) SBR/SiO<sub>2</sub>@POSS (red line), SBR/SiO<sub>2</sub>+POSS (blue line), SBR/SiO<sub>2</sub>@POSS-0 (black line) and SBR/SiO<sub>2</sub>-TMMS (dot-dashed line) nanocomposites.

$G''$  is connected to the rates of network breakdown and re-assembly. In general, at low strain the network is still able to reorganize after each deformation, and the composite shows a behavior which affects the  $G''$  values. Instead, at high deformations, the strain amplitude is high enough to destroy the filler network, and the influence on  $G''$  becomes negligible<sup>113</sup>. Thus, loss modulus curves vs strain allow to identify the maximum strain at which the composite is able to withstand to the mechanical solicitation without fracture of the filler network. The higher are the  $G''$  values and the strain at which  $G''$  is maximum, the more compact is the network. In the investigated composites, SBR/SiO<sub>2</sub>@POSS-10 shows a broad maximum at strain

located at  $\sim 30\%$  and the highest  $G''$  values, while SBR/SiO<sub>2</sub>+POSS-10 and the composites without POSS display lower loss modulus and maxima located at strain  $< 10\%$  (Fig 5.2). These issues endorse the ability of SiO<sub>2</sub>@POSS particles in promoting the formation of a compact particle network which enclose rubbery regions, as assessed by TEM investigation (Fig. 5a, c).

After curing (170°C; 10 min, Fig. 5.1b), a marked increase of the modulus either at low or at high strain, i.e. a considerable decrease of the Payne effect, was observed for all the composites. This was much more relevant for the samples containing POSS nanounits and increases as a function of their concentration, resulting in the highest  $G'_0$  and  $G'_\infty$  values for the C-SBR/SiO<sub>2</sub>@POSS-10 nanocomposite. In general, these issues can be associated to the DCP action, which initiates the reaction between POSS methacryl groups and rubber vinyl functionalities, leading to an effective cross-linking<sup>104</sup>. More in depth, the moduli improvement and the reduced hysteresis in C-SBR/SiO<sub>2</sub>@POSS-X can be discussed in terms of polymer interactions with the silica NPs network.

As evidenced by TEM images, SiO<sub>2</sub>@POSS filler is constituted by silica aggregates which are partially connected and surrounded by a thin POSS amorphous shell. Thus, it can be argued that the cross-linking action promoted by the nanocages functionalities is localized on the surface or even inside the SiO<sub>2</sub> aggregates. This may cause an enhanced immobilization of the polymer chains near the NPs surface or within their network, upgrading the mechanical reinforcement of

the composites. These ideas are sustained by the morphology of the C-SBR/SiO<sub>2</sub>@POSS-10 composite, where thin rubbery regions connect the filler aggregates (see Chapter 4, Fig 4.2a and c), by the enhanced interfacial adhesion observed by SEM (Chapter 4, Fig 4.4) and also by the higher degree of cross-linking for C-SBR/SiO<sub>2</sub>+POSS-X revealed by swelling.

The mechanical behaviour of SBR/SiO<sub>2</sub>@POSS-X, both uncured and cured, were compared to those of SBR/SiO<sub>2</sub>+POSS-X composites, in order to highlight the role of the hybrid fillers NPs in providing enhanced functional properties and to understand to which degree the hybrid filler properties could be obtained by in-situ mixing. In particular, figure 5.3 reports the  $G'$  vs strain plots for SBR/SiO<sub>2</sub>@POSS-10 and SBR/SiO<sub>2</sub>+POSS-10 nanocomposites. Before curing, the  $G'_{\infty}$  values resulted very similar for all the composites (Fig. 5.3a). Instead, while no significant differences were detected between SBR/SiO<sub>2</sub>+POSS-10 and its reference sample SBR/SiO<sub>2</sub>+POSS-0, a high  $G'_0$  was measured for the composite prepared with the hybrid filler. As described above, the performance of SBR/SiO<sub>2</sub>@POSS-10 can be attributed to the compact filler network generated by SiO<sub>2</sub>@POSS NPs within the polymer matrix.

The DCP curing leads to an expected decrease of the Payne effect for all the composites, as a result of the modulus increase either at low or at high strain (Fig. 5.3b). In general, both C-SBR/SiO<sub>2</sub>@POSS-10 and C-SBR/SiO<sub>2</sub>+POSS-10 display outstanding reinforcement and much lower Payne effect in comparison to the composites containing exclusively

silica and TMMS. Similar trends have been obtained for the composites with lower POSS loadings. These results point out that the introduction of low amount of OctaMethacrylPOSS in rubber composites of silica silanised with methacryl silane cured with DCP provides mechanical properties which are significantly superior that those commonly reported in the literature<sup>104</sup>.

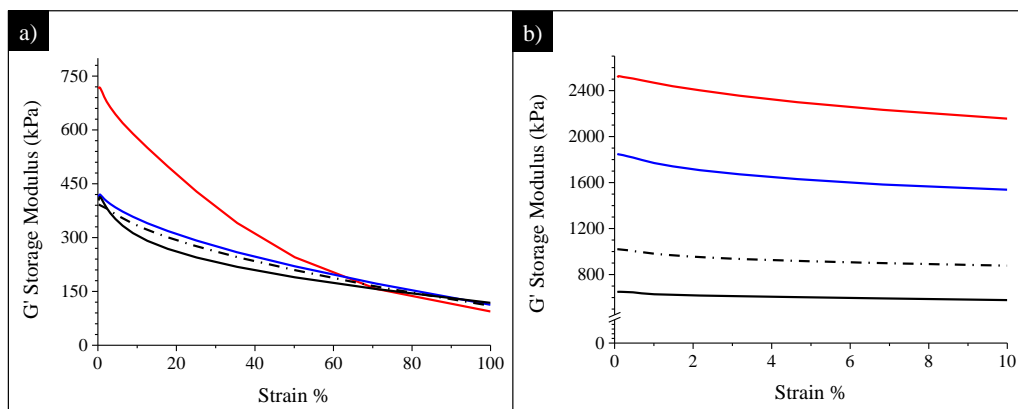


**Figure 5.3.** Comparison among a) uncured and b) cured SBR/SiO<sub>2</sub>@POSS (red line), SBR/SiO<sub>2</sub>+POSS (blue line), SBR/SiO<sub>2</sub>@POSS-0 (black line) and SBR/SiO<sub>2</sub>-TMMS (dot-dashed line) nanocomposites.

However, it must be observed that C-SBR/SiO<sub>2</sub>@POSS-10 exhibits better performance than C-SBR/SiO<sub>2</sub>+POSS-10 nanocomposite. The higher capability of the hybrid nanofiller in upgrading the reinforcement and remarkably decreasing the hysteretical losses may derive from the peculiar surface functionalization with POSS nanounits which, through the high number of reactive functionalities, promote an enhanced networking and the formation of “sticky regions” among the

silica aggregates, immobilizing both filler and rubber, and affording a relevant increase of the mechanical properties.

In C-SBR/SiO<sub>2</sub>+POSS, POSS units are likely grafted to silica NPs with lower efficiency (as compared to C-SBR/SiO<sub>2</sub>@POSS and only during the curing process: the POSS influence still appears significant, though to a lesser extent than in C-SBR/SiO<sub>2</sub>@POSS. We suggest that, in this case, POSS nanounits may interact again with the filler exerting their cross-linking close to the filler surfaces and contributing to the networking, but direct interaction among “free” POSS nanounits and polymer chains may also occur. This lead to the presence of more dispersed and less compact filler aggregates (see Chapter 4, TEM images), and to a lower cross-linking density, resulting in a partial depletion of the functional properties of the composites.

## **5.2 Temperature dependent dynamic-mechanical analysis (DMTA)**

In order to get deeper insights into the influence of the peculiar structure of the SiO<sub>2</sub>@POSS hybrid filler on the mechanical properties of the resulting composites, DMTA analysis was carried out on cured C-SBR/SiO<sub>2</sub>@POSS-10 and C-SBR/SiO<sub>2</sub>+POSS-10 samples (Curing:170°C for 10 min).

Moreover, the results were compared to those obtained by performing the same experiments on pure SBR and SBR/SiO<sub>2</sub>-TMMS nanocomposite.

The experiments have been performed in the laboratory of Institute of Macromolecular Chemistry of Prague in collaboration with Prof. Libor Matejka.

The trend of the  $G'$  vs temperature for SBR nanocomposites is reported in Figure 5.4a.

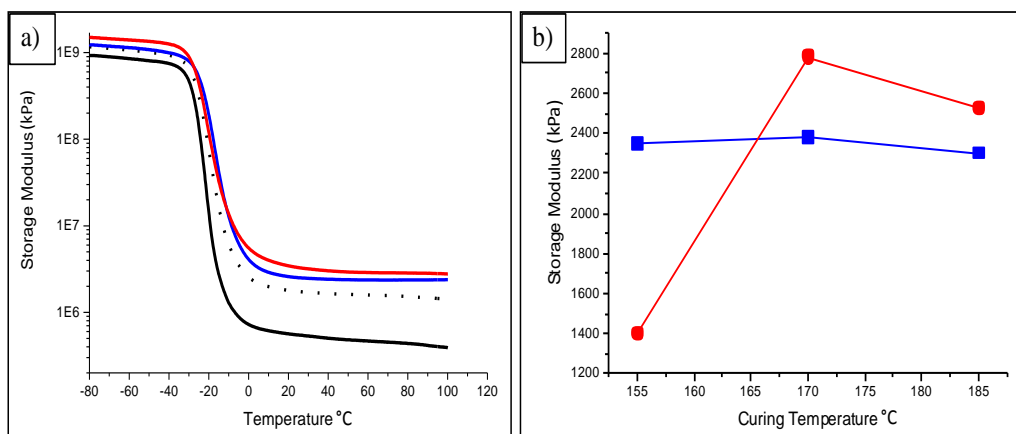


**Figure 5.4:** a) Plot of storage modulus  $G'$  vs. temperature for C-SBR/SiO<sub>2</sub>@POSS-10 (red line), C-SBR/SiO<sub>2</sub>+POSS-10 (blue line), C-SBR/SiO<sub>2</sub>-TMMS (dotted line) and pure C-SBR (black line) nanocomposites. b) Trend of  $G'$  values as a function of the curing temperature for SBR/SiO<sub>2</sub>@POSS-10 (red-line) and SBR/SiO<sub>2</sub>+POSS-10 (blue-line) nanocomposites. (Curing time: 10 min).

In agreement with ODR measurements (see Section 5.1), both C-SBR/SiO<sub>2</sub>@POSS-10 and C-SBR/SiO<sub>2</sub>+POSS-10 display in the rubbery

state higher modulus in comparison to SBR and to the composites containing exclusively silica and TMMS. Moreover, it must be observed that C-SBR/SiO<sub>2</sub>@POSS-10 exhibits better performance than C-SBR/SiO<sub>2</sub>+POSS-10 nanocomposite. This again points out the better capability of the hybrid nanofiller in upgrading the mechanical properties of SBR.

As extensively reported in Chapter 4, the filler networking and distribution and, in turn, the interfacial adhesion and rubber immobilization in these composites are clearly influenced by the curing with DCP. For this reason, DMTA analysis have been also performed on SBR/SiO<sub>2</sub>@POSS-10 and SBR/SiO<sub>2</sub>+POSS-10 nanocomposites cured at 155°C, i.e. under the conditions where dicumylperoxide is in principle less reactive and at 185°C, i.e. the temperature at which the peroxide is surely reacting and the curing is rather complete always cured for 10 min.

The obtained results are summarized in Fig. 5.4b, which shows the trend of the storage modulus for SBR/SiO<sub>2</sub>@POSS-10 and SBR/SiO<sub>2</sub>+POSS-10 nanocomposites as a function of the curing temperature.

At 155°C, for SBR/SiO<sub>2</sub>@POSS-10 composites (red-line in Fig 5.4b), the ineffective DCP activation prevents the network formation, limiting the extent of crosslinking and leading to weak filler–rubber interactions, i.e low adhesion (cfr. SEM and AFM investigation, Chapter 4) and small fraction of rigid polymer chains, as assessed by NMR (cfr. Chapter 4). This results in a very low  $G'$  value and thus in poor mechanical

properties, even worse than those of SBR/SiO<sub>2</sub>+POSS-10 (Fig. 5.4b, blue-line) cured at the same temperature.

At the highest curing temperatures (i.e. 155°C and 185°C), the activation of methacryl groups of both POSS and TMMS induced by the peroxide, promotes the crosslinking between SiO<sub>2</sub>@POSS hybrid filler and polymer chains, enhancing the filler networking and providing rubber immobilization between NPs aggregates. This effect is more evident at 185°C, where SiO<sub>2</sub>@POSS hybrid fillers are completely enclosed in the rubber matrix. As a consequence, the storage modulus value sharply increases and becomes higher than that of SBR/SiO<sub>2</sub>+POSS-10 composites cured under the same conditions. These results are clearly connected to structure of SiO<sub>2</sub>@POSS filler, in which silica NPs aggregates are partially interconnected and surrounded by a thin shell of POSS nanounits, which promote the formation of a tight filler network wherein rubber is immobilized (see SEM, AFM and NMR investigation in Chapter 4).

Instead, no relevant effects of the curing temperature on the storage modulus values have been observed for SBR/SiO<sub>2</sub>+POSS-10 nanocomposites (Fig. 5.4b, blue-line). This behaviour may be ascribed to the competition in these materials, obtained by simply mixing silica, TMMS and POSS with SBR, of the following simultaneous interactions: (i) POSS-POSS, ii) POSS-TMMS, (iii) POSS-TMMS-Silica, (iv) POSS-SBR and (v) TMMS-SBR.

At 155°C (i.e poor activation of DCP), the G' values for SBR/SiO<sub>2</sub>+POSS-10 is much higher than that of SBR/SiO<sub>2</sub>@POSS-10. This may be tentatively associated to the presence of "free" POSS nanounits which

can undergo direct interaction with the polymer chains, increasing the cross-linking and thus improving the mechanical properties.

At 170°C and 185°C, DCP activation initiates the reaction/polymerization among the methacryl groups of SiO<sub>2</sub>-TMMS, OctaPOSS, and vinyl groups of SBR chains. Moreover, POSS units may interact again with silica NPs exerting their cross-linking close to the filler surfaces and contributing to the networking. This leads to the presence of more dispersed and less compact filler aggregates (see TEM, SEM and AFM images in Chapter 4), and to a lower cross-linking density, resulting in G' values still high but significantly lower than those of SBR/SiO<sub>2</sub>@POSS nanocomposites cured under the same conditions.

In summary, the DMTA analysis of SBR nanocomposites confirms the results achieved by ODR and allows to better elucidate the action of SiO<sub>2</sub>@POSS hybrid filler in granting superior mechanical properties.

### 5.3 Tensile Tests

The uniaxial tensile test is the most useful test one can perform on strip material. It generates a stress-strain curve, which characterizes a material's mechanical performance. The test is used to directly or indirectly measure yield strength, tensile strength, elastic modulus, elongation, <sup>114</sup>.

During typical tensile experiment (See Appendix for details), a dog-bone shaped specimen is gripped at two ends and is pulled to elongate at a determined rate to its breakpoint. The standard configuration for tensile testing strip materials is commonly a dog-bone, with wide ends and a narrow middle. The midsection of the sample has a narrower width than the grip section. This concentrates the stress in the test area, so that fracture and most of the strain occur there. Strain is measured in this section, and stress is calculated from the force load on the grips.

In the present study, tensile tests aimed to further shed light on the effects of the POSS incorporation on rubber nanocomposites properties, by evaluating their behaviour also under high deformation conditions.

The experiments have been performed in the laboratory of Institute of Macromolecular Chemistry of Prague in collaboration with Prof. Libor Matejka.

Stress strain profiles for C-SBR/SiO<sub>2</sub>@POSS-10 (red line), C-SBR/SiO<sub>2</sub>+POSS-10 (blue line), C-SBR/SiO<sub>2</sub>-TMMS (dotted line) and C-

SBR pure (black line) composites cured at 170°C for 10min are reported in Fig 5.5.

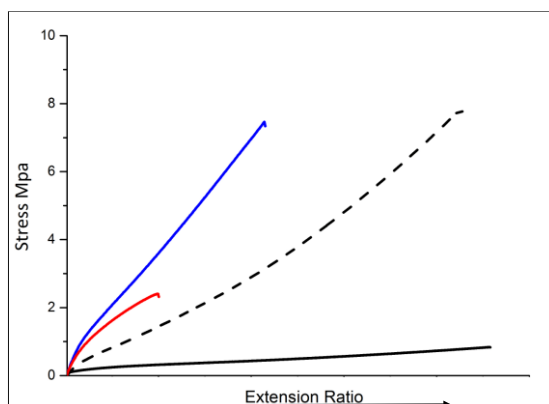


**Figure 5.5:** Tensile Stress-strain profile for C-SBR/SiO<sub>2</sub>@POSS-10 (red line), C-SBR/SiO<sub>2</sub>+POSS-10 (blue line), C-SBR/SiO<sub>2</sub>-TMMS (dotted line) and C-SBR pure (black line) composites cured at 170°C for 10min.

As expected, cured SBR rubber (Fig. 5.5 black line) shows high extensibility and low modulus due to the absence of the filler in the rubber matrix. In this case, dicumylperoxide activates only the chain-chain cross-polymerization of vinyl groups of the rubber thus resulting in a low crosslinking density and consequently in a low modulus and a high extensibility. Instead, for C-SBR/SiO<sub>2</sub>-TMMS nanocomposites (Fig. 5.5 dotted line), the presence of silica aggregates imparts higher modulus to the polymer, while still a significant extensibility is detectable. This latter effect may be ascribed to the crosslinking between methacryl groups of TMMS anchored onto SiO<sub>2</sub> NPs and rubber chains, which may hinder the formation of a compact silica network.

Interestingly, the behaviour of C-SBR/SiO<sub>2</sub>@POSS-10 and C-SBR/SiO<sub>2</sub>+POSS-10 nanocomposites (Fig. 5.5, red line and blue line respectively) is remarkably different.

In detail, both the composites display a higher modulus than SiO<sub>2</sub>-TMMS, supporting the positive effect of POSS nanounits on rubber reinforcement (Fig 5.5). However, it is notable a relevant depletion of the extensibility for these the materials, particularly for C-SBR/SiO<sub>2</sub>@POSS-10 sample.

This behaviour may be associated to the intrinsic properties of the fillers.

In C-SBR/SiO<sub>2</sub>@POSS-10 nanocomposite a tight network is present due to the peculiar surface functionalization of SiO<sub>2</sub> NPs with POSS nanounits which, through the high number of reactive functionalities, provide enhanced filler networking and “sticky regions” among the silica aggregates, immobilizing rubber and affording a relevant increase of the mechanical properties. In fact, as evidenced by TEM images, SiO<sub>2</sub>@POSS hybrid filler is constituted by silica aggregates which are partially connected and surrounded by a thin MethacrylPOSS amorphous shell. The aggregates are covered by rubber layer, the filler-rubber interphases are well interpenetrated and the chains are significantly immobilized as determined by NMR. As a consequence of the rigid network strongly bonded to the polymer, the composite shows the highest modulus and the lowest extensibility and toughness (Fig 5.5, red line).

Instead, in C-SBR/SiO<sub>2</sub>+POSS-10, POSS units are likely anchored to silica NPs with lower efficiency and their grafting may occur only during the

curing process. Thus, although POSS nanounits may interact again with the filler exerting their cross-linking close to the filler surfaces and contributing to the networking, direct interaction among “free” POSS nanounits and polymer chains may also take place. This leads to the presence of more dispersed and less compact filler aggregates and to a lower cross-linking density (cfr. Chapter 4), resulting only in a partial increase of the modulus and to a less remarkable extensibility of the composite (Fig. 5.5, blue line).

In order to better depict the above outcomes, Figure 5.6 shows a schematic proposal of the network influence on the tensile properties in C-SBR/SiO<sub>2</sub>@POSS-10 and C-SBR/SiO<sub>2</sub>+POSS-10 nanocomposites.

In detail, the **dog-bones** represent the **samples specimens** utilized for the measurements; **F** is the **force applied** from the instruments until the breakdown of the samples; the **dotted line** is the **fracture point**. When **F** is applied, the variation in terms of network formation induces relevant differences in the extensibility properties. As observed in Fig. 5.5, the presence of a rigid network strongly bonded to the polymer in SBR/SiO<sub>2</sub>@POSS nanocomposites reduces/prevents the elongation of dog-bones (Fig. 5.6, left-side) much more than in SBR/SiO<sub>2</sub>+POSS, where more dispersed and less compact filler aggregates constitute the sample (Fig. 5.6, right side). This suggests that, at the **fracture point**, the good adhesion between filler and polymer (i.e. the presence of a tight network immobilizing rubber chains) in SBR/SiO<sub>2</sub>@POSS composite, supplies higher strength, superior mechanical properties but much lower extensibility than for SBR/SiO<sub>2</sub>+POSS (see Fig. 5.5).

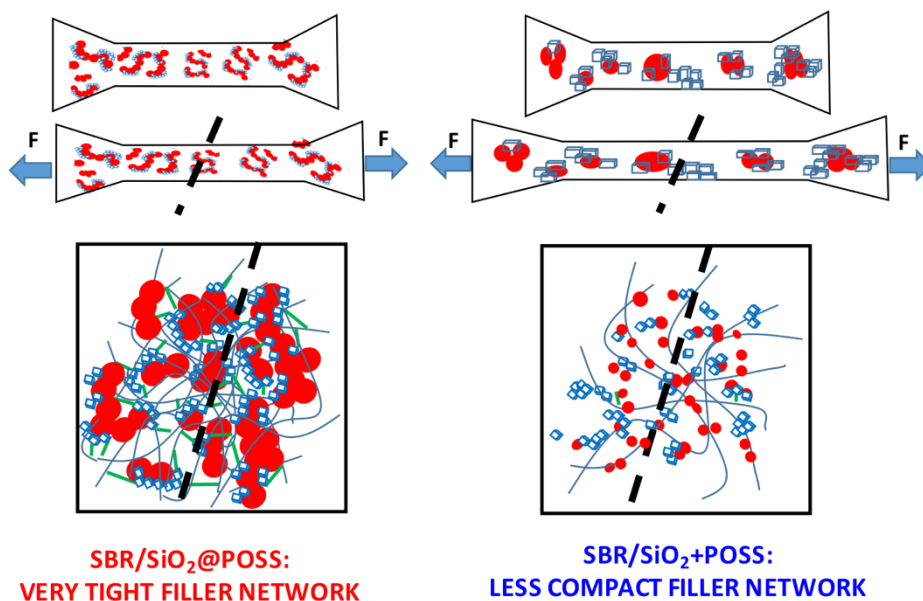


**Figure 5.6:** Schematic of the effect of the filler network in SBR/SiO<sub>2</sub>@POSS and SBR/SiO<sub>2</sub>+POSS nanocomposites on their extensibility at the fracture point.

#### **5.4 SiO<sub>2</sub>@MonoPOSS: a probe for understanding the role of POSS nanocages in SiO<sub>2</sub>@POSS hybrid filler**

In order to better understand the role of OctaPOSS units in SiO<sub>2</sub>@POSS in promoting the cross-linking action, the networking and, in turn, the reinforcement, the mechanical properties C-SBR/SiO<sub>2</sub>@MonoPOSS-10 nanocomposites were also evaluated

The trends of the storage modulus ( $G'$ ) as a function of strain obtained by ODR and the tensile stress-strain profiles for C-SBR/SiO<sub>2</sub>@POSS-10, and C-SBR/SiO<sub>2</sub>@MonoPOSS-10 composites (Curing:170°C for 10 min), are reported in Figure 5.7.

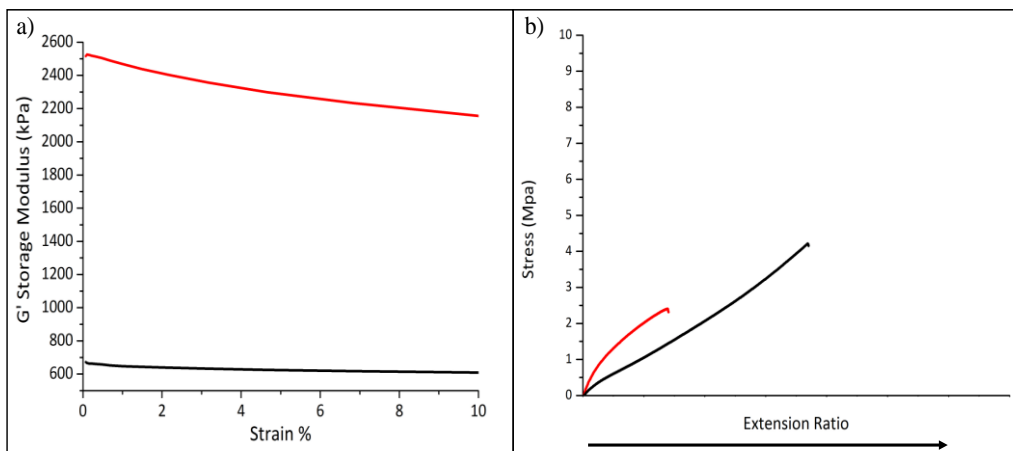


**Figure 5.7** a) Storage modulus  $G'$  vs strain plot and b) tensile stress-strain profiles for C-SBR/SiO<sub>2</sub>@POSS-10 (red line) and C-SBR/SiO<sub>2</sub>@MonoPOSS-10 (black line) composites. (Curing:170°C for 10 min)

As expected, SBR/SiO<sub>2</sub>@MonoPOSS-10 (blackline) shows lower modulus than C-SBR/SiO<sub>2</sub>@POSS-10 (red line) as well as much higher extensibility and toughness (Fig 5.7 a and b). This behavior may be explained considering the structure of SiO<sub>2</sub>@MonoPOSS nanofiller, in which most of the methacryl functionalities of SiO<sub>2</sub>-TMMS have been condensed with the only reactive methacryl group of MonoPOSS. Since, the other seven alkyl functionalities of MonoPOSS are basically poorly reactive, only few functional groups should be then available for filler-filler interaction or reaction with the rubber chains. Accordingly, SEM characterization of SBR/SiO<sub>2</sub>@MonoPOSS nanocomposites (see Chapter 4) shows aggregates with lower dimensions, a sharper adhesion interface between filler and rubber matrix. Moreover, <sup>1</sup>H

NMR revealed smaller fraction of the immobilized chains. This results in the decrease of the storage modulus, while the extensibility remains still high (Fig 5.7).

These results confirm that the outstanding mechanical properties and the remarkably high rigidity observed in SBR/SiO<sub>2</sub>@POSS nanocomposites, derives from the ability of SiO<sub>2</sub>@POSS hybrid filler in supplying a high number of reactive functionalities still available for the interaction with the rubber chains, promoting the formation of a tight filler network, immobilizing rubber among the silica aggregates, and affording a relevant increase of the reinforcement.



**Chapter 6**  
**Conclusions**

## Conclusions

The research activity of my PhD was focused on exploring the possibility to employ Polysilsesquioxanes (PSQs) with different molecular structure (cage or ladder-like) as innovative fillers in rubber nanocomposites, potentially exploitable in tires formulation.

In the first part of the work, a novel SiO<sub>2</sub>@POSS hybrid nanofiller, where silica NPs and POSS belong to the same functional structure, was synthesized through silanization of commercial SiO<sub>2</sub> with methacrylsilane and successive reaction with small loadings of OctaMethacrylPOSS in the presence of dicumylperoxide (DCP), a common initiator of polymerization and curing agent.

SiO<sub>2</sub>@POSS hybrid NPs have been then used to prepare by *ex-situ* blending styrene butadiene rubber (SBR) nanocomposites. Their morphological, swelling and mechanical properties, were comprehensively investigated and compared to those of composites obtained by simply introducing mixtures of SiO<sub>2</sub> and OctaMethacrylPOSS in the polymer matrix (SBR/SiO<sub>2</sub>+POSS).

In detail, TEM microscopy investigation revealed that cured SBR/SiO<sub>2</sub>@POSS nanocomposites, display a tight filler network, in which thin rubbery regions separate the NPs aggregates. Instead, when POSS is mixed with silica within the rubber matrix (i.e SBR/SiO<sub>2</sub>+POSS samples), more dispersed and only partially interconnected silica aggregates were detected. Moreover, a detailed inspection of the nanocomposites, by means of SEM and AFM on fractured surfaces, revealed the presence of continuous surfaces for SBR/SiO<sub>2</sub>@POSS

composites with high interfacial adhesion between filler particles and rubber. Conversely, sharper interfaces with significant boundaries between the two phases were detectable for SBR/SiO<sub>2</sub>+POSS samples. Finally, swelling experiments showed that the reticulation degree for SBR/SiO<sub>2</sub>@POSS nanocomposites is definitively higher than that of SBR/SiO<sub>2</sub>+POSS.

To further shed light on this macroscale behavior, we studied the variation of segmental dynamics of polymer chains in the prepared systems at the molecular level by <sup>1</sup>H-NMR. According to the morphological and swelling results, SiO<sub>2</sub>@POSS/SBR nanocomposites exhibit the highest fraction of rigid domains and surface confined polymer chains, as reflected by the broadening of all the detected NMR signals.

These properties greatly affect the functional features of the composites.

In fact, the dynamic-mechanical analysis performed on the cured SBR/SiO<sub>2</sub>@POSS composites, indicated the presence of POSS, even at very low loadings (5 phr), induces a remarkable increase of the modulus either at low or at high strain and a considerable decrease of the hysteresis. Moreover, by comparing the performances of SBR/SiO<sub>2</sub>@POSS with those of nanocomposites obtained by simple addition of SiO<sub>2</sub> and POSS in the polymer matrix, it turned out that the silica grafting with POSS determines a more positive effect on the mechanical properties.

This has been associated to the peculiar structure of SiO<sub>2</sub>@POSS, constituted by NPs aggregates partially interconnected and decorated

by POSS nanounits which, thanks to the high number of reactive functionalities, promote the formation of a tight filler network which immobilizes filler and rubber, afford a relevant reinforcement and improve the hysteretical properties.

In the second part of the thesis, a similar strategy has been applied for study of the properties of PB nanocomposites including PSQs with tailorable cage or ladder-like structure.

SH-NBBs were synthesized from 3-mercaptopropyltrimethoxysilane by using the in situ water production (ISWP) process and have been then used to prepare by *swelling*, polybutadiene rubber (PB) nanocomposites. NMR confirmed a preferential formation of cage-like compared to ladder-like structures and the narrowing of the species distribution over long reaction times. Swelling experiments and, more in depth,  $^1\text{H}$  NMR revealed a significant relation between SH-NBBs architecture and their interactions with the polymer, suggesting that nanocages may really provide effective chemical or physical interactions at the polymer-NBBs interface, resulting in a restricted polymer chains mobility.

In summary, the whole results suggest that the utilization of PSQs significantly improve the rubber reinforcement, decreasing the energy loss under strain, and leading also to a potential reduction of filler utilization in the tires formulation. Moreover, though this work focused on rubber nanocomposites, we expect that the presented approach

may supply new scientific and technological opportunities for the designing of other advanced polymer nanocomposites, which require remarkable mechanical strength and low deformability simultaneously (e.g materials for friction and wear applications, protective coatings, etc.), thus expanding the potential application of these new materials in the modern industry.



## References

- [1] T. Sabu and S. Ranimol, *Rubber Nanocomposites: Preparation, Properties and Applications*, (2010), John Wiley & Sons.
- [2] V.E. Borisenko and S. Ossicini, *What is What in the Nanoworld: A Handbook on Nanoscience and Nanotechnology*, (2008), Wiley.
- [3] G. Kickelbick, *Hybrid Materials: Synthesis, Characterization, and Applications*, (2007), Wiley.
- [4] P. Gómez-Romero and C. Sanchez, *Functional Hybrid Materials*, (2004), Wiley.
- [5] S. Mihara, Ph.D thesis, University of Twente, (2009).
- [6] T. Sabu and J.M. Hanna, *Progress in rubber nanocomposites*, Woodhead Publishing Series in Composites Science and Engineering: Number 75, (2017) Elsevier.
- [7] Ramier, J. Gauthier, C. Chazeau, L. Stelandre and L. Guy, *J. Polym. Sci., Part B: Polym. Phys.* (2007), 45, 286–298.
- [8] Baeza, G. P. Genix, A.-C. Degrandcourt, C. Petitjean, L. Gummel, J. Schweins, R. Couty, M. Oberdisse, *J. Macromolecules* (2013), 46, 6621–6633.
- [9] I. Mora-Barrantes, L. Ibarra, A. Rodriguez, L. Gonzalez and J. L. Valentin, *J. Mater. Chem.*, (2011), 21, 17526–17533.
- [10] A. K. Bhowmick, *Current topics in elastomers research*, CRC Press–Taylor & Francis Group, Broken Sound Parkway, NW, (2008).
- [11] S. Pavlova and P. G. Khalatur, *Soft Matter* (2016), 12, 5402–5419.
- [12] B. Guo, F. Chen, Y. Lei and W. Chen, *Polymer Journal* (2010), 42, 319–325.

- [13] Choose Green Report, Low rolling resistance tires.
- [14] L. Wahba, M. D'Arienzo, R. Donetti, T. Hanel, R. Scotti, L. Tadiello and F. Morazzoni, *RSC Advances* (2013), 3, 5832–5844.
- [15] R. Scotti L. Wahba M. Crippa, M. D'Arienzo, R. Donetti, N. Santo and F. Morazzoni, *Soft Matter*, (2012),8, 2131-2143
- [16] R. Scotti, L. Conzatti, M. D'Arienzo, B. Di Credico, L. Giannini, T. Hanel, P. Stagnaro, A. Susanna, L. Tadiello and F. Morazzoni, *Polymer* (2014), 55, 1497–1506.
- [17] L. Tadiello, M. D'Arienzo, B. Di Credico, T. Hanel, L. Matejka, M. Mauri, F. Morazzoni, R. Simonutti, M. Spirkova and R. Scotti, *Soft Matter* (2015), 11, 4022–4033.
- [18] A. Blume, *Rubber World*, (2002), 86, 30.
- [19] C.-W. Nan, Y. Shen and J. Ma, *Annual Review of Materials Research*, (2010), 40,131–51
- [20] F. Thurn and S. Wolff, *Kautsch. Gummi Kunstst*, (1975), 28, 733.
- [21] H. Roelig, *Rubber Chem. Technology*, (1939), 12, 284
- [22] W.S.J. Naunton and J.S.R. Warning, *Trans. Inst. Rubber Ind.*, (1939), 14, 340
- [23] S.D. Gehman, D.E. Woodford and R.B. Stambaugh, *Ind. Eng. Chem*, (1941), 33, 1032.
- [24] R.B. Stambaugh, *Ind. Eng. Chem.*, (1942), 34, 1358
- [25] A. Blume, S. Uhrlandt, *Am. Chem. Soc.*, Rubber Div. Meeting, Akron, Ohio (2000).
- [26] A.R.Payne, *Rubber Plast Age*, (1961), 963.
- [27] A. R. Payne, *Rubber Chem.Technology*. (1971), 44, 440.
- [28] A. I. Medalia, *J.Interface.Sci.*, (1970), 32, 115.

- [29] G. Kraus, *Rubber Chem. Technol.*, (1971),44, 199.
- [30] G. Tsagaropoulos and A. Eisenberg, *Macromolecules* (1995), 28, 6067–77.
- [31] G. Tsagaropoulos and A. Eisenberg, *Macromolecules* (1995), 28, 396–8.
- [32] V. Arrighi, I. McEwen, H. Qian and M. Prieto, *Polymer* (2003), 44, 6259.
- [33] A Papon, K. Saalwächter, K. Schäler, L. Guy, F- Lequeux, and H-Montes, *Macromolecules*, (2011), 44, 913–922
- [34] K. Saalwächter, *J. Am. Chem. Soc.*, (2003), 125, 48, 14684–14685
- [35] S. Bandyopadhyay, D. K. Tripathy and S.K. De., *Rubber Chem. Technol*, (1996), 69, 675.
- [36] Deggusa AG, Applied Technol., Advanced Filler, Produkt information PI321 and PI335.
- [37] L. Wahba, M. D'Arienzo, S. Dirè, R. Donetti, T. Hanel, F. Morazzoni, M. Niederberger, N. Santo, L. Tadiello and R. Scotti, *Soft Matter*. (2014), 10, 2234-2344
- [38] E. Ayandele, B. Sarkar and P. Alexandridis, *Nanomaterials*, (2012), 2, 445–475
- [39] K. N. Raftopoulos and K. Pielichowski, *Progress in Polymer Science* (2016), 52, 136–187.
- [40] Kuo S.W., *ACS Central Science* (2016), 2, 62–64.
- [41] D. B. Cordes, P. D. Lickiss and F. Rataboul *Chem. Rev.* (2010), 110, 2081–2173.
- [42] S. W. Kuo and F. C. Chang, *Progress in Polymer Science* (2011), 36, 1649–1696.

- [43] A. Fina, O. Monticelli and G. Camino, *J. Mater. Chem.* (2010), 20, 9297–9305.
- [44] K. Tanaka and Y. Chujo, *J. Mater. Chem.* (2012), 22, 1733–1750.
- [45] A. L. Goffin, E. Duquesne, J. M. Raquez, H. E. Miltner, X. Ke, M. Alexandre, G. Van Tendeloo, B. Van Meleb and P. Dubois, *J. Mater. Chem.* (2010), 20, 9415–9625.
- [46] S.W. Kuo, F. Feng and C. Chang, *Progress in Polymer Science* 36 (2011) 1649–1696.
- [47] H. Zhou, Q. Yea and J. Xu, *Mater. Chem. Front.*, (2017).
- [48] F. Brown, L. H. Vogt, A. Katchman, J. Eustance, K. M. Kiser and K. W. Krantz, *J. Am. Chem. Soc.* (1960), 82, 6194–6195.
- [49] S. Yamamoto, N. Yasuda, A. Ueyama, H. Adachi and M. Ishikawa, *Macromolecules*, (2004), 37, 2775–2778.
- [50] A. S. Lee, S. S. Choi, H. S. Lee, K. Y. Baek and S. S. Hwang, *Dalton Trans*, (2012), 41, 10585–10588.
- [51] A. S. Lee, S. S. Choi, H. S. Lee, K. Y. Baek and S. S. Hwang, *J. Mater. Chem.*, (2010), 20, 9852–9854.
- [52] A. S. Lee, S. S. Choi, H. S. Lee, K. Y. Baek and S. S. Hwang, *J. Polym. Sci., Part A: Polym. Chem.*, (2011), 49, 5012–5018.
- [53] A. S. S. Lee, J. H. Lee, J. Lee, S. M. Hwang and C. Min Koo, *J. Mater. Chem. A*, (2014), 2, 1277
- [54] T. S. Haddad and J. D. Lichtenhan, *Macromolecules* (1996), 29, 7302–4.
- [55] A. Romo-Uribe, P. T. Mather, T. S. Haddad and J. D. Lichtenhan, *J. Polym. Sci. Part B: Polym. Phys* (1998), 36, 1857–72.

- [56] L. Matějka, I. A. Kroutilová, J. D. Lichtenhan and T.S. Haddad, *European Polymer Journal* (2014), 52, 117–126.
- [57] K. Y. Cho, A. S. Lee, H. Jeon, S. Park, M. Jang, H. Yoon, S. Hong, K. Baek and S. S. Hwang, *Polymer* 77 (2015) 167-176.
- [58] O. Bianchi, L.G. Barbosa, G. Machado, L. B. Canto, R. S. Mauler and R. V. B. Oliveira, *J. Appl. Polym. Science*, (2013), 128, 811–827.
- [59] G. Pan, J. E. Mark and D. W. Schaefer, *Journal of Polymer Science: Part B* (2003), 41, 3314–3323.
- [60] V. Joshi, M. Srividhya, Mayank Dubey, A. K. Ghosh and Anubhav Saxena, *J. Appl. Polym. Science* (2013), 130, 92–99.
- [61] T. Vokatá, M. Twomey, E. Mendez and J. H. Moon, *Journal of Polymer Science: Part A* (2015), 53, 1403–1412.
- [62] J. H. Jeon, K. Tanaka and Y. Chujo, *Journal of Polymer Science: Part A* (2013), 51, 3583–3589.
- [63] K. Tanaka, S. Adachi and Y. Chujo, *Polymer Chemistry* (2009), 5690–5697.
- [64] F. X. Perrina, D. M. Panaitescu, A. N. Frone, C. Radovici and C. Nicola, *Polymer*, (2013), 54, 2347–2354
- [65] A. Kosmalka, A. Strąkowska and M. Zaborski, *Materials Science Forum* (2012), 714, 175-181.
- [66] F. Carniato, C. Bisio, E. Boccaleri, M. Guidotti, E. Gavrilova and L. Marchese, *Chemistry*, (2008), 8098–8101.
- [67] M. Bhagiyalakshmi, R. Anuradha and H. T. Jang, *Materials*, (2010), 265–273.
- [68] K. Szwarc, K. Siwinska-Stefanska, B. Marciniak, and T. Jesionowski, *Physicochemical Problems of Mineral Processing*, (2012), 181–192.

- [69] K.Szwarc, F. Ciesielczyk, and T. Jesionowski, *Journal of Nanomaterials*, (2009), 13, 254–26.
- [70] M. Handke, B. Handke, A. Kowalewska and W. Jastrzebski, *Journal of Molecular Structure*, (2009), 3, 924–926.
- [71] E. Borovin, E. Callone, B. Papendorf, G. Guella and S. Dirè, *J. Nanosci. Nano-technol.* (2015).
- [72] E. Borovin, E. Callone, F. Ribot, and S. Diré, *Eur. J. Inorg. Chem.* (2016), 2166–2174.
- [73] K. Nagdi, *Rubber as an Engineering Material: Guideline for Users*, Carl Hanser Verlag (1993).
- [74] J.R. White and S.K. De, *Rubber Technologist's Handbook*, Rapra Technology (2001).
- [75] V. Duchacek and A. Kuta, *J. Appl. Polym. Sci.* (1993), 47, 743–748.
- [76] G. Heideman, Ph.D. Thesis, University of Twente, Enschede Netherlands, (2004).
- [77] G. Heideman, R.N. Datta and J.W.M. Noordermeer, *Rubber Chem. Technol.* (2004), 77,512–541.
- [78] C.G. Moore and M. Porter *Rubber Chem. Technol.* (1963), 36, 547–557.
- [79] W. C. Endstra and C. T. J. Wreesman in “Elastomer Technology Handbook,” N. P. Cheremisinoff, ed., CRC Press, Ann Arbor, (1993).
- [80] J. B. Class, Rubber Division, ACS, Indianapolis, IN, May 5-8, (1998).
- [81] A. H. Johansson, Fall Technical Meeting, Rubber Division, ACS, Cleveland, (2003).
- [82] L. H. Palys and P. A. Callais, *Rubber World* (2003), 229(3), 35
- [83] P. R. Dluzneski, *Rubber Chem. Technol.* (2001), 7.4, 451

- [84] R.C. Keller, *Rubber Chem. Technol.* (1988), 61, 238
- [85] L.D. Loan, *Rubber Chem. Technol.* (1967), 40, 149.
- [86] E. Borovin, PhD thesis, University of Trento, Department of Industrial Engineering, (2015).
- [87] C. Bressy, V. Ngo, F. Ziarelli and A. Margaillan, *Langmuir* 2012, 28, 3290–3297.
- [88] F. Bauer, H. Ernst, U. Decker, M. Findeisen, H.J., Gläsel, H. Langguth, E. Hartmann, R. Mehnert and C. Peuker, *Macromolecular Chemistry and Physics*, (2000), 2654–2659.
- [89] K. Szwarc-Rzepka, F. Ciesielczyk and T. Jesionowski, *Journal of Nanomaterials* (2013), Article ID 674237.
- [90] C. G. Allen, D. J. Baker, J. M. Albin, H. E. Oertli, D. T. Gillaspie, D. C. Olson, T. E. Furtak and R. T. Collins, *Langmuir* (2008), 24, 13393–13398
- [91] M. D'Arienzo, M. Redaelli, B. Di Credico, S. Polizzi, R. Scotti and F. Morazzoni, *RSC Adv.* (2016), 6, 52987–52997.
- [92] M. Crippa, E. Callone, M. D'Arienzo, K. Müller, S. Polizzi, L. Wahba, F. Morazzoni and R. Scotti, *Applied Catalysis B: Environmental* (2011), 104, 282–290
- [93] A. Testino, I.R. Bellobono, V. Buscaglia, C. Canevali, M. D'Arienzo, S. Polizzi, R. Scotti and F. Morazzoni, *J. Am. Chem. Soc.* (2007), 129, 3564.
- [94] S. Brunauer, P.H. Emmet and E. Teller, *J. Am. Chem. Soc.* (1938), 60, 309
- [95] R. Di Maggio, E. Callone, F. Girardi and S. Diré, *Journal of Applied Polymer Science* (2012), 125, 1713–1723.

- [96] F. Graziola, F. Girardi, R. Di Maggio, E. Callone, E. Miorin, M. Negri, K. Müller and S. Gross, *Prog. in Organic Coatings* (2012), 74, 479–490.
- [97] V. Mittal, *Characterization Techniques for Polymer Nanocomposites*, (2012), Wiley
- [98] P. Deepalekshmi, J. M. Hanna, K.C. Arup and T. Sabu, *Rubber Nanocomposites: Latest Trends and Concepts* (2013), Springer.
- [99] S. Fu, X. Q. Feng, B. Lauke and Y. Mai, *Composites: Part B* 39 (2008) 933–961
- [100] S. Aoyama, T. Park, C. W. Macosko, T. Ougizawa and G. Haugstad, *Langmuir*, (2014), 30-43
- [101] X. Yong Gan, *Int J Mol Sci.* (2009) , 10, 5115–5134.
- [102] S.C. Tjong, *Materials Science and Engineering*, (2006),53, 73–197
- [103] L.F. Valadares, C.A.P. Leite and F. Galembeck, *Polymer*, (2006) 47, 672–678
- [104] N. Tsubokawa and H. Ishida, *Journal of Polymer Science: Part B* (1992), 2241–2246.
- [105] L. Gonzalez, A. Rodriguez, A. Marcos and C. Chamorro, *Rubber Chemistry and Technology*, (1995), Vol 69.
- [106] B.W. Ellis, G. N. Welding, *Rubber Chem. Technol.* (1964), 37, 571-575.
- [107] P.J. Flory, J. Rehner, *J. Chem. Phys.* (1943), 11, 521-526.
- [108] J. Brus, M. Urbanová and A. Strachota, *Macromolecules*, (2008), 41 , 372–386.
- [109] J. Brus, M. Urbanová, I. Kelnar, and J. Kotek, *Macromolecules*, (2006), 39, 5400–5409.
- [110] J. Brus and J. Dyba, *Polymer* 41,(2001) 5269-5282.

- [111] G. Maier, D. Goritz and G. K. Kautsch, *Polymer* (1996);118-21;
- [112] A.P Meera. *J. Phys. Chem. C* (2009),113, 17997178002.
- [113] K. S. W. Sing, D. H. Everett, R. A. W. Haul, L. Moscou, R. A. Pierotti, J. Rouquérol and T. Siemieniowska, *Pure and Applied Chemistry* (1985), 57, 603–619.
- [114] Technical Tidbits, *Brush Performance Alloys*,(2011), 27



**Appendix**  
**Characterization methods**

The aim of this Appendix is to resume the analytical techniques employed for the characterization of SiO<sub>2</sub>@POSS hybrid and SH-NBBs nanofillers and their relative nanocomposites and in order to understand the structure-properties relationship of the materials.

### **A1.1 Attenuated Total Reflectance Fourier Transform Infrared Spectroscopy (ATR-FTIR)**

The surface chemistry of examined materials can be determined qualitatively by vibrational spectroscopy. The absorption of infrared radiation at different wavelengths is associated with the vibrational modes of different bonds. ATR spectroscopy uses the phenomenon of total internal reflection in a crystal. The radiation undergoes a total internal reflection when the angle of incidence at the interface between the crystal and the material is greater than the critical angle (Fig. A.1)

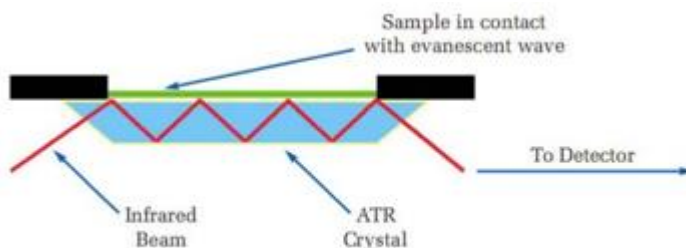


**Figure A.1:** ATR-FTIR

The beam penetrates a fraction of a wavelength beyond the reflecting surface. When the material is in close contact with the reflecting surface, the beam loses energy at the wavelength there the material

absorbs. The radiation resultant is measured (absorption energy) and plotted as a function of the wavelength.

The Attenuated Total Reflectance Fourier Transform Infrared spectroscopy (ATR-FTIR) in the range 4000-6000  $\text{cm}^{-1}$  was used to check the effective silanization of silica particles and the presence of POSS molecules on the silica surface. Moreover, FT-IR was also employed for the characterization of pure SH-NBBs\_30h and SH-NBBs\_80 and for the relative PB/Y%NBB\_Hh nanocomposites. The measurements were performed by a Perkin Elmer Spectrum 100 instrument. (1  $\text{cm}^{-1}$  resolution spectra, 650-4000  $\text{cm}^{-1}$  region, 32 scan).

### **A1.2 Thermal analysis (TGA)**

Thermo-gravimetric analysis (TGA) is a technique that allows the measurement of the weight changes of sample materials as a function of the temperature in a controlled atmosphere. During a thermal treatment of the filler it is possible to determine the amount of functionalizing molecules allocated on the surface, the amount of solvent and humidity physically adsorbed on the surface and in the pores, and its thermal stability. The instrument used for doing this kind of analysis is composed of four parts: analytic thermos-balance, heating oven, gas injector (inert or reactive gases) and a computer for instrument control in order to collect and process the data obtained. The heart of the instrument consists in a light horizontal arm (balance) immersed in a magnetic field on which the sample pan is allocated. A

special optical sensor controls the position of the pan. For each mass sample loss, the arm moves inducing an electric current which is recorded as a signal by the machine. In detail, the instrument records a graph which reports the loss of the mass as a function of time or temperature and the first derivative curve of the mass loss (DTGA).

A thorough understanding of the result provided by the instrument allows to explain the processes, which take place in the sample, during the thermal treatment. For every small mass loss, it is possible to determine the correspondent temperature at which the sample loses the maximum amount and then hypothesize the kind or reaction which occurs. Thermogravimetric analysis was used to characterize SiO<sub>2</sub>-TMMS and SiO<sub>2</sub>@POSS hybrid nanofillers and to obtain the amount of functional groups on silica surface by subtracting the weight loss by the pristine SiO<sub>2</sub>. The analysis was carried out by Thermo Gravimetric Analysis (TGA) on Mettler Toledo TGA/DSC1 Star System. The sample powders were heated in air from 30 to 1000°C. Thermal profile was the following: 30-150°C at 2°C min<sup>-1</sup>; dwell at 150°C for 120 min; 150-1000°C at 5°C min<sup>-1</sup>.

This technique was also used to check the effective presence of the SH-NBBs in the PB matrix. The analysis was carried out by the same instrument with the same thermal profile using a piece of the composites.

### **A1.3 Nitrogen physisorption measurements**

Specific surface area, external surface area and porosity (pore volume and pore size distribution) was measured out by physical adsorption of  $N_2$ . Regarding the porosity, in particular for pore diameter, an official classification was proposed by the International Union of Pure and Applied Chemistry (IUPAC)<sup>7</sup>: micropores (pore size  $< 2$  nm), mesopores (pore size between 2 nm and 50 nm) and micropores (pore size  $> 50$ ).

Adsorption is a phenomenon in which a fluid interacts with the surface atoms of solid by Van der Waals or weak forces (energies of interaction between adsorbent and adsorbed is in the order of 20 kJ/mol). Among the fluids used for the physical adsorption measurements,  $N_2$  is the most chosen because it is chemically inert and condenses at  $-196^\circ\text{C}$ .

The increase of the amount of adsorbed fluid corresponds to a variation of pressure in dynamic equilibrium. Isotherm function represents the change of the equilibrium expressed as volume of the adsorbed gas as function of the relative pressure  $p/p_0$ , where  $p$  is the pressure of the vapor and  $p_0$  is its saturation pressure.

At low relative pressure the smallest pores are filled with nitrogen.

As the pressure is increased further, larger pores are filled; near the saturation pressure, all pores are filled. The total pore volume is determined by the quantity of gas adsorbed near the saturation pressure.

The desorption isotherm rarely overlaps with that of adsorption, creating an hysteresis, due to the presence of pores in the adsorbent

material. By studying the hysteresis shape it is possible to determine the total pore volume and size distribution of the pores.

The IUPAC classification recognizes six basic types of isotherms and four different types of hysteresis (Fig A.2): I isotherm is typical for microporous solids and chemisorption isotherms; type II is observed on finely divided non-porous solids, type III and type V are typical for vapor adsorption (e.g. water vapour on hydrophobic materials) and type IV and V feature a hysteresis loop, finally, the rare type VI steplike isotherm is seen on special types of carbons. Regarding the hysteresis, it is due to desorption on mesopores which occurs at lower pressures than those at which adsorption in similar-sized pores would take place.

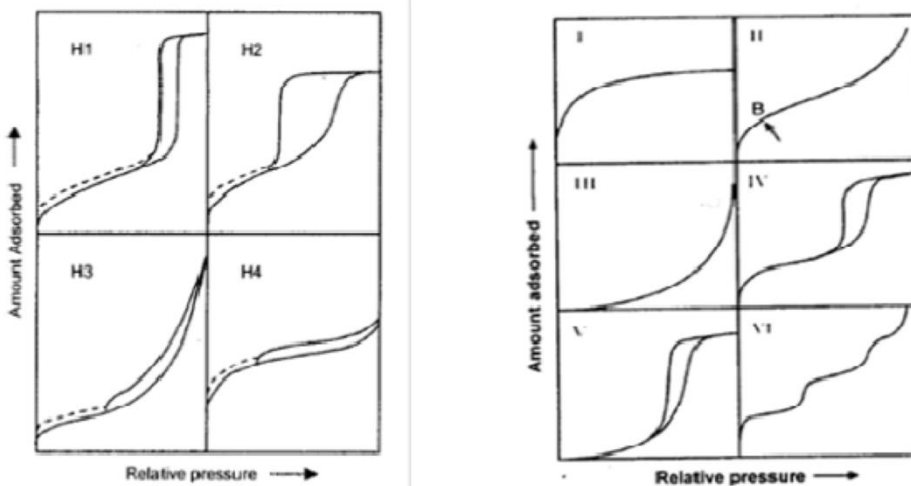


**Figure A.2:** Classification of gas adsorption hysteresis and isotherms.

There are 4 types of hysteresis shape,: H1(associated with solid homogeneous pore size), H2 (porous solids in which the distribution of the shape and size of the pores is not uniform and pores are not

intersected with each other), H3 (solid pore forming flat shape (cracks) of non- uniform size); H4 (solid pore forming flat shape (cracks) of uniform size).

Different models can be applied to different regions of the adsorption isotherms to evaluate the specific surface area (e.g. BET method, Dubinin method, Langmuir adsorption isotherm, etc.), or the micro-and mesopore volume and pore size distributions (e.g. BJH method, Horvath and Kawazoe method, Saito- Foley method, etc.). The microporous volume is determined by the t-plot method of de Boer, while mesopore size and volume are determined by the Kelvin equation.

Nitrogen physisorption measurements on SiO<sub>2</sub> Rhodia NPs, SiO<sub>2</sub>-TMMS and SiO<sub>2</sub>@POSS hybrid filler in order to highlight the effect on functionalization on the aggregation/porosity of the fillers. The analysis were carried out by a Quantachrome Autosorb-1 apparatus. The specific surface area ( $SSA_{BET}$ , BET method) was measured after evacuation at 150°C for 16 h.

#### **A1.4 Solid State NMR**

Solid-state NMR (MAS-NMR) spectroscopy is a kind of nuclear magnetic resonance (NMR) spectroscopy, characterized by the presence of anisotropic interactions. Magic-angle spinning (MAS) is a technique often used to perform experiments in solid-state NMR spectroscopy.

By spinning the sample (usually at a frequency of 1 to 100 kHz) at the magic angle  $\theta_m$  (ca.  $54.74^\circ$ , where  $\cos^2\theta_m=1/3$ ) with respect to the direction of the magnetic field, the normally broad lines become narrower, increasing the resolution for better identification and analysis of the spectrum.

In any condensed phase, a nuclear spin experiences a great number of interactions. The main three interactions (dipolar, chemical shift anisotropy, quadrupolar) often lead to very broad and featureless lines. However, these three interactions in solids are orientation-dependent and can be averaged by MAS. The nuclear dipole-dipole interaction, between magnetic moments of nuclei averages to zero only at the magic angle,  $\theta_m$ .

Another important technique is Cross Polarization. When combined with MAS, polarization from abundant nuclei like  $^1\text{H}$ ,  $^{19}\text{F}$  and  $^{31}\text{P}$  can be transferred to dilute or rare nuclei like  $^{13}\text{C}$ ,  $^{15}\text{N}$ ,  $^{29}\text{Si}$  in order to enhance signal to noise and reduce waiting time between successive experiments.

$^{29}\text{Si}$  and  $^{13}\text{C}$  NMR experiments were performed on  $\text{SiO}_2@\text{POSS}$  hybrid fillers to more effectively assess the silica functionalization by POSS.

Multinuclear solid state NMR analyses were carried out with a Bruker 400WB spectrometer operating at a proton frequency of 400.13 MHz. MAS NMR spectra were acquired with cross polarization (CP) and single pulse (SP) sequences. CP experiments:  $^{13}\text{C}$  frequency: 100.48 MHz, contact time 2000  $\mu\text{s}$ , decoupling length 5.9  $\mu\text{s}$ , recycle delay: 5 s, 2k scans;  $^{29}\text{Si}$  frequency: 79.48 MHz,  $\pi/2$  pulse 3.9 $\mu\text{s}$ , decoupling

length 6.3  $\mu$ s, recycle delay: 10 s, 2k scans. SP sequence:  $\pi/4$  pulse 3.9 $\mu$ s, recycle delay 100s, 2k scans. Samples were packed in 4 mm zirconia rotors, which were spun at 6.5 kHz under air flow. Adamantane and Q8M8 were used as external secondary references. Si units are labeled according to the usual NMR notation: T<sub>n</sub> and Q<sub>n</sub> represent trifunctional SiCO<sub>3</sub> and tetrafunctional SiO<sub>4</sub> units, respectively and n is the number of oxo-bridges.

In order to determine the amount of rigid domains and to probe degree of immobilization of polymer segment by determining signal line-widths for SBR/SiO<sub>2</sub>@POSS-X\_Y and SBR/SiO<sub>2</sub>+POSS-X\_Y and PB/NBBs\_Xh nanocomposites, <sup>1</sup>H NMR MAS spectra were recorded spectra at frequency of  $\omega_r/2\pi = 15$  kHz as well as under static conditions. The static <sup>1</sup>H NMR spectra were simulated, decomposed to individual spectral component.

To compensate for frictional heating of the spinning samples, all NMR experiments were measured under active cooling. The sample temperature was maintained at 305 K. Precise temperature calibration was performed on Pb(NO<sub>3</sub>)<sub>2</sub> using a calibration procedure described in literature.

The experiments have been performed in the laboratory of Institute of Macromolecular Chemistry of Prague in collaboration with Prof. J. Brus and Prof. L. Matejka and in the Klaus Laboratory of Trento in collaboration with Dr. E. Callone and Prof. S. Dirè.

### **A1.5 Scanning Electron Microscope (SEM)**

A scanning electron microscope (SEM) is a type of electron microscope that produces images of a sample by scanning it with a focused beam of electrons. The electrons interact with atoms in the sample, producing various signals that contain information about the sample's surface topography and composition. The apparatus consists in a column in which the electron beam is accelerated, a sample chamber in UHV condition to avoid collision of the beam with air molecules, a secondary electron detector (SED) and a computer connected to the instrument (Fig A.3).

The most common SEM mode is detection of secondary electrons emitted by atoms excited by the electron beam. The number of secondary electrons that can be detected depends, among other things, on the angle at which beam meets surface of specimen, i.e. on specimen topography. By scanning the sample and collecting the secondary electrons that are emitted using a special detector, an image displaying the topography of the surface is created.

The types of signals produced by an SEM include secondary electrons (SE), reflected or back-scattered electrons (BSE), photons of characteristic X-rays and light (cathodoluminescence) (CL), absorbed current (specimen current) and transmitted electrons.

The signals result from interactions of the electron beam with atoms at various depths within the sample. In the most common or standard detection mode (secondary electron imaging or SEI), the secondary electrons are emitted from very close to the specimen surface. Consequently, SEM can produce very high-resolution images of a

sample surface, revealing details less than 1 nm in size. Back-scattered electrons (BSE) are beam electrons that are reflected from the sample by elastic scattering. They emerge from deeper locations within the specimen and consequently the resolution of BSE images is generally poorer than SE images. However, BSE are often used in analytical SEM along with the spectra made from the characteristic X-rays, because the intensity of the BSE signal is strongly related to the atomic number (Z) of the specimen. BSE images can provide information about the distribution of different elements in the sample. Characteristic X-rays are emitted when the electron beam removes an inner shell electron from the sample, causing a higher-energy electron to fill the shell and release energy. These characteristic X-rays are used to identify the composition and measure the abundance of elements in the sample. Due to the very narrow electron beam, SEM micrographs have a large depth of field yielding a characteristic three-dimensional appearance useful for understanding the surface structure of a sample.

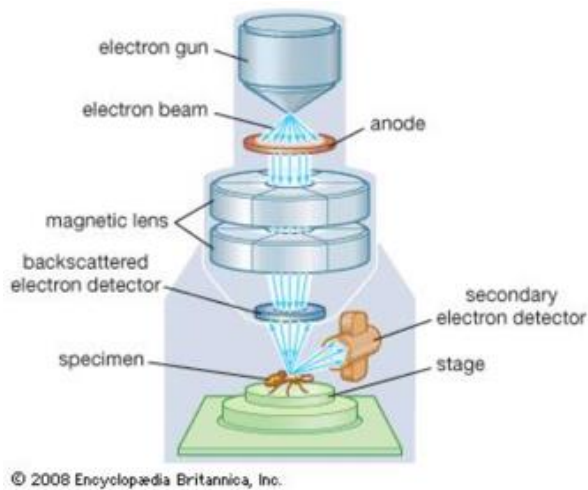


**Figure A.3:** Scheme of SEM apparatus

Microscope Quanta 200 FEG (FEI) was used for the characterization of SBR/SiO<sub>2</sub>@POSS-X<sub>1</sub>Y<sub>1</sub> and SBR/SiO<sub>2</sub>+POSS-X<sub>2</sub>Y<sub>2</sub>. The samples were fractured in liquid nitrogen, sputtered with thin platinum layer (4nm of Pt, deposited using vacuum sputter coater SCD 050 (Leica)) and observed at the accelerating voltage 30 kV using both secondary electrons detector (SE) and backscattered electrons detector (BSE). SE and BSE micrographs showed mostly topographic and material contrast, respectively.

The experiments have been performed in the laboratory of Institute of Macromolecular Chemistry of Prague in collaboration with Prof. M. Slouf and Prof. L. Matejka.

### **A1.6 High-Resolution Transmission Electron Microscopy (HRTEM)**

HRTEM is a technique that allows to obtain images of a nanostructured material at a much higher resolution than SEM. The apparatus is made of an electron beam source, a series of electromagnetic lenses (at least 5) to accelerate the electron beam at very high speed (up to 100KeV), and an imaging system of the electrons going through the sample, which converts the diffraction pattern into a 2D image. Going into detail, the technique makes use of both transmitted electrons and electrons generated by interaction of the beam with the sample, that are elastically scattered in the direction of the imaging system. This means that the imaging system receives a diffraction pattern, that is reconstructed by the projection lens into a 2D image of the sample.

Finally, the imaging plate on the bottom converts the incident electrons into visible light by fluorescence, and the visible image is detected by a CCD camera. The resolution depends mainly on the speed of the electron beam used, and modern HRTEM apparatus are able to resolve features as small as few nanometers. Morphological characterization of SiO<sub>2</sub>@POSS and SiO<sub>2</sub>-TMMS fillers were performed on a Jeol 3010 High resolution Transmission Electron Microscope (HRTEM) operating at 300kV with a high-resolution pole piece (0.17nm point to point resolution) and equipped with a Gatan slow-scan 794 CCD camera. The powders were suspended in isopropanol, and a 5mL drop of this suspension was deposited on a holey carbon film supported on 3 mm copper grid for HRTEM investigation.

Transmission electron microscopy was also employed for the morphological characterization of cured and uncured SBR/SiO<sub>2</sub>@POSS and SBR/SiO<sub>2</sub>+POSS nanocomposites. The main principles are already described with the difference that an electron beam of lower energy has to be employed in order to avoid the destruction of the polymer matrix, and the sample preparation is more complicated. In particular, the investigation of both uncured and vulcanized composites was carried out by using a Zeiss EM 900 microscope. Ultrathin sections (about 50 nm thick) of composites were obtained with a Leica EM FCS cryo-ultramicrotome equipped with a diamond knife, by keeping the samples at -130°C.

The experiments have been performed in the laboratory of University Cà Foscari of Venezia in collaboration with Prof.S.Polizzi.

### A1.7 Swelling experiments

Swelling and extraction experiments were performed on cured nanocomposites SBR/SiO<sub>2</sub>@POSS ,SBR/SiO<sub>2</sub>+POSS and PB/Y%NBB\_Xh to evaluate the cross-linking density ( $\nu$ ). Samples of 10x10x2 mm<sup>3</sup> (0.20±0.02 g) were immersed in close vessels filled with 10 mL of toluene at 25 °C for three days in the dark to avoid photodegradation reactions. Toluene swells the composites and extracts the polymer chains not bound to silica or not crosslinked. It was replaced daily by fresh solvent to eliminate all the extractable chains. Finally, the swollen mass was weighted and dried till constant mass under vacuum at 70 °C for 12 h.

In order to evaluate the cross-linking density of the cured nanocomposites, the volumetric fraction of the swelled rubber  $V_r$  was calculated according to the following equation:

$$V_r = \frac{(m_d - fm_0) \cdot \rho_p^{-1}}{(m_d - fm_0) \cdot \rho_p^{-1} + m_{so} \cdot \rho_s^{-1}}$$

where:  $m_0$  and  $m_d$  are the mass of the composite specimen before and after swelling/extraction experiments, respectively;  $m_{so} = (m_{sw} - m_d)$  is the weight of the solvent in the swollen mass;  $m_{sw}$  is the weight of the swollen mass;  $\rho_p = 0.94 \text{ g}\cdot\text{cm}^{-3}$  is the SBR density;  $\rho_s = 0.87 \text{ g}\cdot\text{cm}^{-3}$  is the toluene density;  $f$  is the fraction of the filler in the composites, as determined by TGA. The cross-link density  $\nu$ , i.e. the number of network chains per gram bounded on both ends by crosslinks, was calculated according the Flory-Rehner equation:

$$\nu = \frac{[\ln(1-V_r) + V_r + \chi V_r^2]}{-2 \cdot \rho_p \cdot V_s \cdot (V_r)^{1/3}}$$

where  $V_s=105.91$  is the molar volume of toluene and  $\chi$  is the Flory solvent-polymer interaction term, which is 0.472 for toluene-SBR.<sup>33</sup>

The experimental uncertainty on the calculated  $\nu$  values does not exceed  $\pm 10$  %.

### **A1.8 Atomic Force Microscopy (AFM)**

Atom force microscopy is a microscopic technique from the family of Scanning Probe Microscopies (SPM), which groups all the techniques that use a probe to scan a surface in a raster pattern and to create an image. In particular, AFM exploits the contact on an ultra sharp tip (few nanometers large) with an almost flat surface which is kept on an equilibrium distance of few nanometers from the tip. The tip is mounted on a flexible cantilever. The equilibrium position corresponds to a minimum of energy due to the compensation of the attractive Van der Waals force with the repulsive electrostatic force acting between the charged tip and the surface. The cantilever can have a starting deflection in the equilibrium position. During the scan, as the tip encounters higher or lower surface features, it further deflects to keep the equilibrium distance. The deflection is in the range of nanometers or even angstroms, but can be measured with high accuracy by a laser beam which is reflected by a cantilever into a diode detector. The piezoelectric tube is hence stimulated to modify the z position as a consequence of the cantilever deflection detected by the laser-diode

system, in order to keep the equilibrium position. From the piezo tube z displacement it is possible to obtain an height image of the material. This is the original operating mode, also referred to as contact mode AFM (Fig A.4).

Conversely, operating in tapping mode, the cantilever is oscillated at a constant frequency between an alternating attractive and repulsive force, while the tip scans the surface. Two similar height images are in this case obtained: since the oscillation amplitude changes causes the piezo tube to displace, one image is obtained by the change in amplitude (Amplitude Error Image) and another is obtained from the z displacement (height Image). Generally speaking, in contrast to height signal, the amplitude error signal shows contrast only at the interface, where the height changes sharply. During the oscillations, when the tip is in close contact to the surface, a repulsive force is exerted. This can be divided into two component (in-phase and out of phase), that correspond to an elastic repulsion rather than an inelastic one. The factors influencing the ration between the two components include adhesive forces between tip and the sample, and the modulus of the surface feature examined. The overall elastic vs inelastic component is summerized by a phase signal recorded at each point of scanning, that can be transferred into an image (phase image), which gives qualitative information about the local stiffness of the material, in other words, the materials heterogeneities.

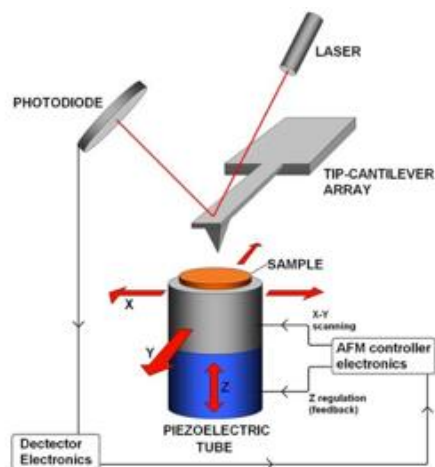


**Figure A.4:** Scheme of AMF experiment

To sum up, AFM measurements conducted in tapping mode give three simultaneous images (Height, Amplitude Error, Phase) of the materials surface that give a morpho-mechanical description of his heterogeneities at the nanoscale. The bulk morphology was evaluated by imaging the fracture area after previous freeze-fracturing of cured composites at the temperature of liquid nitrogen. Investigation of the topography surface was done by an atomic force microscope (MultiMode Digital Instruments Nanoscope Dimension IIIa), equipped with the SSS-NCL probe, Super Sharp Silicon SPM-Sensor (NanoSensor Switzerland; spring constant 35 N/m, resonant frequency 170 kHz). Measurements were performed on SBR/SiO<sub>2</sub>@POSS-X and SBR/SiO<sub>2</sub>+POSS-X nanocomposites cured at different temperature for 10 min under ambient conditions using the tapping mode AFM technique. Surface images were taken by scanning sizes from 1 to 50um. Investigations on the crude materials was not possible because of their high stickiness. The experiments have been performed in the

laboratory of Institute of Macromolecular Chemistry of Prague in collaboration with Prof. M.Spirkova and Prof. L. Matejka.

### **A1.9 Oscillating Dish Rheometry (ODR) and stress-strain measurements**

ODR measurements of the uncured SBR/SiO<sub>2</sub>@POSS and SBR/SiO<sub>2</sub>+POSS nanocomposites composites was performed by Rubber Process Analyzer (RPA 2000, Alpha Technologies) by applying a shear stress mode (Fig A.5).

The testing chamber is composed by an upper moving part (rotor), with cone geometry and a lower part with plate geometry. The torque acting on the rotor during oscillation can be transformed into a value of modulus and divided into a real and an imaginary part, giving the Storage Modulus  $G'$ , associated with an elastic response, and the Loss Modulus  $G''$ , associated with a viscous response. The ratio between  $G''$  and  $G'$  ( $\tan\delta$ ) is a predictive number of the energy dissipated from the tire during usage.



**Figure A.5:** Rubber Process Analyzer (RPA 2000, Alpha Technologies)

The strain sweep tests were carried out at 70°C and 1 Hz from 2 to 100% elongation. Same measurements was also performed on cured composites, after vulcanizing the crudes sample in the testing chamber at the optimum temperature. In this case the train sweep was carried out at 70°C and 10Hz, from 0.2 to 10 % elongation. Specimens were cut by using a Constant Volume Rubber Sample Cutter (CUTTER 2000, Alpha Technologies); the dimensions were 3.5cm diameter and  $\approx 0,2$  cm thick, the weight  $4.5 \pm 0.3$  g. Two measurements were carried out for each sample and the average value was reported.

### **A1.10 Dynamo Mechanical Thermal Analysis (DMTA)**

Dynamo mechanical measurements of the final material can be also conducted along a wide temperature range, above and below the glass transition temperature of the material. The main interest in using DMTA as an additional dynamo mechanical technique are the identification of the correct glass transition temperature more precisely than DSC, as seen by the mechanical relaxation of polymer chains, and second, the identification of the relaxation modes different from the glass transition. In fact, while increasing the temperature other chain relaxation phenomena can occur, as a result of increasing entropy: for example, in polar polymers hydrogen bonds can break upon a certain temperature, allowing new segmental movements to take place, or in filled polymers the chains interacting with the filler surface can increase their mobility at temperatures that are different from the main glass transition. The instrument setup is composed by a thermostated chamber, in which the sample is a rectangular slab, champed on the upper part with a static clamp, and on the lower part with a moving clamb.

Dynamic mechanical characterization of the SBR/SiO<sub>2</sub>@POSS and SBR/SiO<sub>2</sub>+POSS nanocomposites cured at different temperature for 10 min was performed by a TA Ares G3 instrument by applying a shear stress mode. Temperature dependence of the complex shear modulus of rectangular samples (5 x 1 x 0.25cm<sup>3</sup>) was measured by oscillatory shear deformation at a constant frequency and deformation amplitude.

The experiments have been performed in the laboratory of Institute of Macromolecular Chemistry of Prague in collaboration with Prof. L. Matejka.

### **A1.11 Tensile Tests**

Tensile testing is a fundamental materials science test in which a sample is subjected to a controlled tension until failure. The results from the test are commonly used to select a material for an application, for quality control, and to predict how a material will react under other types of forces. Properties that are directly measured via a tensile test are ultimate tensile strength, maximum elongation and reduction in area. From these measurements the following properties can also be determined: Young's modulus, Poisson's ratio, yield strength, and strain-hardening characteristics. Uniaxial tensile testing is the most commonly used for obtaining the mechanical characteristics of isotropic materials. For anisotropic materials, such as composite materials and textiles, biaxial tensile testing is required. The common testing machine has two crossheads; one is adjusted for the length of the specimen and the other is driven to apply tension to the test specimen. There are two types: hydraulic powered and electromagnetically powered machines.

The machine must have the proper capabilities for the test specimen being tested. There are four main parameters: force capacity, speed, precision and accuracy. Force capacity refers to the fact that the machine must be able to generate enough force to fracture the specimen. The machine must be able to apply the force quickly or

slowly enough to properly mimic the actual application. Finally, the machine must be able to accurately and precisely measure the gauge length and forces applied; for instance, a large machine that is designed to measure long elongations may not work with a brittle material that experiences short elongations prior to fracturing.

As shown in Figure A.6, during a typical tensile experiment, a dog-bone shaped specimen is gripped at its two ends and is pulled to elongate at a determined rate to its breakpoint; a highly ductile polymers may not reach its breakpoint. Figure A.6 shows also the standard configuration for tensile testing strip materials. This shape is commonly referred to as a dogbone, with wide ends and a narrow middle. The grips of the testing apparatus hold the specimen firmly at the wide ends. The midsection of the sample has a narrower width than the grip section. This concentrates the stress in the test area, so that fracture and most of the strain occur here. Strain is measured in this section, and stress is calculated from the force load on the grips. If any strain or deformation occurs outside of the test area, the test results will be inaccurate. However, if the fracture occurs outside of the area in which the strain is measured, the test results must be thrown out. It is therefore a good idea to prepare multiple samples if using straight-sided pieces.

Tensile tests were carried on the SBR/SiO<sub>2</sub>@POSS-X<sub>Y</sub> and SBR/SiO<sub>2</sub>+POSS-X<sub>Y</sub> out using an Instron 5800 apparatus at 25 °C and a crosshead speed of 50 mm min<sup>-1</sup>. For each sample five dog bones were prepared and the average value was evaluated.

The experiments have been performed in the laboratory of Institute of Macromolecular Chemistry of Prague in collaboration Prof. L. Matejka.

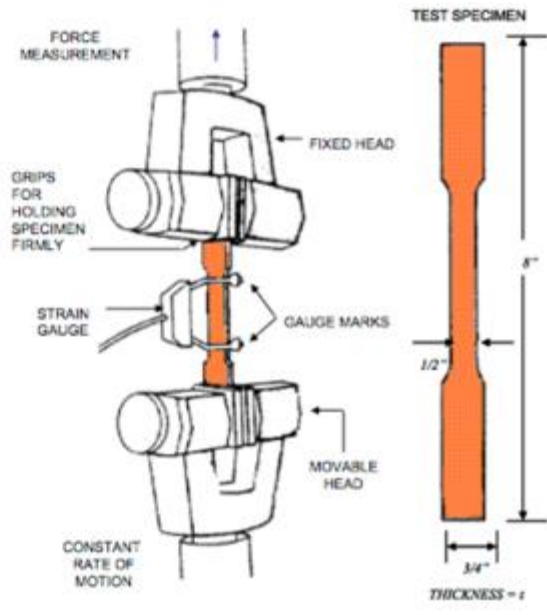


Figure A.6: Tensile test experiment



## **List of Abbreviations**

NPs	Nanoparticles
PSQs	Polysilsequioxanes
POSS	Polyhedral Oligomeric Silsesquioxanes
LPSQs	Ladder-like Polysilsesquioxanes
LPMASQ	Ladder-like Poly(Methacryloxypropyl)Silsesquioxane
PTMS	Phenyltrimethoxysilane
PDVF	Polyvinylidene fluoride
PMMA	Poly(methyl methacrylate)
PS	Polystyrene
PE	Polyethylene
HNBR	Hydrogenated Nitrile Butadiene Rubber
DCP	Dicumylperoxide
ISWP	in-situ water production
PB	Polybutadiene
NR	Natural Rubber
IR	Isoprene Rubber
SBR	Styrene Butadiene Rubber
BR	Butadiene rubber
TMMS	Trimethoxysilyl)propylmethacrylate
6PPD	N-(1,3-dimethylbutyl)-N'-phenyl-p-phenyldiamine
RPA	Rubber Process Analyzer

McPTMS	Mercaptopropyl)trimethoxysilane
DBTL	Dibttyltindilaurate
CIAA	Chloroacetic Acid
PrOH	1-Propanol